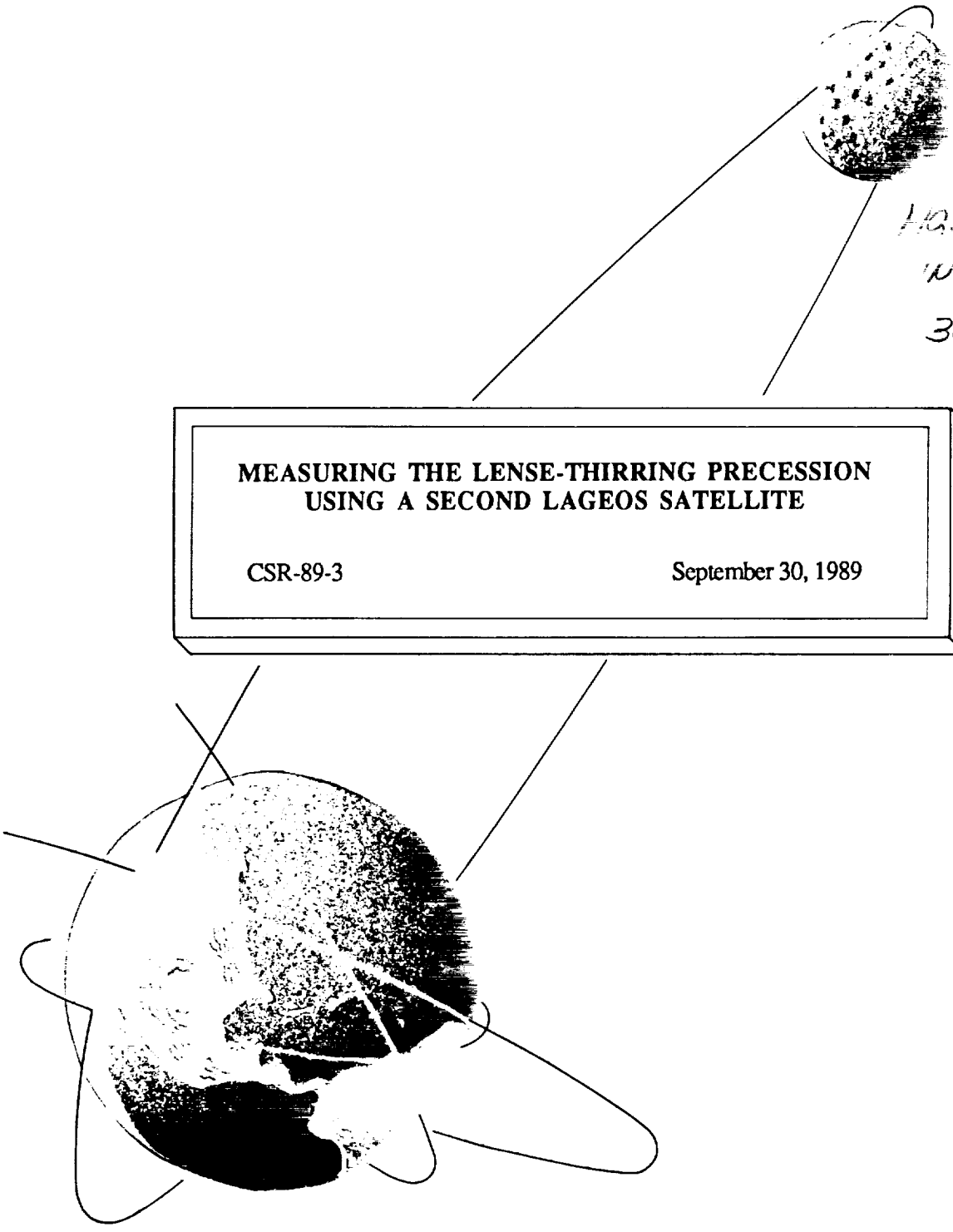

MEASURING THE LENSE-THIRRING PRECESSION USING A SECOND LAGEOS SATELLITE

CSR-89-3 September 30, 1989

CENTER FOR SPACE RESEARCH

THE UNIVERSITY OF TEXAS AT AUSTIN AUSTIN, TEXAS

MEASURING THE LENSE-THIRRING PRECESSION USING A SECOND LAGEOS SATELLITE

B. D. Tapley and I. Ciufolini

Results of a Joint NASA/ASI Study

Report No. CSR-89-3

Center for Space Research
The University of Texas at Austin
Austin, Texas 78712

September 30, 1989

FOREWORD

The final report for the joint NASA/ASI study consists of three sections:

1. A summary of the objectives, accomplishments, and conclusions of the research performed by the Center for Space Research and the Agenzia Spatiale Italiana,
2. Appendix A, which describes in detail the comprehensive simulation and covariance analysis of the Lageos-3 experiment which was performed by the Center for Space Research under NASA Grant No. NAGW-1330,
3. Appendix B, which is bound under separate cover and which describes the various investigations performed by the members of the Agenzia Spatiale Italiana concerning selected aspects of the Lageos-3 mission.

The investigation teams appreciate the numerous stimulating discussions held with the Science Advisory Group and are indebted to NASA and ASI for their support of this investigation.

TABLE OF CONTENTS

Measuring the Lense-Thirring Precession Using A Second Lageos Satellite

B. D. TAPLEY

Center for Space Research, The University of Texas at Austin, Austin, Texas U.S.A.

I. CIUFOLINI

IFSI-CNR, Consiglio Nazionale delle Ricerche, Frascati, Italy

INTRODUCTION

The procedures by which space measurements can contribute to the understanding of gravitation, as one of the four fundamental forces in the universe, is documented in the National Research Council report, *Strategy for Space Research in Gravitational Physics in the 1980's.* The report, which was prepared by the Space Science Board (SSB) Committee on Gravitational Physics (CGP) in 1981, identifies the measurement of the dragging of inertial frames by a rotating mass as the highest priority experiment in the class of experiments requiring a dedicated spacecraft.

The dragging of inertial frames is a consequence of Einstein's General Relativity [*Misner et al.*, 1973]. In this theory, a nonrotating, spherical mass produces the standard and well-tested Schwarzschild field. If the sphere is rotating, then the gravitomagnetic field occurs, whose strength, in the weak field and slow motion limit, is proportional to the angular velocity of the sphere. In the weak field approximation of the Kerr metric, the gravitomagnetic field is given by [*Thorne et al.*, 1986]:

$$\vec{H} = \vec{\nabla} \times \vec{\beta} = 2 \left[\frac{\vec{J} - 3(\vec{J} \cdot \hat{r})\hat{r}}{r^3} \right]$$

where $\vec{\beta} = \left[0, 0, -\frac{2J}{r^3} \right]$ is the gravitomagnetic or Lense-Thirring potential, and $\vec{J}$ is the angular

momentum of the central body.

Oersted [1820] proved that electric currents produce magnetic fields; general relativity predicts that mass currents produce gravitomagnetic fields. The importance of observing the effect of the gravitomagnetic field can be summarized as follows. First, this field can be considered as a "new" field of Nature, which is analogous to the magnetic field in electrodynamics, and has not been directly measured previously. Second, the measurement of the gravitomagnetic field will provide experimental support of the general relativistic formulation of the Mach principle: that the local inertial frames are determined or at least influenced by the mass-energy distribution and currents in the universe [*Wheeler*, 1988]. Finally, the demonstration of this effect will be of significant importance in high-energy astrophysics. Some theories of energy storage, power generation, jet formation and jet alignment of quasars and active galactic nuclei are in fact based on the existence of the gravitomagnetic field of a supermassive black hole [*Thorne et al.*, 1986].

The dragging of the orbital plane (and the orbital angular momentum) of a test particle orbiting in the field of a rotating body is included among the various effects due to the gravitomagnetic field. In the case of central force motion, the orbital plane can be thought of as an enormous gyroscope which is dragged in the direction of rotation of the central body. This dragging of the whole orbital plane is described by the formula for the rate of change of the longitude of the node, discovered by *Lense and Thirring* [1918]:

$$\dot{\Omega}^{L\text{-}T} = \frac{2J}{a^3(1-e^2)^{3/2}}$$

where a is the satellite semimajor axis, e is the eccentricity, and J the angular momentum of the central body. This fact is significant when evaluating concepts for using space-based measurements to observe the Lense-Thirring nodal drag.

The report prepared by the SSB/CGP identifies two possible ways of measuring the frame-dragging effect. They are:

1. Placing a gyroscope in Earth orbit and monitoring the precession of its spin due to the Earth's rotation.
2. Placing two counter-rotating, drag-free satellites in polar orbit to monitor the relative precession of their orbital angular momentum vectors.

The current approach for measuring the frame-dragging or Lense-Thirring effect has been based on the orbiting gyroscope approach and is to be realized by the Gravity Probe B mission [*Everitt et al.*, 1974; *Parkinson et al.*, 1987]. Although the SSB/CGP report notes the need for an independent confirmation of the effect for a measurement of this importance, the counter-orbiting polar satellite approach was not given detailed consideration because of the apparent difficulty in making the measurement and because of the cost implied in the need for two satellites and two different launch vehicles.

Ciufolini [1986] proposed an additional method for measuring the induced Lense-Thirring nodal precession using of a pair of non-polar, Earth-orbiting satellites. This approach took advantage of the existing Lageos satellite (Lageos-1) [*Cohen and Smith*, 1985] by proposing a new Lageos-type satellite (Lageos-3), which is:

1. Physically identical to Lageos-1,
2. Placed in an orbit with identical altitude and eccentricity and with an inclination supplementary to the Lageos-1 orbit, and
3. Tracked with satellite laser ranging (SLR).

This configuration was proposed as a means of eliminating the influence of errors in our knowledge of the longitudinally independent part of the Earth's gravitational field on the combined or additive nodal precession. For a single satellite, the errors in the Earth's gravity

field model cause orbit errors which mask the predicted precession due to the Lense-Thirring effect. Since Lageos-1 is already in orbit, the dual Lageos satellite configuration has the advantage of requiring the launch of a single comparatively inexpensive satellite, and the present proposed plan calls for the program costs to be shared between the U.S. (NASA) and Italy (Agenzia Spaziale Italiana (ASI)).

Further study of the concept has noted that the configuration has a number of additional advantages; in particular, the lifetime of the passive Lageos satellites is predicted to be essentially limitless (estimated as 500,000 years before reentry), allowing continual monitoring and improvement in the determination of the frame-dragging effect. The potential for repeated measurement of the Lense-Thirring effect allows the possibility of improving the measurement accuracy. The accuracy with which the measurement can be made depends on the accuracy of laser ranging systems and the accuracy of the models for the forces which act on the satellite. The accuracy of both are improving steadily. The global SLR tracking system has undergone substantial improvement during the last decade. The number of regularly operating sites exceeds 25 stations at present, with many of the best systems having single-shot range accuracies approaching the one-cm level. Millimeter-level ranging technology is well underway toward development. The force models on Lageos-1 have improved to the level where dynamically continuous long-arc solutions over 12 years can be obtained. The rms of measurement fit including both model and measurement errors is around the 5 cm level during the last few years. (See Figure 1 and Figure 2 in Appendix A-1.)

The ability of the global SLR systems to range with accuracies at the 1 cm level has been used to perform measurements of tectonic motion, through station coordinate determination at the level of a few parts in 10^9 for monthly averages, and Earth orientation, with a precision of the order 1–2 milliarcsecs for 3-day averages [*Tapley et al.*, 1985; *Smith et al.*, 1985; *Christodoulidis*

et al., 1985]. The SLR data have been used to obtain significant improvements in our knowledge of the Earth's gravity field [*Tapley et al.*, 1988b; *Marsh et al.*, 1988; *Christodoulidis et al.*, 1988; *Cheng et al.*, 1989]. The feasibility of the proposed measurement of the Lense-Thirring precession of the Lageos-1/Lageos-3 satellite configuration has been examined in the light of the current maturity of the SLR tracking system.

Preliminary computations by the Center for Space Research (CSR) aimed at demonstrating the feasibility of the proposed relativity experiment, along with preliminary studies of several important error sources by ASI [*Bertotti and Ciufolini*, 1988], produced positive results. Initial error analyses [*Ciufolini*, 1987, 1988, 1989] predicted that a measurement of the Lense-Thirring precession, with about a 10% accuracy, should be possible for this important test of gravitational physics. After reviewing the preliminary results, an ad hoc NASA committee established to examine the proposed mission concluded that the initial studies did not consider several important effects and that a more extensive study would be required to establish the feasibility of the experiment.

In response to this conclusion, NASA and ASI formed study groups in May 1988 for the purpose of performing a comprehensive analysis of the experiment and demonstrating the feasibility through a comprehensive numerical simulation. A Lageos-3 Science Advisory Group was formed to provide guidance for the two investigations. The membership of the Science Advisory Group is given in Table 1. As shown in Table 2, four meetings with the Science Advisory Group were held: an initial meeting to define the complexity of the force model effects to be included, a second meeting to review the final simulation design and assess final decisions on the force model, a third meeting to review the initial results from the analytic analysis and numerical simulation of the experiment, and a final meeting to review the final results and conclusions.

The objective of the research described in this document was to perform a complete numerical simulation and error analysis for the proposed experiment with the objective of establishing an accurate assessment of the feasibility and the potential accuracy of the measurement of the Lense-Thirring precession. Consideration was given to identifying the error sources which limit the accuracy of the experiment and proposing procedures for eliminating or reducing the effect of these errors. Analytic investigations were conducted to study the effects of major error sources with the objective of providing error bounds on the experiment. The study was conducted as a joint effort by NASA and ASI, and the results obtained in the individual study efforts are documented in Appendix A and Appendix B, respectively.

The benefits of a Lageos-3 mission are not restricted to tests of relativity. In the area of geodynamics, the addition of Lageos-3 to the complement of other satellites tracked by SLR will improve results in all of the applications currently in progress. These include crustal motion monitoring, determination of gravity and tidal parameters, and of particular importance, maintenance of reference frames and monitoring of Earth rotation. The same orbital symmetry that allows the detection of the Lense-Thirring precession will improve substantially the capability of SLR measurements to provide rapid service measurement of universal time (UT1). The errors in the model for the tidal and nontidal time variations in the even zonal gravitational potential of the Earth, oceans and atmosphere, which are the primary limitations on the long-period accuracy of the UT1 determination using Lageos-1, are cancelled with the Lageos-1/Lageos-3 satellite configuration.

OBJECTIVES OF THE STUDY

The primary goal of the study is to demonstrate through the analysis of realistic simulated data that satellite laser ranging to two Lageos satellites, orbiting with supplemental inclinations, collected for a period of 3 or more years, can be used to verify the Lense-Thirring precession. An

ancillary objective is to develop a comprehensive covariance analysis for the solution. The covariance analysis will establish the uncertainty in the estimate of the Lense-Thirring scale parameter, L, due to errors in the SLR data and errors in the other aspects of the dynamical and measurement model. In both numerical simulation and covariance analysis, it is important to establish an accurate value for the expected magnitudes of the model uncertainties, as well as their functional form. In establishing the error models and the technique used to translate these errors into the predicted uncertainty in L conservative estimates were adopted to prevent undue optimism in the error estimate.

In response to previous evaluations of the proposed experiment, both gravitational and nongravitational forces, which contribute significant perturbations, were identified for detailed consideration. The main perturbations considered in this study are:

- Neutral and charged particle drag, in particular inhomogeneities and anisotropies in the charged particle drag (fluctuating pressure due to charged particle precipitation in the auroral zones, systematic charged particle currents in the inner Van Allen belt and anisotropic fluctuations in the residual atmospheric drag driven by solar activity),
- Thermal thrusting generated from heating by infrared of the Earth radiation and the thermal lag of the Lageos retroreflectors [*Rubincam*, 1987],
- Thermal thrusting from the re-emission by the satellite of heat from the Sun interacting with eclipsing by the Earth [*Slabinski*, 1988],
- Radiation pressure due to the Earth albedo, both the diffuse and specular components, and the effect of the direct Earth infrared radiation pressure [*Rubincam et al.*, 1987],
- The periodic, secular, seasonal and stochastic variations in the Earth's gravity field.

The achievement of symmetry in the orbit of the second Lageos satellite is a critical factor, and the range of orbital injection error that can be tolerated was treated as a specific parameter in

the study. The analysis also assessed the sensitivity of the error in L to the expected deviation of the injection from the condition of perfect symmetry. The results of this study will be used to determine the feasibility of achieving the required accuracy with current launch vehicles.

Finally, the sensitivity of the accuracy of the estimate to the duration of the experiment was evaluated. The analysis indicates that a duration of approximately three years is a minimum. The temporal variation of the longitudinally independent components of the gravitational field, due to Earth and ocean tides and atmospheric circulation, were found to be one of the more important factors, and requires a long duration experiment to separate the effect of errors in these models from the Lense-Thirring parameter.

INVESTIGATION RESULTS

Center for Space Research

The primary objectives of the CSR study were to use a complete numerical simulation of the proposed experiment to demonstrate the experiment feasibility and to perform a comprehensive covariance analysis to establish the accuracy of the experiment and the sensitivity to measurement errors, dynamic model errors, and orbit injection conditions. In this study, the dynamical effect of the gravitomagnetic interaction was modeled as a scaled perturbing acceleration for each of the two satellites involved in the computation. The scaling parameter, L, is modeled such that the prediction of general relativity will correspond to a value of $L = 1$. In the analysis of the simulated SLR tracking data, an estimate of the value of L and its uncertainty was determined. The SLR data were generated using locations from a current set of globally distributed tracking stations with simulated ranging errors modeled after actual SLR tracking statistics. Range measurements to both satellites were combined in a simultaneous solution in which the orbital parameters of both satellites, the value of L, and other common force and

kinematic model parameters were estimated. The details of the experiment design and the numerical simulations are given in Appendix A-1.

The primary model errors were identified as the geopotential, the solid Earth and ocean tides, and the surface forces. An analysis of the Lageos-1 range residuals from the latest CSR long-arc 8801 [*Tapley et al.*, 1988a] was performed in order to evaluate the nature and magnitude of the errors which remain in the current modeling of Lageos-type satellites. There was concern expressed, initially, regarding the models for the surface forces, particularly those representing the thermal effects that apply to Lageos-type satellites. Much of the effort in the preliminary stages of this analysis was devoted to identifying and understanding the possible mechanisms which can induce nongravitational forces on Lageos-1 in order to be sure that these forces are not critical to the Lense-Thirring measurement. In addition to quantifying the effect on the semimajor axis and node, it was noted for the first time that the thermal thrusting has an important effect on the orbit inclination [*Center for Space Research*, 1989].

Comparable attention was devoted to understanding the effects of the solid Earth and ocean tides. The sensitivity to errors in the tide models will be reduced by performing the experiment over a sufficiently long period of time, nominally three years, so that their effects will average out. Tides or quasi-periodic atmospheric pressure variations whose periods (in a space-fixed system) are close to the nodal periods of either Lageos-1 or Lageos-3 could cause changes in the satellite orbits that look like secular effects over the three-year experiment duration, but the results of this study indicate that there is insufficient power in the tidal spectrum near these critical resonance bands to seriously affect the measurement.

The numerical simulation was designed to emulate as closely as possible the procedure to be used in the proposed experiment. Simulated laser range data were generated in a manner which duplicated the distribution of the actual laser tracking of Lageos-1 during a three-year mission. In

the initial definition of the simulated experiment, there was concern expressed by the Science Advisory Group that, if the analysts who would be processing the data processed *a priori* knowledge of the true value for L and the other perturbed parameters, they would tend to be biased in their choice of the parameters to be estimated. This concern was addressed by adopting a blind simulation procedure in which the CSR analysts would not know the true value for any of the approximately 1550 individual error sources, including the true value of L. The extensive modifications to the orbit determination program, and the thorough testing required, resulted in some delay in completing the simulation and providing the final report, but the resulting system performed well and will provide a valuable simulation tool for future studies.

The results of the six blind solutions are summarized in Table 3, where the difference between the CSR estimate and the true value of L is listed. The scatter of the simulation solutions was 8%, and the mean of the differences between the estimate and true value of L was zero. In comparison, a covariance analysis for each case, based on considering the effect of errors in the non-estimated parameters similar to those included in the simulation, indicated that the 1-σ uncertainty in the estimate of L varied between 5 and 7%. The results are displayed graphically in Figure 1, where each solution is shown with respect to the true value and the size of the 95% confidence interval as predicted by the consider-covariance analysis. The covariance analysis could not consider the effect of the stochastic error sources and would be expected to predict a smaller uncertainty; otherwise, the agreement between the simulation results and the covariance analysis is remarkably good. The combination of the six simulations, supported by consistent results from the consider error analysis, indicate that the Lense-Thirring precession should be measurable at the 8% accuracy level. The fact that only one solution out of six deviated by as much as 15% is entirely consistent with this error assessment.

The simulation results include the effects of all modeled errors, but they do not allow one to quantify the contribution of the individual sources of error. Thus, the covariance analysis was necessary in order to construct the error budget for the Lense-Thirring measurement which is displayed in Table 4. The error in the gravitational model is the primary contributor to the overall error. The constant errors in the mean values of the Earth's geopotential and tide model are expected to contribute about 4 to 5%. The effect of errors in the even zonal harmonics are proportional to the size of the Lageos-3 orbit injection errors, with a conservative assessment of 3% for each 0.1° error in the inclination. The unmodeled thermal forces were found to cause a little less than a 3% uncertainty, while the contribution of the errors in the model for the Earth radiation pressure (reflected optical and reradiated infrared) was approximately 1%. The uncertainty due to the remaining parameters was generally negligible. The various stochastic errors not amenable to the consider analysis, particularly the seasonal variations in the geopotential, are conservatively estimated to contribute an additional 5%.

Further confidence in the experiment is obtained by evaluating the accuracy of the dynamic model parameters recovered along with the Lense-Thirring parameters. The dynamic model parameters which are likely to corrupt the Lense-Thirring parameter include GM of the Earth, the $J_2, J_3, \dot{J}_2$, and $\dot{J}_3$ coefficients of the Earth's geopotential, the k_2 tide coefficient and the Lageos-1 and Lageos-3 solar reflectivities. As shown in Appendix A-1, Table 9 the values of these parameters, recovered simultaneously with the Lense-Thirring parameter, showed excellent agreement with the values adopted for these parameters in the overall simulation. This illustrates again the contention that the Lense-Thirring parameter is uniquely separated from the other dynamic model parameters in the case of satellites with supplementary inclinations.

An important concern in this analysis is whether any significant error source has been ignored. It could be argued, for example, that the errors assumed for the thermal thrusts are

optimistic, since the existing model does not completely model the observed variations in Lageos drag. However, even if the thermal forces were 100% larger than those assumed for this investigation, an assumption that appears unlikely based on the existing analysis, the error estimate increases from 8% to only 10%. While there are certainly significant systematic errors remaining in the Lageos residuals, they can generally be explained by errors in the models for the known physical effects, such as the year-to-year fluctuation in the seasonal changes of the Earth's gravity field. These errors have been included in the 8% overall error estimate given in Table 4. The thermal forces on the Lageos satellite represent essentially the limit of the forces that can be affecting the satellite significantly. *Ciufolini* [1989] has examined a wide variety of lesser forces and found that the maximum effects of those not already considered in this analysis were generally much less than 1% of the Lense-Thirring precession. Since reasonable limits on the known forces have been determined and used in this simulation, the existence of a large, unsuspected force with a new physical mechanism must be considered very unlikely. A similar argument applies to possible measurement errors which would be large enough, have just the right time dependence, and be common to all stations over the three-year period. While such an effect is impossible to rule out, it must be considered to be a remote possibility and should not be included in a 1-σ error estimate. It would appear that the 3-σ error estimate of 24% would adequately include the effect of such unlikely errors.

Agenzia Spatiale Italiana

The following discussion summarizes the main results of the study of the nongravitational perturbations. The details of the analytical studies are given in Appendix B.

It is reasonably certain that neutral and charged particle drag explains part of the Lageos-1 semimajor axis decay. To study the effect on the node node, four cases were considered:

1. The exosphere is co-rotating with the Earth,
2. The charged exosphere is rotating about the Earth's geomagnetic axis,
3. The worst case, involving variations of the average particle drag, from essentially 0 to approximately 5×10^{-12} m/s^2,
4. The worst case of charged particle drag, corresponding to high charging of the satellite (sporadic, anomalous potentials of –600 Volt, once per orbit, for a few tens of seconds).

The result of the investigation is that, even in the most extreme conditions, the secular nodal drag will never exceed a few tenths of a percent of the Lense-Thirring effect (Appendix B-1).

Regarding the thermal thrust due to anisotropic re-emission of Earth infrared radiation and re-emission of solar radiation modulated by eclipses, this effect has been studied both by the ASI group [*Afonso et al.*, 1989] and by the CSR group [*Center for Space Research*, 1988, 1989]. In the case of heating by the infrared radiation from the Earth, the ASI study found a maximum secular nodal precession of 2% of the Lense-Thirring effect, corresponding to a worst case for the spin axis orientations of Lageos-1 and Lageos-3, one along the Earth spin axis and the other perpendicular to it. In the case of heating by sunlight modulated by eclipses, the largest secular and long periodic terms can be at most 1% of the Lense-Thirring effect, corresponding to the worst values of some thermal parameters considered. These figures refer to the maximum effect of thermal thrust; however,

1. The orientation and the rotation rate of the spin of Lageos-1 and Lageos-3 can be measured and modeled (see below), and
2. The knowledge of the thermal and optical properties can be substantially improved through various measurements.

Therefore, according to formulas (8) and (20) of Appendix B-2, and because of partial cancellation of the overall effect over a period of a few years, the sum of the unmodeled secular

nodal drifts of Lageos-1 and Lageos-3 due to this effect should be less that 1% of the Lense-Thirring effect.

Because of the importance of knowing the spin orientation and spin rate of Lageos-1 and Lageos-3, to allow accurate modeling of the thermal thrust on laser-ranged satellites, the rotational dynamics of Lageos-1 must be studied to determine the temperature anisotropy and the ensuing radiation recoil effect. For this purpose, a model is proposed in Appendix B-3 for the torques acting on Lageos-1 due to eddy currents and gravity gradients.

Concerning the Earth's albedo, the CSR and ASI investigations show that the error in the Lense-Thirring measurement, due to Earth-reflected radiation pressure on Lageos-1 and Lageos-3, would not exceed a few percent of the gravitomagnetic effect. However, improvements are achievable by modeling the Earth's albedo. Furthermore, many of the terms in the expression for the nodal precession due to the Earth albedo are linearly dependent on $\cos I$ and therefore give, for the two satellites, nodal precessions equal in magnitude but opposite in sign, thus substantially reducing the uncertainty due to Earth's albedo.

Similar arguments can be applied to concerns about the direct radiation pressure on Lageos-type satellites due to infrared radiation from the Earth. On the basis of a paper by *Sehnal* [1981], *Ciufolini* [1987] has pointed out that the main latitudinal effect is equal in magnitude but opposite in sign for Lageos-1 and Lageos-3. Furthermore, the CSR group has shown that the Lageos-1 secular nodal effect is much smaller than the value previously calculated by *Sehnal* [1981], i.e., the total secular effect is ≈2 mas/year. Therefore, due to the small size of the effect and the cancellation of the J_2 part, the error in modeling the direct effect of Earth's infrared radiation on the node is substantially negligible.

CONCLUSIONS

The following conclusions, drawn from the numerical and analytic investigations described in Appendices A and B, are:

1. The results of a number of simulations and covariance analyses, including six blind tests which involved simulated data with a wide variety of unknown error sources, indicate that, with a high level of confidence, two Lageos-type satellites in orbits with supplementary inclinations can measure the Lense-Thirring precession of the satellite orbit planes with an estimated precision of 8% (1 σ). The 8% uncertainty is based on a conservative assessment of the error in the parameters recovered in the numerical simulation and the uncertainties assigned by a comprehensive covariance analysis. While tides, thermal forces and seasonal variations of the gravity field are among the largest contributors to the uncertainty, no error source exceeding 5% was identified. Since the error models adopted were generally conservative, the actual accuracy of the recovery of the Lense-Thirring precession parameter is likely to be better than 8%. With the development of improved models for the geopotential and tides, which are the main sources of error, the accuracy of the measurement will be improved.
2. Since the satellite lifetimes are essentially limitless, repeated measurements can be made in successive three-year experiments. To the extent that the errors which limit the accuracy are random, repeated measurements would lead to an increased accuracy.
3. The error in the Lense-Thirring precession recovery due to the nongravitational perturbations, will not exceed a few percent of the Lense-Thirring effect. The primary contributor to this error is the thermal thrust from Earth infrared radiation and from sunlight plus eclipses and to uncertainties in the reflected and diffused Earth albedo. The knowledge of the nongravitational perturbations can be improved by measurement of the

thermal, optical and rotational parameters of Lageos-type satellites. This procedure will substantially reduce the error due to incorrect modeling of these perturbations.

4. The ability to improve the lump-sum zonal contributions of geopotential error during the estimation process will allow maximum allowable injection errors for Lageos-3 to be larger than the 0.1° in inclination error originally specified. As shown in Appendix A-2, the injection errors required to ensure that this effect contributes no more than a 1-σ variation of 3% is $\Delta a \leq 30$ km, $\Delta e \leq 0.2$ and $\Delta i \leq 0.12°$. These injection errors are easily attainable with current satellite launch capabilities.

5. The secular, periodic, and stochastic time variations of the even zonals have been shown to preclude any satellite combination other than the supplementary inclination approach. Even if the constant part of the Earth's gravity field could be determined with sufficient accuracy from a combination of historical and modern data from multiple satellites, the time variations in the even zonals during the period of the experiment would also have to be determined with a very high accuracy if the effect is to be modeled. However, with the supplementary inclination for Lageos-1 and Lageos-3, the effect of the time variations in the even zonals on the orbit nodes will cancel to a high degree of precision.

REFERENCES

Afonso, G., F. Barlier, M. Carpino, P. Farinella, F. Mignard, M. Milani, and A. M. Nobili, Orbital effects of Lageos' seasons and eclipses, *Ann. Geophys. A*, in press, 1989.

Bertotti, B., and I. Ciufolini, An experiment to measure the gravitomagnetic force with laser ranged satellites, Dipartimento di Fisica Nucleare e Teorica della Università, via Bassi, 6-Pavia, Italy, June 9, 1988.

Center for Space Research, The University of Texas at Austin, Semiannual Report for NASA

Grant No. NAGW-1330, December 30, 1988.

Center for Space Research, The University of Texas at Austin, Annual Report for NASA Grant No. NAGW-1330, May 3, 1989.

Cheng, M. K., R. J. Eanes, C. K. Shum, B. E. Schutz, and B. D. Tapley, Temporal variations in low degree zonal harmonics from Starlette orbit analysis, *Geophys. Res. Lett.*, *16*(5), 393, 1989.

Christodoulidis, D. C., D. E. Smith, R. Kolenkiewicz, S. M. Klosko, M. H. Torrence, and P. J. Dunn, Observing tectonic plate motions and deformations from satellite laser ranging, *J. Geophys. Res.*, *90*(B11), 9249–9263, 1985.

Christodoulidis, D. C., D. E. Smith, R. G. Williamson, and S. M. Klosko, Observed tidal braking in the Earth/Moon/Sun system, *J. Geophys. Res.*, *93*(B6), 6216, 1988.

Ciufolini, I., Measurement of the Lense-Thirring drag on high-altitude, laser-ranged artificial satellites, *Phys. Rev. Lett.*, *56*(4), 278–281, January 1986.

Ciufolini, I., The Lageos Lense-Thirring precession and the Lageos nongravitational nodal perturbations – I, *Celest. Mech.*, *40*, 19–33, 1987.

Ciufolini, I., Lageos-3, *Proceedings of NASA Workshop on Relativity and Gravitation Experiments in Space*, Annapolis, Maryland, June 28–30, 1988.

Ciufolini, I., A comprehensive introduction to the Lageos gravitomagnetic experiment, *Int. J. Mod. Phys. A*, *4*, 3083, 1989.

Cohen, S. C., and D. E. Smith, Lageos scientific results: Introduction, *J. Geophys. Res.*, *90*, 9217–9220, 1985.

Everitt, C. W. F., W. M. Fairbank, and L. I. Schiff, The gyroscope experiment. I. General description and analysis of gyroscope performance, in *Experimental Gravitation: Proceedings of the International School of Physics "Enrico Fermi,"* ed. B. Bertotti,

Academic, New York, 331–360, 1974.

Lense, J., and H. Thirring, ber die Einfluss der Eigenrotation der Zentralkrper auf die Bewegung der Planeten und Monde nach der Einsteinschen Gravitationstheorie, *Phys. Zeitschr., 19*, 156, 1918; English translation by B. Mashhoon et al., *Gen. Relativ. Gravit., 16*, 711, 1984.

Marsh, J. G., F. J. Lerch, B. H. Putney, D. C. Christodoulidis, D. E. Smith, T. L. Felsentreger, B. V. Sanchez, S. M. Klosko, E. C. Pavlis, T. V. Martin, J. W. Robbins, R. G. Williamson, O. L. Colombo, D. D. Rowlands, W. F. Eddy, N. L. Chandler, K. E. Rachlin, G. B. Patel, S. Bhati, and D. S. Chinn, A new gravitational model for the Earth from satellite tracking data: GEM–T1, *J. Geophys. Res., 93*(B6), 6169, 1988.

Misner, C. W., K. S. Thorne, and J. A. Wheeler, *Gravitation*, Freeman Press, San Francisco, 1973.

Oersted, H. C., *Experimenta Circa Effectum Conflictus Electrici in Acum Magneticum*, Copenhagen, 1820.

Parkinson, B. W., C.W.F. Everitt, and J. P. Turneaure, The Gravity Probe B relativity gyroscope experiment: An update on progress, *Aerospace Century XXI, 64*, 1183, 1987.

Rubincam, D. P., Lageos orbit decay to infrared radiation from the Earth, *J. Geophys. Res., 92*, 1287, 1987.

Rubincam, D. P., P. C. Knocke, V. R. Taylor, and S. Blackwell, Earth anisotropic reflection and the orbit of Lageos, *J. Geophys. Res., 92*, 11662, 1987.

Sehnal, L., Effects of the terrestrial infrared radiation pressure on the motion of an artificial satellite, *Celest. Mech., 25*, 169, 1981.

Slabinski, V. J., Lageos acceleration due to intermittent solar heating during eclipse periods, *Proceedings of 19th Regular Meeting of Division on Dynamical Astronomy-American Astronomical Society*, Gaithersburg, Maryland, July 25–26, 1988.

Smith, D. E., D. C. Christodoulidis, R. Kolenkiewicz, P. J. Dunn, S. M. Klosko, M. H. Torrence S. Fricke, and S. Blackwell, A global geodetic reference frame from Lageos ranging (SL5.1AP), *J. Geophys. Res.*, *90*(B11), 9221–9233, 1985.

Space Science Board, Committee on Gravitational Physics, *Strategy for Space Research in Gravitational Physics in the 1980's*, National Research Council, National Academy Press, Washington, D.C., 1981.

Tapley, B. D., B. E. Schutz, and R. J. Eanes, Station coordinates, baselines, and Earth rotation from Lageos laser ranging: 1976–1984, *J. Geophys. Res.*, *90*(B11), 9235–9248, 1985.

Tapley, B. D., B. E. Schutz, R. J. Eanes, and M. M. Watkins, Analysis of a twelve-year Lageos long arc, *Eos Trans. AGU*, *69*(16), 1988a.

Tapley, B. D., C. K. Shum, D. N. Yuan, J. C. Ries, and B. E. Schutz, An improved model for the Earth's gravity field (TEG–1), *Proceedings of Chapman Conference on Progress in the Determination of the Earth's Gravity Field*, Ft. Lauderdale, Florida, 1988b.

Thorne, K. S., R. H. Price, and D. A. MacDonald, Eds., *Black Holes, the Membrane Paradigm*, Yale University Press, New Haven and London, 72, 1986.

Wheeler, J. A., Geometrodynamic steering principle reveals the determiners of inertia, *Int. J. Mod. Phys. A*, *3*, 2207, 1988.

TABLE 1. LAGEOS-3 SCIENCE ADVISORY GROUP

NAME	AFFILIATION
Peter Bender, Chairman	U. Colorado
John Anderson	JPL
John Armstrong	JPL
John Breakwell	Stanford
Demos Christodoulidis	JPL
Francis Everitt	Stanford
Edward Guinan	Villanova
Ron Hellings	JPL
Robert King	MIT
Irwin Shapiro	CFA
David Smith	GSFC
Rainer Weiss	MIT
Ex Officio:	
Bruno Bertotti	U. Pavia
Ignazio Ciufolini	IFSI-CNR
Edward Flinn	NASA HQ
Roberto Ibba	ASI
Warner Miller	Kirtland AFB, NM
George Newton	NASA HQ
Robert Stachnik	NASA HQ
Byron Tapley	U. Texas

TABLE 2. SCHEDULE OF MEETINGS

May 28, 1987, Goddard Space Flight Center, Greenbelt, MD

Ad Hoc Committee on Lageos-3

May 28, 1988, Contract Initiation

April 8, 1988, Baltimore International Airport, Baltimore, MD

First Meeting of Lageos-3 Science Advisory Group

September 8, 1988, University of Texas, Austin, Texas

Second Meeting of Lageos-3 Science Advisory Group

December 5, 1988, Stanford University, Palo Alto, CA

Third Meeting of Lageos-3 Science Advisory Group

May 22, 1989, Days Inn, Greenbelt, MD

Presentation of results to Lageos-3 Science Advisory Group

TABLE 3. RESULTS OF LENSE-THIRRING SIMULATION BLIND ANALYSIS

Case	True Value of L-T Scale	UT/CSR Solution	Solution Difference	Estimated Uncertainty
1	0.55	0.47	0.08	0.06*
2	1.38	1.32	0.06	0.06
3	0.08	0.02	0.06	0.05
4	0.86	0.83	0.03	0.07
5	1.83	1.98	-0.15	0.07
6	0.94	1.02	-0.08	0.07

Mean of difference = 0.0 RMS of difference = 0.08

* 0.06 can interpreted as 6% of the nominal General Relativity prediction of 1.0

TABLE 4: ESTIMATED ERROR BUDGET FOR LENSE-THIRRING MEASUREMENT

Geopotential (other than even zonals) + tides	5%
Earth radiation pressure	1%
Uncertainty in other relativistic effects [1]	1%
Earth- and solar-induced thermal forces [2]	3%
Even zonal geopotential (per 0.1° inclination injection error) [3]	3%
Other errors (such as random and stochastic errors included in simulation but not in covariance analysis) [4]	5%

	RSS Error
assuming 0.1° injection error or less	8%
assuming 0.2° injection error	10%
assuming 0.3° injection error	12%

Notes:

1) The only significant uncertainties are in the amount of geodesic (or de Sitter) precession and in the exact value of the PPN parameter γ.

2) The effect of the solar heating was based on the conservative assumption that no modeling is possible.

3) The result of 3% error per 0.1° inclination injection error assumes an equal influence of error in the semimajor axis and eccentricity, but the bounds on the semimajor axis and eccentricity injection errors are less demanding than the bounds on inclination. As a result, the predicted effect on the Lense-Thirring estimate is considered to be conservative.

4) Consider-covariance analysis results were augmented by an additional 5% to account for the effect of time-correlated stochastic errors (such as the seasonal variations in the geopotential, drag, and observation biases), which were included in the simulation, but could not be included explicitly in the covariance analysis.

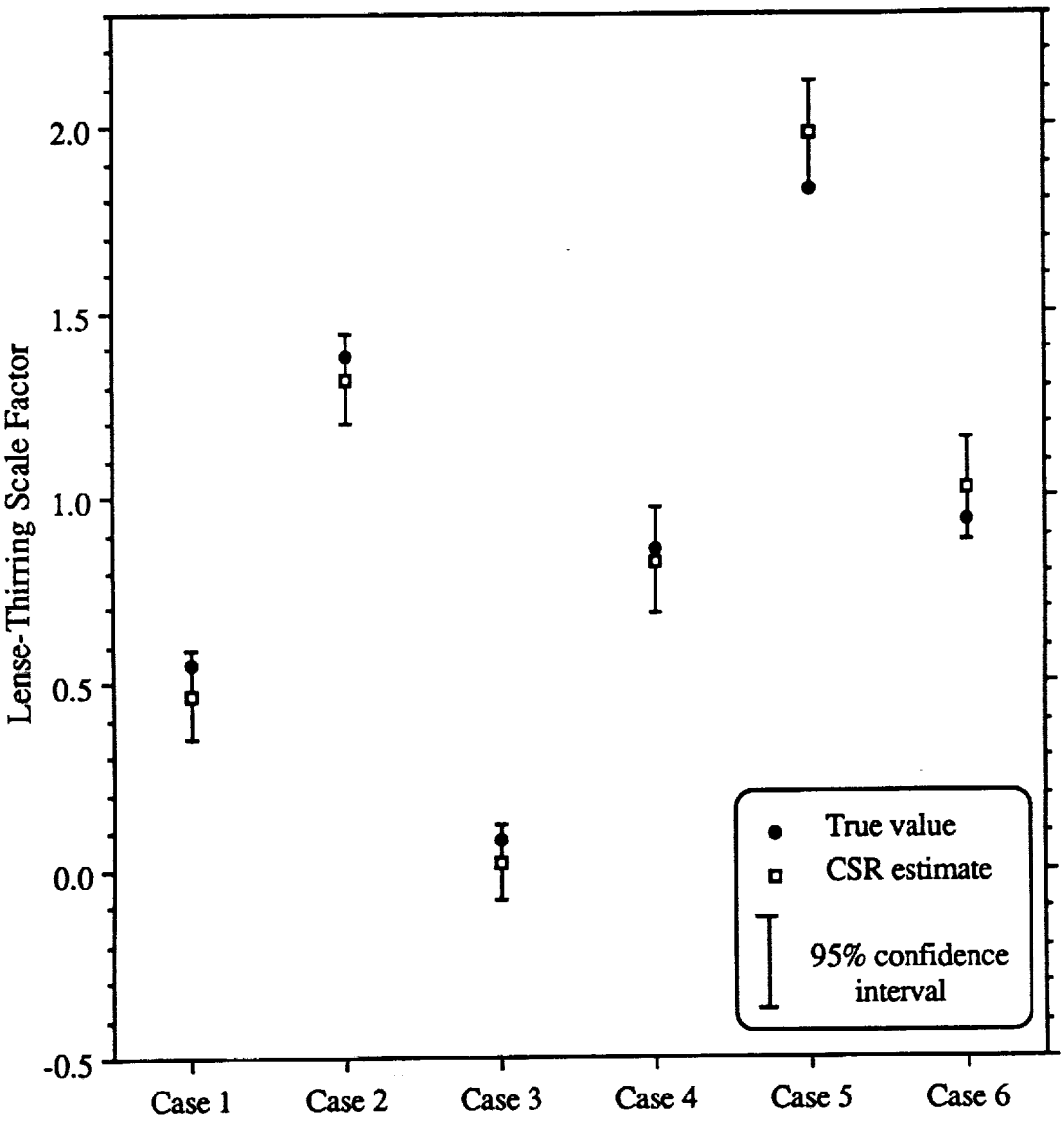

Figure 1. Estimate of Lense-Thirring parameter from blind data cases

APPENDIX A

Center for Space Research Investigations

NASA Grant No. NAGW-1330

Principal Investigator: Byron D. Tapley

A-1. Simulation of an Experiment to Measure the Lense-Thirring Precession Using a Second Lageos Satellite (John C. Ries, Richard J. Eanes, Michael M. Watkins, and Byron D. Tapley)

A-2. Orbit Injection Error Analysis for the Proposed Lageos-3 Mission (Stefano Casotto)

APPENDIX A-1

Simulation of an Experiment to Measure the Lense-Thirring Precession Using A Second Lageos Satellite

by
John C. Ries, Richard J. Eanes, Michael M. Watkins,
and Byron D. Tapley

SIMULATION OF AN EXPERIMENT TO MEASURE THE
LENSE-THIRRING PRECESSION USING
A SECOND LAGEOS SATELLITE

SIMULATION OF AN EXPERIMENT TO MEASURE THE LENSE-THIRRING PRECESSION USING A SECOND LAGEOS SATELLITE

John C. Ries, Richard J. Eanes, Michael M. Watkins and Byron D. Tapley
Center for Space Research, The University of Texas at Austin
Austin, Texas 78712 USA

SUMMARY

The results of a number of simulations and covariance analyses performed at the University of Texas Center for Space Research, including six blind tests in which the analysts processed simulated data with a wide variety of unknown error sources, indicate that using two Lageos-type satellites in orbits with supplementary inclinations will allow the measurement of the Lense-Thirring precession of the satellite orbit planes with an estimated precision of 8% (1 σ). While tides, thermal forces and seasonal variations of the gravity field are among the largest contributors to the uncertainty, no error source exceeding 5% was identified. Because of a degree of conservatism adopted in many of the error models, it is suggested that, with the development of better models for the main sources of error, the accuracy of the measurement could be improved significantly.

I. INTRODUCTION

A method for measuring the relative nodal precession of a pair of Earth-orbiting satellites, caused by the gravitational dragging of the orbit plane of each satellite by the Earth's rotation (the Lense-Thirring precession [*Lense and Thirring,* 1918]) as predicted by General Relativity has been proposed [*Ciufolini,* 1986]. In the proposed experiment, a new Lageos-type satellite (Lageos-3), which is identical to Lageos-1, placed in an orbit whose inclination is symmetric about the polar axis with respect to Lageos-1 and tracked with satellite laser ranging (SLR) can be used to eliminate the influence of errors in our knowledge of the longitudinally independent (zonal) part of the Earth's gravitational field on the additive nodal precessions of the two satellite orbit planes. Elimination of

this source of error will allow direct observation of the Lense-Thirring precession of the bisector of the satellite orbit planes. Uncertainties in our knowledge of the even degree zonal harmonics (and their secular, tidal and seasonal variations) mask the predicted precession due to the Lense-Thirring effect for a single satellite, but the use of two satellites, orbiting with supplementary inclinations and identical eccentricities and altitudes, will cause those model errors to cancel.

The University of Texas Center for Space Research (CSR), under NASA grant NAGW-1330, has conducted a comprehensive numerical simulation and covariance analysis of the proposed mission to 1) determine the experiment feasibility, 2) determine the magnitude of the error that can be expected in such a measurement, and 3) identify the error sources which limit the measurement accuracy. The numerical simulation was designed to emulate as closely as possible the procedure to be used in the proposed experiment. Thus, simulated laser range data were generated for a simplified tracking network composed of only eight laser stations with ranging precision comparable to the better laser stations currently operating. The current global SLR network contains 15 to 20 operational stations and the adoption of eight stations for the study provides a conservative, if not pessimistic, assumption for the tracking network distribution. The simulated data from the eight stations were sampled in a manner which attempted to duplicate the distribution of the actual laser tracking of Lageos, but with some conservatism in the amount of data obtained to reflect the possible conflict of tracking Lageos and Lageos-3 with other satellites (such as Lageos-2, Starlette, Stella, etc.), although current plans to provide multi-satellite tracking at each laser tracking site will minimize the potential for this conflict.

A three-year orbit was adjusted in a preliminary solution to fit the simulated SLR data for each satellite. The three-year time frame was selected to agree with the time interval for the proposed experiment. The simulated data contained a comprehensive set of satellite force model and measurement model errors. In the preliminary solutions, a small set of satellite dependent

parameters were estimated to achieve reasonably good fits to the simulated data. The information from both satellites was combined in a simultaneous solution for the individual satellite parameters as well as the parameters common to both satellites, such as a few low degree zonals, selected ocean tide coefficients, station coordinates and the Lense-Thirring scale parameter. A scaling factor for the Lense-Thirring precession, whose value would be 1 in Einstein's general relativity, was introduced into the simulation to represent the degree to which the Lense-Thirring precession is present. A parameterization of this sort is amenable to least-squares estimation techniques, allowing the estimation of the parameter, as well as the uncertainty in the estimate based on the expected errors in other parameters.

The feasibility of the proposed experiment depends on the type and magnitude of errors present in the modeling of the forces on Lageos-type satellites, and the acceptability of the simulation depends on the fidelity of the models chosen to represent those errors. Because of the nonlinear, multi-dimensional nature of the orbit dynamics, error sources which do not directly affect the node of Lageos-type satellites can still affect other orbit parameters, which in turn may affect the recovery of model parameters which do affect the node. It is important that all significant error sources be included, but the magnitude of the errors should be neither optimistic nor unreasonably pessimistic. Thus, careful analysis of the errors which remain in the current Lageos orbit is required.

The purpose of this report is to document the results presented at the various meetings with the Lageos-3 Science Advisory Group (SAG). There are, however, occasional differences between those results and the material presented here. These differences generally represent improvements or expansion of the analysis. Some of the changes are responses to the concerns raised by the SAG, while other changes have been made to improve the clarity of the analysis.

Nomenclature

In the following discussion, the real Lageos spacecraft will be referred to generally as Lageos, whereas the simulated satellites will be referred to as Lageos-1 and Lageos-3. In this analysis, the formulas for the relativistic effects will include only the parameterized post-Newtonian parameters, β and γ. The parameter used to scale the general relativity prediction of the Lense-Thirring precession will be denoted by L, which is not a standard relativity parameter, but has been added for the purpose described above. Errors in L will be referred to as a percent of the general relativistic prediction of 1; thus, for example, a 6% error will indicate an error in the measurement of the Lense-Thirring parameter L of 0.06.

Random errors of a given magnitude will represent a randomly chosen error from a Gaussian distribution with zero mean and a standard deviation equal to the specified value. Random noise refers to a similar process, but indicates that multiple realizations will be used (such as for individual 5-day values of polar motion or point-by-point data noise) rather than a single initial random error in a parameter (such as a station coordinate or geopotential coefficient). Stochastic process errors will refer to errors which vary with time in a stochastic manner. The primary model used to simulate the effect of these errors is a first-order autoregressive (Markov) process defined by *Box and Jenkins* [1970].

II. PRELIMINARY ANALYSES

First-order analyses of the measurement of the Lense-Thirring precession using two Lageos satellites in supplementary orbits have indicated that the measurement should have an uncertainty on the order of 10% [*Ciufolini*, 1986, 1987, 1988, 1989]. In those studies, a number of error sources were considered, but a rather simplistic approach was used in which the effect of each error on the orbit node-rate was compared with the size of the Lense-Thirring precession. This type of analysis is useful more in a qualitative sense; it is helpful in identifying error sources which are likely to be

significant, but since it neglects a number of important nonlinear dynamical couplings, it is less able to quantify the uncertainty precisely in the actual Lense-Thirring measurement. The analysis adopted a conservative approach by estimating the maximum effect of the various errors considered, resulting in a reported maximum statistical error of 12% [*Ciufolini*, 1989].

The cancellation of the Newtonian gravity induced nodal precession was demonstrated in an initial simulation performed at the Center for Space Research using a more rigorous parameter estimation approach [*CSR*, 1988]. This approach includes all of the interactions between the various error sources, the estimated parameters and the tracking scenario. The sources of error were limited to measurement noise and constant errors in the parameters for the Earth gravity model, the solid Earth and ocean tide model, the solar and Earth radiation pressure models, and the tracking station coordinates. The realizations of the gravity model errors were based on a mapping of the error in the coefficients of the GEM-T1 [*Marsh et al.*, 1988] gravity model covariance matrix into a set of errors for each coefficient in the geopotential model. The Earth and ocean tide errors were chosen to be 10% of their nominal value with the distribution randomly selected. The Earth radiation pressure error was 100% of the total modeled effect; the solar radiation pressure reflectivity error was 20%. Random errors in each station coordinate with a standard deviation of 5 cm were assumed. There was no injection error assumed for the Lageos-3 satellite; i.e., Lageos-3 was in a perfectly supplementary orbit and had the same semimajor axis and eccentricity as Lageos-1. The preliminary simulation had as its objective the demonstration of the cancellation of the effect of errors in the even degree zonal harmonics.

When the Lense-Thirring parameter, L, was estimated in the presence of these errors, the recovered value agreed with the general relativity value to within 3%. Since this represented only a single realization of the possible errors, a consider-covariance analysis was also performed. Estimating the same parameters as in the simulation, but considering errors in the remaining

parameters (data noise, remainder of the gravity field, other ocean tides, and station coordinates) resulted in an uncertainty in L of less than 4%. Thus the simulation and the covariance analysis produced similar results. The estimated uncertainty was less than half the 10% predicted in the error analysis given in *Ciufolini* [1986]. Although most of the important error sources had been included in these simulations, the error model was incomplete. In particular, the model did not contain random or stochastic errors, which are from a class of errors that could not be removed by the estimation of most or all of the available parameters. That is, the structure of the satellite force model was assumed to be known, and only the values of the force model parameters were unknown. Increasing this preliminary error estimate by a factor of two to account for the lack of knowledge of some components of the force model would have been reasonable.

Consequently, the success of the preliminary simulation was a necessary, but not sufficient, condition for asserting the feasibility of the experiment, since several possible errors were not considered. The simulation did demonstrate the cancellation that is necessary for a successful mission.

Principal Error Sources

The primary model errors have been identified as the geopotential, the solid Earth and ocean tides, and the surface forces on the Lageos-type satellites. While models for all of these effects exist, the models are not complete, nor are the values for the parameters in the models known precisely. In the initial phase of the study, there was concern expressed regarding the models for the surface forces, particularly those representing the thermal effects that apply to Lageos-type satellites. Much of the effort in the preliminary stages of this analysis was devoted to identifying and understanding the possible mechanisms which can induce nongravitational forces on Lageos-1 in order to be sure that these forces are not critical to the Lense-Thirring measurement.

Based on the formulation of *Kaula* [1966] describing the effect of the geopotential on a satellite orbit, it can be shown that the errors in the zonal gravity coefficients will cancel if the inclinations of the two satellites are supplementary, and if the semimajor axis and eccentricity are identical. Since these conditions are unlikely to be met exactly, the error in knowledge of the coefficients of the Earth's gravity field is an important consideration, and the magnitude of the errors in the zonal coefficients will determine the allowable margin of error in the orbit injection of Lageos-3. An analysis by *Casotto* [1989] is included in Appendix A-2 which quantifies the increase in the uncertainty of the Lense-Thirring measurement due to error in the injection conditions (i.e., the degree to which the semimajor axis, inclination and eccentricity of the Lageos-3 orbit differ from the ideal values).

The most important effect of the solid Earth and ocean tides on the Lense-Thirring experiment is that they induce periodic variations in the Earth's gravity coefficients, particularly the even zonals. The sensitivity to errors in the tide models will be reduced by performing the experiment over a sufficiently long period of time, nominally three years, so that their effects will average out. Tides or quasi-periodic atmospheric pressure variations whose periods (in a space fixed system) are close to the nodal periods of either Lageos or Lageos-3 could cause changes in the satellite orbits that look like secular effects over the three-year experiment duration, but the results of this study indicate that there is insufficient power in the tidal spectrum near these critical resonance bands to seriously affect the measurement.

The surface forces on Lageos-type satellites consist of radiation pressure and atmospheric drag. While the atmosphere is very tenuous at the Lageos altitude, there are still enough charged and uncharged particles to cause noticeable drag on the satellite [*Smith and Dunn*, 1980; *Rubincam*, 1980, 1982; *Afonso et al.*, 1985; *Drozyner*, 1988]. The dominant force, however, is the effect of radiation pressure from the Sun. The reflectivity of the satellite surface can be estimated, but errors

in the modeling of the effect of shadowing by the Earth and Moon have the possibility of causing significant orbit errors. There is also the radiation pressure exerted on the satellite by light reflected from the Earth and by heat which has been absorbed and reradiated by the Earth. Like the geopotential, any zonal variation in the Earth's albedo or emissivity should cancel out, provided that the two satellites have identical reflectivities. The sensitivity to differences in the surface properties of the two satellites and the effects of longitudinal variations of the Earth's radiation are factors which are considered in the investigation.

In addition to the incident radiation forces described above, recent investigations at the NASA Goddard Space Flight Center (NASA/GSFC) indicate that heat, absorbed and reradiated anisotropically by the satellite itself, can also produce a significant acceleration. The primary along-track effect of the force produced by this anisotropic thermal radiation has been modeled routinely for Lageos by an empirically determined function which was restricted to acting along-track. Recent studies, however, indicate that much of the observed "drag" in the Lageos orbit may be explained by the mechanism proposed by Rubincam [*Rubincam*, 1987, 1988]. These studies have produced a more reasonable error model for the simulation and will eventually lead to models which can be used in the actual orbit determination of Lageos and Lageos-3.

Lageos Residual Analysis

An analysis of the Lageos range residuals from the latest CSR long arc 8801 [*Tapley et al.*, 1988a] was performed in order to evaluate the nature and magnitude of the errors which remain in the current modeling of Lageos-type satellites. The SLR data from 1976 to 1988 were fit with a single dynamically consistent orbit where an appropriate set of satellite parameters and geopotential and ocean tide coefficients were simultaneously estimated. The SLR tracking stations which provided data for this solution are shown in Figure 1. The resulting rms (root mean square) fit was 20 cm, although the fit to the data after 1980 was considerably better than the fit to the earlier data.

The number of stations tracking and the rms of the range residuals in each 15-day interval are shown in Figure 2. The improvement in the rms fit is consistent with the overall improvement in the ranging accuracy of the SLR systems. The residuals from the laser ranges were projected into equivalent mean orbit element errors for 6-day intervals in order to determine the nature and possible sources of the remaining errors (see Section IV for graphical representations of the orbit element residuals and their spectral content). There were a number of conclusions:

1. There has been a steady improvement in the quality and quantity of SLR data. The 6-day fits are now able to attain 3 to 5 cm residual rms, and the normal point precision is approaching the millimeter level. The factors which limit the precision of the fits over 6-day arcs are predominantly short period gravity errors, station coordinate and Earth orientation errors and measurement biases (range biases, timing biases and tropospheric correction biases).
2. Most of the errors remaining in the Lageos long-arc residuals come from errors in diurnal and semidiurnal tides, annual variations in the even zonal coefficients of the geopotential, annual and semiannual variations in the odd zonals [*Cheng et al.*, 1989], and thermal imbalance forces. Any variations in the even zonals which do not cancel out will affect the ability to measure the Lense-Thirring precession. This is one of the important reasons for using satellites with supplementary inclinations. Even if the average value of the even zonals could be determined with sufficient accuracy from multi-satellite solutions, there would still be the problem of determining the temporal variations in the even zonals during the period of the mission. Without the cancellation from supplementary inclinations, the variations in the even zonals would cause variations in the nodal precession that could be confused with the Lense-Thirring precession.
3. The current implied accuracy in determining the inclination of the Lageos orbit over a 6-day period is typically better than 0.5 mas (rms). There are, however, systematic variations in the

inclination residuals that can exceed 3 mas. These are mainly due to mismodeled diurnal and semidiurnal tides, which will be estimated as part of the experiment. Errors in these tides will still remain after their estimation, and at least a three-year averaging period is required to further reduce their effect on the measurement of the Lense-Thirring precession.

III. SIMULATION MODEL AND ADOPTED ERRORS

The procedure for generating the simulated data for the definitive blind test experiments involved adding the capability for generating random errors to the data simulation program and setting up a procedure for allowing the data to be generated in a controlled or blind mode. The following sections describe the details of the simulation procedure.

Measurement Model and Tracking Scenario

The measurement model for the simulation consisted of laser range data taken from eight SLR tracking stations with corrections for atmospheric delay, station motion due to plate tectonics and tides, the satellite center-of-mass offset, and the relativistic light time correction. Table 1 summarizes the tracking scenario. Normal point laser range data were created at 3-minute intervals during a three-year period when either satellite was visible at any of the stations during their scheduled tracking shift. Since Lageos and Lageos-3 would be in competition with other satellites for tracking, a network of only eight stations was adopted to provide a conservative amount of tracking data for the simulation. These stations, illustrated in Figure 3, were specified as a subset of the current laser tracking network in Figure 1, with most of the stations located in the northern hemisphere. Thus, if the lack of a uniformly distributed tracking station network were to cause a problem, this choice of stations should reveal it.

There was an attempt made to simulate the effect of data outages due to weather or station downtime. The decimation of the data by randomly eliminating 75% of the passes for each satellite,

combined with the limited tracking schedules adopted, created gaps in the tracking that should represent the data outages due to these effects. For example, Figure 4 contains a histogram of a portion of the simulated data for HOLLAS, the SLR station at Mt. Haleakala, Hawaii, which was on a 5-days-per-week tracking schedule in the simulation. It is apparent that the data success is very conservative, with many 6-day intervals containing only one, two or even no passes from this station.

No special assumptions were made concerning extended or optimized tracking schedules. Each station was assumed to track for a single eight-hour shift that was fixed for the entire three-year mission, and four of the eight stations tracked only five days per week, as is common for many of the NASA stations. Thus the amount of tracking for each satellite varied as the node precessed with respect to the ground stations, as can be seen in the data distribution histograms shown in Figure 5. The data yield for Lageos and the simulated data for Lageos-1 show the same periodic character, while Lageos-3 shows a higher frequency variation due to its faster ground track precession rate. It is also apparent in Figure 5 that there was considerably less data generated in the simulation than the total actually obtained for Lageos from all stations during the three-year period of 1984–86. That is, the Lageos yield is approximately three times the yield for Lageos-1 and Lageos-3.

Dynamical Model

The force models were based on the models currently in use at CSR in the analysis of the Lageos satellite laser range data. The force models included the nonspherical geopotential perturbations with the coefficients defined by the NASA/GSFC gravity model GEM-T1 [*Marsh et al.*, 1988] up to degree and order 20, the Newtonian *n*-body perturbations due to the Sun, Moon, and planets with positions and masses given by the JPL planetary ephemeris DE-200 [*Newhall et al.*, 1983], solid Earth and ocean tides, solar radiation pressure (with Earth and Moon shadowing), Earth radiation pressure, an empirical along-track acceleration (or "drag"), and the relativistic perturbations. A

model for the thermal drag forces induced by asymmetric heating of the satellite by the Earth has also been introduced [*Rubincam*, 1987].

Relativity Modeling

There are a number of relativistic effects which must be included in the satellite orbit determination model if the Lense-Thirring experiment is to be valid. A recent test in which the complete formulation in the solar-system barycentric frame was compared to the simpler geocentric formulation verified that equivalent results can be obtained in either formulation [*Ries et al.*, 1988]. The geocentric formulation is generally used for near-Earth satellite orbit determination, and it is the model which will be used for the Lense-Thirring experiment.

The relativistic correction to the acceleration of an artificial Earth satellite is [*Huang et al.*, 1989]:

$$\Delta\ddot{\mathbf{r}} = \frac{GM_E}{c^2 r^3}\left[[\,(2\beta+2\gamma)\frac{GM_E}{r} - \gamma(\dot{\mathbf{r}}\cdot\dot{\mathbf{r}})\,]\,\mathbf{r} + (2+2\gamma)(\mathbf{r}\cdot\dot{\mathbf{r}})\,\dot{\mathbf{r}}\right]$$
$$+ 2(\Omega\times\dot{\mathbf{r}})$$
$$+ L(1+\gamma)\frac{GM_E}{c^2 r^3}\left\{\frac{3}{r^2}\left[\mathbf{r}\times\dot{\mathbf{r}}\right]\left[\mathbf{r}\cdot\mathbf{J}\right] + \left[\dot{\mathbf{r}}\times\mathbf{J}\right]\right\},$$

where

$$\Omega \approx (\frac{1}{2}+\gamma)(\dot{\mathbf{R}}_{ES})\times\left[\frac{-GM_S\,\mathbf{R}_{ES}}{c^2 R_{ES}^3}\right],$$

and $\mathbf{J}$ is the Earth's angular momentum per unit mass ($\mathbf{J} = 9.8\times10^8$ m^2/sec). The vector $\mathbf{r}$ is the geocentric satellite position, and $\mathbf{R}_{ES}$ is the position of the Earth with respect to the Sun. GM_E and GM_S are the gravitational coefficients for the Earth and Sun, respectively. The parameter L is the Lense-Thirring parameter added for the purpose of the least-squares estimation and consider-covariance analysis. The form of the acceleration is from *Weinberg* [1972], although *Will* [1981] has

a different, but equivalent, form. It can be seen that the estimate of L is dependent on the knowledge of the relativity parameter γ. However, the general relativity value of 1 for γ is currently considered to have been verified to better than 1% [*Shapiro et al.*, 1976], and thus it introduces no significant uncertainty in the estimate of L. The estimate of L is also dependent on the knowledge of the geodesic (or De Sitter) precession [*De Sitter*, 1916], represented by Ω, which amounts to about 17.6 mas/yr in the Lageos orbit node [*Ciufolini*, 1986]. This is not considered to be a limiting factor, since the general relativity prediction of geodesic precession has been verified to at least the 2% level [*Shapiro et al.*, 1988], which is about 1% of the Lense-Thirring precession. Some analysis still remains in the area of the relativistic effect of the oblateness of the Earth [*Soffel et al.*, 1988]. Preliminary results indicate that this effect may be as much as 1–2% of the Lense-Thirring precession, but it is expected that this can be modeled to sufficient accuracy to eliminate it as a significant source of error.

Measurement Model Errors

A number of different measurement errors were included in the simulated laser range data, and these are summarized in Table 2. The observational errors were composed of 1 cm random noise and several kinds of stochastically varying biases. While these errors are small for the higher quality ranging stations and are not considered to have any direct effect on the Lense-Thirring measurement, there is an indirect effect caused by data that contains errors other than simply random noise. Like many of the minor error sources, these systematic observation errors subtly affect the Lense-Thirring measurement by introducing spurious signals in the residuals that impede the recovery of all parameters, thereby affecting the Lense-Thirring measurement indirectly. The remaining measurement errors were of a kinematic nature, reflecting errors in the knowledge of the location of the tracking stations with respect to the Earth and the orientation of the Earth with respect to inertial space. Some of these parameters also affect the dynamical model, but their contributions are

generally felt much more directly in the measurement model.

Observational Errors

The observational errors can be broadly divided into three types:

1. Biases (improperly calibrated system delays, erroneous survey of the calibration target, and errors in the station software are examples of possible sources),
2. Time tag biases (local clock problems, incorrect application of time transfer, and station software errors are examples), and
3. Troposphere correction biases (biases in the meteorological data, biases in the tropospheric refraction correction model, and variations in the pressure, temperature and water vapor as the line-of-sight changes over a pass which cannot be accommodated in a model based on atmospheric information at the ground station are some possible error sources).

It is possible to evaluate the size of the range biases in laser tracking through collocation tests in which two or more laser stations are located close to each other as they attempt to range to a common satellite. The Matera collocation report [*NASA/GSFC*, 1988], for example, indicates that the biases were less than 2 cm even for the high noise Matera fixed site and about 0.5–1.0 cm for the higher precision MTLRS units. For this analysis, a stochastic model for the biases was adopted with an rms of 2 cm and a correlation time of approximately 10 to 20 days. To verify that the amplitude and correlation time were realistic, the biases generated for the simulated data where averaged into monthly bins and compared to monthly estimates of the biases in the real Lageos data from several tracking stations. In Figure 6, the biases from the Royal Greenwich Observatory (RGO) and MOBLAS-7 are compared to the simulated biases for these sites. It can be seen that the simulated errors are at least as large as, and have variations similar to, the real biases. However, the real biases are estimated from the post-fit residuals from the Lageos long-arc. They therefore contain not only the actual range biases, but also the effect of other error sources, including residual orbit error and

troposphere errors. The actual range biases are likely to be smaller than the plots indicate, and the collocation comparisons appear to confirm this. Thus, the simulation approach used here leads to a degree of conservatism, since the simulated range biases are larger than those expected in the real tracking data, and the simulated errors are further augmented by separately modeled errors in the troposphere correction.

The bias in the troposphere refraction correction was included using a time dependent first-order process with a standard deviation of 0.2%. The standard deviation value is considered to be the average precision of the *Marini and Murray* [1973] refraction correction model for laser range data above 10 degrees elevation. The time biases were generated with a standard deviation of 2 microseconds, although the stations attempt to keep the precision of the time tags to the microsecond level. The timing errors generated by this procedure exhibited the same level of agreement with the time bias estimates from the Lageos residuals as was shown for the range biases. The correlation time for the time tag errors was varied between 10 and 20 days, but the troposphere biases were generated with a correlation time varying between 1 and 2 days, based on the assumption that the troposphere errors were likely to vary from day to day.

Nutation, Precession, Earth Orientation

Assuming that nutation, precession and Earth orientation will be determined by very long baseline interferometry (VLBI), uncertainties in the orientation of the Earth with respect to inertial space were introduced in several ways in order to obtain as realistic a spectrum of errors as possible. The 5-day values of x_p, y_p and UT1 were corrupted with 1 mas random noise, while the nutation corrections proposed by *Herring* [1986, 1988] were corrupted by 1.0 mas random noise in 5-day intervals, plus 0.1 mas random errors in the amplitude of the long period components and 0.05 mas random errors in the short period components. In addition, a 0.1 mas/yr random error was included in the precession in right ascension, and the mean obliquity was also perturbed by 0.1 mas. The

level of errors assumed are a conservative representation of the operational accuracies of the VLBI Earth rotation solutions [*Herring*, 1986].

Station Coordinates and Plate Motion

In addition to the 5 cm random errors in each cartesian component, several other types of uncertainties in the station locations were introduced. The plate velocities for each station were perturbed by 1 cm/yr random errors in all three cartesian components, these errors being conservatively based on *Minster and Jordan* [1978, 1987] and *Watkins et al.* [1988]. Even if stations were on the same plate, they were still assigned different velocity errors, since this could represent deformation within the plate or perhaps some local phenomenon. The velocity errors were not constrained to the horizontal plane in order to include the effect of possible subsidence or uplifting in the area of the tracking station. The plate velocity errors also had the effect of simulating some long-period polar motion error, since the net rotation of the velocity errors was non-zero. The geometric tide corrections for each station were perturbed by 5%, both in the h_2 and l_2 components. These errors are generally larger than the uncertainties given in *Herring* [1986], but they were used to include errors such as mismodeled ocean loading and other periodic station perturbations.

Dynamical Model Errors

The preliminary analyses indicate that the dynamical model errors are the most crucial factor in the measurement of the Lense-Thirring precession. In order to avoid the optimism of the initial simulations, errors were included in this analysis in every aspect of the dynamical model. Only the indirect planetary perturbations were not corrupted, since they are not expected to have any significant error for Lageos, as long as all of the important planets are included in the modeling. The dynamical model errors are summarized in Table 3 and are described in more detail in the following sections.

Geopotential

The spherical part of the gravity field of the Earth, as well as the overall scale of the geocentric frame, is determined by the Earth's gravitational coefficient, GM. The accuracy of the latest determination of GM is estimated to be about 0.001 km^3/s^2 [*Ries et al.*, 1989], but errors several times this value were included in some cases. This generally had no effect on the Lense-Thirring parameter recovery, since GM was always estimated, but it did require that GM be tuned during the preliminary orbit fits when the error was too large.

The nonspherical portion of the gravity field of the Earth is usually represented by a spherical harmonic expansion, with the zonal harmonics representing the longitude independent portion [*Kaula*, 1966]. The errors in the model for the constant part of the gravity field were generated based on the covariance of the NASA/GSFC geopotential solution, GEM-T1 [*Marsh et al.*, 1988]. A list of the GEM-T1 variances and covariances for the even zonals is given in Table 2 of Appendix A-2. Several different realizations were generated so that the six blind tests did not all have the same gravity model error. Because of the insensitivity of Lageos to the high degree and order coefficients, only the coefficients up to degree and order 20 were included.

Postglacial rebound, which is primarily attributed to the viscous relaxation in the mantle, has been observed through the changes of the Earth's zonal harmonics using the geodetic satellites, Starlette and Lageos. The secular variations in the first two zonal harmonics, $\dot{J}_2$ and $\dot{J}_3$ were given errors in the range of +5 to −35 ($\times 10^{-12}$ yr^{-1}). These errors are larger than the error estimates in *Rubincam* [1984], *Yoder et al.* [1983] and *Cheng et al.* [1989], but they were chosen conservatively in order to account for errors in the secular rates of the zonal harmonics above degree 3 as well as any long-period variations which would appear secular over the time span of a three-year mission.

In addition to the secular variations and the periodic variations caused by tides (described below), there are also seasonal changes which are the result of a number of mechanisms, primarily

the redistribution of air and water mass [*Gutierrez and Wilson*, 1987; *Chao*, 1988]. The lumped effect of the variations in the even and odd zonal harmonics have been determined using Lageos and Starlette, and the year-by-year variations are a significant fraction of the average annual and semiannual effects [*Tapley et al.*, 1988a; *Cheng et al.*, 1989]. Figures 7a and 7b plot the observed variations in the Lageos and Starlette orbit nodes, respectively. The annual variation is clear in both plots, but it can be seen that there is a significant difference in the annual variation from year to year.

In order to simulate the observed errors, a second-order autoregressive process was used which was capable of generating quasi-periodic variations when properly initialized [*Box and Jenkins*, 1970]. Some examples of the realizations for the seasonal variation in J_2 are plotted in Figure 8. Seasonal variations were generated for 10 low-degree geopotential coefficients (C_{20}, C_{21}, S_{21}, C_{22}, S_{22}, C_{30}, C_{31}, S_{31}, C_{32}, S_{32}). The Lageos node residuals shown in Figure 7a were used to initialize the time series for the annual variations in the even degree terms, while the eccentricity residuals (not shown), which contain annual and semiannual variations, were used to generate the perturbations to the odd degree terms. The inclusion of these seasonal variations provided model errors that could not be accommodated perfectly by any of the adjusted parameters.

Tides

The gravitational effect of the Sun and Moon deform the Earth and its oceans, causing periodic variations in the gravitational attraction of the Earth on satellites in orbit. The conventional form for expressing this effect is in terms of spherical harmonic coefficients, identical to the constant part of the Earth's gravity field except that the coefficients of the tide model have temporal variations which are functions of the motion of the Sun and Moon [*Eanes et al.*, 1983].

The major part of the solid Earth tide effect is modeled with a frequency independent Love number $k_2 = 0.30$ (ratio of the response of the second degree component of the Earth's gravitational potential to the applied potential due to the Sun and Moon) and a phase lag of 0.0 degrees. This

Love number is used for all frequencies of the Earth's response, which varies from very long period (18.6 years) to semidiurnal. The tidal potential is evaluated in the time domain from ephemerides of the Moon and Sun, such as the JPL DE-200 planetary ephemeris [*Newhall et al.*, 1983]. The remainder of the solid Earth's response is modeled as frequency dependent corrections to the frequency independent part by using the model developed by *Wahr* [1981] for the long period, diurnal and semidiurnal tides. Ocean tides are modeled in UTOPIA through a set of constant spherical harmonic coefficients that originate from 11 lines computed by *Schwiderski* [1980] in terms of a discrete set of frequencies with amplitude and angular argument given by *Cartwright and Tayler* [1971]. The angular arguments are computed from linear combinations of the mean elements of the Sun and Moon. Interaction effects are included explicitly by adding additional tidal lines at frequencies including the mean orbital rates of both solar and lunar elements. The nominal values of the tide coefficients used in this analysis were derived from the NASA/GSFC GEM-T1 tide model [*Christodoulidis et al.*, 1988; *Marsh et al.*, 1988].

The value of k_2 is fairly well determined, and only a 3% error was applied. Since k_2 was always estimated and was recovered accurately, this was not a significant source of error. In the initial simulations, errors in the frequency dependent tides were assumed to be 10% of their nominal value. However, examination of the the error estimates in *Christodoulidis et al.* [1988] indicated that this assumption was optimistic, and a more conservative error model was adopted for the final simulation. A 20% error, with a 2 mm maximum, was assumed for the semidiurnal tide components. The diurnal and long period tide components appeared to be less accurately determined, and 30% and 40% errors, along with 6 mm and 15 mm maximums, were assumed for the diurnal and long period tide components, respectively. The maximum error ceiling was applied in case a 3-σ realization happened to occur for one of the larger tides, but this turned out to be a rare occurrence.

Solar Radiation Pressure

The acceleration of the Lageos satellite due to the photon pressure from the Sun is a fairly complex function in spite of the simplicity of the shape of Lageos. The solar "constant," for example, is estimated to vary by about 0.1% [*Willson and Hudson*, 1988], but the lack of intercalibration of the pyroheliometers causes a disparity in the various measurements of the solar irradiance of up to 0.3% [*Willson*, 1978; *Mecherikunnel et al.*, 1988]. In addition, the *a priori* knowledge of the overall reflectivity of the satellite is limited, but, fortunately, the solar radiation pressure has a very distinct signature which separates well from other forces, allowing the accurate estimation of the reflectivity parameter (actually a scale parameter for the entire solar radiation pressure force). However, there is some uncertainty concerning the exact shape of the Earth's shadow, since the atmosphere attenuates some of the light near the edge of the shadow (either due to clouds or simply refraction) [*Haley*, 1973]. There is also concern that the numerical integration procedure may generate significant orbit error because of the use of step sizes which greatly exceed the time spent in the penumbra portion of the shadow. When this occurs, the integrator is integrating a different function than the correct one. This error is expected to average out to some degree, and the estimation of arc parameters (initial conditions, empirical drag, etc.) also absorbs some of the error.

In order to include the effect of these uncertainties, random errors were applied to the reflectivities of both satellites and the radius of the Earth used to calculate the shadow boundary, and a different stepsize and order were implemented in the integrator so that the shadow crossings did not occur at exactly the same times for the data simulation and the data analysis.

Earth Radiation Pressure

The Earth constitutes the next largest source of radiant energy for artificial satellites. The model in UTOPIA for the radiation pressure in the optical (shortwave) and infrared (longwave) regions is

based on the model by *McCarthy and Martin* [1977], in which the portion of the Earth's surface visible to the satellite is divided into discrete segments, and the radiation from each segment is calculated and vectorially summed to obtain the total force on the satellite [*Knocke and Ries*, 1987; *Knocke*, 1989]. The model for the Earth's albedo and emissivity is composed of a zonal-only spherical harmonic representation, with the coefficients based on the analysis of *Stephens et al.* [1981]. The adoption of such a model is based on two arguments, the first being that variations in the Earth radiation parameters show a dominant latitudinal dependency with a somewhat weaker longitudinal dependency [*Lochry*, 1966]. Also, in the absence of resonance, it is likely that the Earth's rotation will tend to average out any long period orbital effects from the longitudinal variations in albedo and emissivity. A similar argument applies to concerns about local areas that are significantly different from the average. Spots that are particularly cold, for example, like the tops of some high clouds, would occupy only a small fraction of the area viewed by Lageos at its high altitude. Furthermore, such spots would not be long-lived, and are not likely to be resonant with Lageos, so their effects are subsumed as a contribution to the overall average effect.

The effect of the Earth's radiation pressure on the Lageos orbit node predicted by UTOPIA is compared to *Rubincam and Weiss* [1985] and *Sehnal* [1981] in Table 4a [from *Knocke*, 1989]. The UTOPIA node rate prediction was obtained numerically by comparing a one-year trajectory which included the component of the Earth radiation pressure being investigated with a trajectory whose force model excluded the particular component. It was found that the node rate induced by the shortwave (optical) component of the Earth radiation pressure varied from year to year. The cause is likely to be due to a dependence on the orbital eccentricity and the location of the argument of perigee. As can be seen in Table 4a, the average of the optical component from two different years appears to be in good agreement with *Rubincam and Weiss* [1985], whose analysis ignored the eccentricity. There is considerable disagreement with *Sehnal* [1981]. It appears that the formula

derived by Sehnal has been incorrectly evaluated for Lageos, with the result that it is too large by more than an order of magnitude. The value used by Sehnal for the area-to-mass ratio of Lageos is not specified, and an effort has been made to contact the author concerning the possible error, but, at this time, nothing has been received.

Some experiments were performed in *Knocke* [1989] in which the zonal model was expanded to include longitudinal variations, but there was little effect on the Lageos orbit, since only the zonal components appeared to contribute significantly to the long period orbital evolution. Additional complexity in the albedo model was added when diurnal variations and the effects of anisotropic reflection were included. The diurnal variations are the changes in the Earth's reflectivity which are dependent on the Sun's zenith angle; for example, there might generally be more clouds in the morning and evening than at noon. The anisotropic effects are due to the fact that many of the Earth's surfaces are not necessarily perfectly diffusely reflecting surfaces. *Rubincam et al.* [1987], for example, made use of satellite radiometer measurements of the ocean to study the effect of a hypothetical severe hemispherical asymmetry in the Earth's directional reflectance in an attempt to explain some of the "drag" observed on Lageos. *Knocke* [1989] used Nimbus-7 radiance data to develop an anisotropic reflection function for 10 latitude bands, and these functions were combined with the diurnal variation model to create an advanced Earth radiation pressure model.

When the effects of the advanced and diffuse models on the Lageos orbit were compared, it was found that the advanced model, with its longitudinal, anisotropic and daily variations, predicted long period orbit perturbations that were very similar to those predicted by the nominal, purely diffuse model. However, the effect of Earth radiation pressure on the node as predicted by the advanced model was less than the diffuse model, implying that the results of the simulation may actually represent an upper bound on the effect of Earth radiation pressure model errors.

Taking the diffuse model as a conservative error model, the analysis of the effect of Earth radiation pressure on the nodes of Lageos-1 and Lageos-3 is shown in Table 4b. It can be seen that the effect is about 10% of the the Lense-Thirring precession on each satellite individually, but due to the supplementary inclinations, the result on the Lense-Thirring measurement would be only a 1% error, assuming identical satellite masses, areas and reflectivities.

The Lageos-3 satellite will be constructed to be nearly identical to the Lageos satellite in size and mass, but there will likely be some difference in the surface properties due to a lack of documentation on the surface treatments for the Lageos satellite. The overall reflectivity of Lageos, the parameter referred to simply as the solar reflectivity, is estimated from the solar radiation pressure model to be about 0.13. This quantity represents a "lumped" effect over the whole satellite and is not the actual surface reflectivity.[1] That is, of the total incident radiation from the Sun, much of it is reflected in equal and opposite amounts, leaving only a net 13% additional momentum transfer. The total force on the satellite is then 1.13 times the incident radiation pressure, the 1.00 coming from the incident momentum and the 0.13 coming from the reaction to the reflected part.

The Starlette satellite is an independently built satellite, but the current CSR estimate of its reflectivity is about 0.12. Thus, letting the simulated surface properties of Lageos-3 be as different from Lageos as is Starlette amounts to (1.13 – 1.12)/1.12, or about a 1% imbalance. This would cause an additional 0.1% error in the Lense-Thirring measurement. Clearly, the difference in the surface properties of Lageos-1 and Lageos-3 can be much larger without seriously affecting the cancellation, and this argument applies to both the optical and infrared reflectivities of the two

1 It is instructive to note that a perfectly specularly reflecting sphere, whose surface reflectivity is 1, has an overall reflectivity of 0, since the reflected energy is reradiated isotropically with no net momentum transfer beyond the incident amount [*Lochry*, 1966]. In the extreme opposite case, a perfectly reflecting flat plate normal to the Sun would reflect 100% of the incident radiation back at the Sun, resulting in an overall reflectivity coefficient of 1. Thus, a satellite's reflectivity coefficient will always be in the range of 0 to 1.

satellites. There is very little information concerning the reflectivity of Lageos in the infrared, but it can be seen that it is unlikely that the surfaces will be so different as to seriously degrade the cancellation.

One caveat should be noted. The simulation assumed that Lageos-3 had the same argument of perigee as Lageos-1 at the start of the mission. It has been noted that the actual node rate due to the optical component at any given time will be dependent on the location of the perigee, and the level of cancellation shown in Table 4b may differ for other choices of the initial perigee for Lageos-3. However, the Lageos and Lageos-3 perigees move through more than a full revolution during the three-year period of the mission, and the three-year averages for orbits with non-matched initial perigee should cancel as well as the one year averages in Table 4b.

The analysis above indicates that completely ignoring the modeling of the Earth radiation pressure would have very little effect on the measurement of the Lense-Thirring precession. For completeness, however, random errors of 0.03 were applied to all of the coefficients of the Earth albedo and emissivity model. In the case of the J_0 coefficient of the albedo or emissivity, for example, an error of 0.03 is equivalent to 3% of total Earth radiation pressure force acting on the satellite. In addition, random errors of 0.01 (the same level of difference between Lageos and Starlette) were applied to the individual reflectivities for the optical and infrared components of each satellite.

Thermal Forces and Atmospheric Drag

Thermal forces on the Lageos satellite have been identified to be a significant source of error for the Lense-Thirring measurement. Since this force has only recently been considered and the investigations are still continuing, a more comprehensive discussion of the force and its error model is appropriate.

After subtracting most of the known forces acting on the Lageos satellite, there still remains a significant along-track acceleration which is reducing the semimajor axis by approximately 1 mm per day. The mean of the observed acceleration over the entire arc is about −3.5 picometer/s^2 (pm/s^2), with fluctuations that are sometimes as large as the mean. The largest variations (or spikes) always occur when the Lageos satellite is experiencing eclipsing of the Sun by the Earth, although every eclipsing interval does not necessarily generate a spike. Thus, both the mean and the variations require an explanation.

A thermal drag model, a variant on the Yarkovsky effect [*Burns et al.*, 1978], has been proposed by *Rubincam* [1987] which is able to account for much of the observed average along-track acceleration. The heat from the Earth is absorbed by the laser retroreflectors, and because Lageos is spinning, the heat distribution is uniform longitudinally, but not latitudinally. This creates a temperature imbalance between the northern and southern hemispheres of the satellite, generating a thrust along the spin axis as the heat is re-emitted (Figure 9). If the heat was re-emitted immediately, the thrust would have no net effect averaged over one orbital revolution of the Lageos satellite. Due to the combination of the geometry of the reflector mounting and the materials used, there is enough thermal inertia that some of the heat is not emitted immediately, but rather, is delayed until the satellite has moved a significant distance along its orbit. This delay causes the thermal thrust to have a non-zero average in the along-track direction if the spin axis of the satellite is oriented in or close to the orbital plane (see *Rubincam* [1987] for a fuller explanation). The improved model in *Rubincam* [1988] accounts for the heat transport more precisely, as evidenced by the extremely good agreement with the engineering data.

The model for the "Earth Yarkovsky" effect,[2] the thermal lag-induced acceleration due to Earth heating, is represented in this investigation as

$$\ddot{\mathbf{r}} = -2\,\alpha \sin\delta \cos\left[u - \delta\right] \mathbf{s}$$

where u is the argument of latitude of the satellite, and the vector s is the spin axis direction, which is assumed for Lageos to be in the same direction as the spin axis at the moment of the final orbit injection [*Rubincam*, 1987]. The nominal value of the magnitude of the thermal acceleration, $2\alpha\sin\delta$, is approximately 6.3 pm/s^2 and the current estimate for the thermal delay angle, δ, is 55° [*Rubincam*, 1988]. The model accounts for about 70% of the observed drag, and the remainder can be accounted for by of a combination of neutral atmosphere and charged particle drag [*Rubincam*, 1980; *Rubincam*, 1982; *Afonso et al.*, 1985]. The thermal drag model also predicts periodic variations about the mean with periods of once and twice per node revolution of the Lageos orbit, which is 1050 days.

In order to validate the Earth Yarkovsky model, the effect of thermal drag due to Earth heating was included in a simulated orbit spanning the first 12 years of the real Lageos orbit. The trajectory generated by a force model which included the thermal drag was then used as data in an orbit determination experiment where the thermal drag was excluded, but 15-day empirical along-track accelerations (or drag) where estimated instead. By this procedure, the effect of the thermal drag model on the recovered values of the drag coefficients could be studied, and the effect on other orbit elements could also be examined. The result of using the nominal model described above is

2 The classical Yarkovsky effect, discovered by an Eastern European scientist around 1900, is an acceleration due to a "diurnal" asymmetry in the heating of a body, such as a dust particle in the interplanetary medium. If the body is spinning much faster than its thermal response however, the effect of the "seasonal" asymmetry, due to the hemisphere of the body which is tilted toward the Earth or Sun experiencing greater heating, will be much larger than the effect of the "diurnal" imbalance. Thus, labeling the thermal thrusting effect on Lageos as the Yarkovsky effect is appropriate, since the current thermal forces will develop into the classical Yarkovsky force as Lageos despins.

compared to the observed "drag" in Figure 10, where an additional acceleration of 1 pm/s^2 has been included to account for atmospheric drag. The peculiar variation in the recovered drag is the superposition of a 1050 and 525 day period with amplitudes and phases matching those predicted by *Rubincam* [1987]. From Figure 10, it can be concluded that it is unlikely that thermal drag could account for 100% of the average drag since the amplitude of the 1050 day periodic variation would also increase proportionally, and the agreement with the observed variations would be degraded.

The validity of the Earth Yarkovsky model is supported by examining the effect of thermal drag on the orbital inclination of Lageos. As first reported [*CSR*, 1989], the Earth Yarkovsky effect also leads to a slope in the inclination residual. The slope in the inclination is predicted to be approximately 0.9 mas/year [*Farinella et al.*, 1989]. Figure 11 shows the actual Lageos inclination residuals from Lageos long-arc 8808 [*Tapley et al.*, 1988a] after all other known forces have been modeled and most of the periodic phenomena have been removed. The poorer quality of the early laser data is evident in this figure. The observed inclination slope for Lageos is 1.4 mas/yr, with an uncertainty of about 0.2 mas/yr due to the large variations still remaining. The slope in the Lageos inclination residuals has been a concern for some time, since there seemed to be no reasonable force which could generate an inclination change of this magnitude. It is most convincing that a single model is able to explain much of the average drag, the observed drag variation at the 1050 day period and most of the residual inclination slope. Errors in the modeling of other nongravitational forces are likely to account for the remainder of the inclination slope.

Unfortunately, Earth heating does not account for the large variations that occur during the intervals where Lageos is experiencing shadowing (eclipsing of the Sun by the Earth). One possible mechanism for the large variations during eclipse seasons is the cooling of the satellite during shadowing. Since the spin axis orientation is essentially fixed with respect to the Sun over an orbit, the hemisphere of the Lageos satellite which is experiencing summer (tilted towards the sun) will be

warmer than the opposite hemisphere at every point in the orbit. This temperature difference will be essentially constant except for the additional influence of the Earth heating. Ignoring the Earth's heat (which is accounted for in the Earth Yarkovsky model) and the effect of shadowing for the moment, it can be seen that, because the force generated by the solar heating will be uniform over the orbit, there is no net effect on a circular orbit (except an infinitesimal shift in the orbit center). For a non-circular orbit, there are variations in the orbit inclination and node to first order in the eccentricity, but there are negligible for Lageos because of the small orbit eccentricity [*Anselmo et al.*, 1983; *Farinella et al.*, 1989]. Thus, between eclipse seasons, the Earth Yarkovsky effect plus atmospheric drag should adequately account for the observed drag.

During shadowing, however, the "solar Yarkovsky" effect cannot average out, and there is a net along-track acceleration. Only during those eclipse seasons where the hemispheres were experiencing equal heating ("spring" or "fall"), would there be no solar Yarkovsky effect. *Slabinski* [1988] indicates that this force will result in a positive acceleration most of the time. This is suggested also by Figure 12, where the model for the Earth Yarkovsky effect and atmospheric drag have been removed from the observed drag in the Lageos long-arc (the difference of the two curves in Figure 10). The largest variations tend to be positive, and they occur more often, but there are negative accelerations produced as well.

The magnitude of the solar Yarkovsky acceleration (60 pm/s^2) was not based on expected temperature differences, but rather was chosen simply to give peaks with the same approximate amplitude as those seen in Figure 12. However, the modeling adopted was nearly identical to that derived by *Farinella et al.* [1989], where an estimate of the expected temperature difference was also derived. The only significant difference in that study was the use of a decay time of approximately 50 minutes for the cooling (with a possible uncertainty of a factor of 2), whereas the model in this investigation used a 30 minute decay time. Studies at CSR indicate that the effect of the model is

not particularly sensitive to the choice of the decay time constant in the region of 20 to 50 minutes. As can be seen in Figure 12, where the predicted effect of the Solar Yarkovsky model on the estimated drag is compared to the observed drag after models for the Earth Yarkovsky and atmospheric drag have been removed, the model does not accurately predict even the sign of some of the spikes, while others are predicted reasonably well. There are also occasions when a spike is predicted but not observed.

Thus the thermal force model for Lageos is not yet complete enough for actual orbit determination, although considerable progress is being made by investigators at CSR and elsewhere [*Scharroo et al.*, 1989; *Farinella et al.*, 1989]. The model is, however, much more realistic than any model which considers the force as drag only. The effects of Earth and solar Yarkovsky on the Lageos orbit are plotted for a six-year time span in Figures 13 and 14. It is apparent that the effects on the orbit elements are in some cases quite significant and provide a strong test of the ability to detect the Lense-Thirring effect in the proposed experiment.

A number of choices were possible for the orientation of the Lageos-3 spin axis, but the most conservative approach was considered to be an orientation similar to, but not exactly the same as, Lageos-1. In this orientation, the thermal drag force due to Earth heating on Lageos-3 was nearly at its maximum, but there would be periodic variations introduced as well. Choosing an orientation that was nearly polar would cause little increase in the magnitude of the force while eliminating the periodic variations, and choosing an orientation more nearly parallel to the Earth's equator would decrease the magnitude of the thermal force. This choice could also be justified by the probability that Lageos-3 would be inserted into orbit in a manner similar to Lageos, and thus the Lageos-3 spin axis orientation is likely to be similar to Lageos. The magnitudes of the Earth Yarkovsky acceleration for Lageos-1 and Lageos-3 were varied between 4 and 9 pm/s^2 in the various blind cases. Similarly, the magnitude of the solar Yarkovsky effect was varied between 15 and 75 pm/s^2.

The density of the atmosphere at Lageos altitude is extremely small, yet it is estimated that the combination of neutral particle and charged particle drag could cause an acceleration with a magnitude on the order of one pm/s^2. Early studies attempted to explain the entire observed drag on Lageos in terms of neutral and charged particle drag [*Rubincam*, 1980, *Afonso et al.*, 1985]. The required particle density and electric charge on the Lageos satellite generally appeared to be near the upper limits of what was thought to be possible in order to explain the entire amount of observed drag. Since about 70% of the observed drag is explained with the thermal thrust mechanism, the density and charge required to explain the remaining drag are considered to be reasonable [*Rubincam*, 1988].

A test was performed in which current atmospheric drag models were extrapolated to the Lageos altitude, but since they do not consider the charged particle drag effects, it is not surprising that the predicted drag acceleration was not large enough to account for the remaining drag. There was also very little variability observed in the predicted drag. Thus, an empirical model for the drag was adopted in which the drag acceleration was generated as a stochastic process with a 1-day correlation time, an rms of 1 pm/s^2 rms about a mean that was varied between -1 and -1.5 pm/s^2. A sample realization of this process is illustrated in Figure 15.

The effect of combining the thermal thrusts and stochastic drag on the estimated values for the 15-day empirical drag coefficients can be seen in Figure 16. The daily samples of the drag are not entirely smoothed by the 15-day averaging. By comparing Figure 16 to Figure 10, it can be seen that the resulting variations in the drag estimates from the simulated data are quite similar to those observed in Lageos. The mean is about -3.5 pm/s^2, and the long period variation is the 1050-day periodicity caused by the Earth Yarkovsky effect. The rms of the scatter about the mean is about 1 pm/s^2 for both the real and the simulated drag coefficient estimates.

IV. SIMULATION PROCEDURE AND RESULTS

Simulation Procedure

The numerical simulation was designed to emulate as closely as possible the procedure to be used in the proposed experiment. Thus, simulated laser range data were generated and sampled in a manner which attempted to duplicate the distribution of the actual laser tracking of Lageos. A three year orbit was adjusted in a preliminary solution to fit the simulated SLR data for each satellite for each of the six cases. In the preliminary solutions, a small set of satellite dependent parameters was estimated to achieve reasonably good fits to the simulated data.

After the preliminary orbits had been obtained, information equations were written which contained the partial derivatives of all the parameters which were to be estimated or considered. The information equations were combined in CSR's Large Linear System Solver (LLISS) into a form suitable for obtaining solutions and performing consider-covariance analysis with the Consider Analysis Program (CONAN). The compaction of three years of data from each satellite into a single information matrix allowed the efficient execution of a large number of experimental solutions.

Data Generation

In the initial definition of the simulated experiment, there was concern expressed by the Science Advisory Group that, if the analysts who would be processing the data possessed *a priori* knowledge of the true value for L and the other perturbed parameters, they would tend to be biased in their choice of the parameters to be estimated. This concern was addressed by adopting a blind simulation procedure in which the CSR analysts would not know the true value for any of the approximately 1550 individual error sources, including the true value of L. The capability to achieve the blind simulation of the SLR data was accomplished after considerable modifications to the University of Texas Orbit Processor Program (UTOPIA) to allow most of the errors, in both the model parameters

and in the time varying stochastic processes, to be generated automatically. The few remaining parameters could then be easily perturbed by hand by the two SAG members, John Armstrong and Bob King, who assumed responsibility for preparing the simulated data set. The automatic capability for generating most of the random errors was important since it is would be difficult to fully understand the computer operating system, its editing program and the intricacies of the inputs to a complex orbit determination program within the few days available to the two SAG members. It was critical that the simulated data be generated in a manner consistent with the software used in the estimation process so that the resulting analysis did not fail for the wrong reason. It was also necessary that the ability to specify the seeds for the various random errors be included, so that any of the computer runs could be duplicated exactly in case anomalies were noted later. The extensive modifications, and the thorough testing required, resulted in some delay in completing the simulation and providing the final report, but the resulting system performed well and will provide a valuable simulation tool for future studies.

Data Processing

Before the combined Lageos-1/Lageos-3 solution could be performed, it was necessary to converge preliminary orbits which attained reasonably good fits to the simulated data. The preliminary estimates of the orbits were obtained using, in an iterative fashion, a linearized least-squares estimation procedure. The highly nonlinear orbit determination and parameter estimation problem can be converted into a linear estimation problem by an expanding in a Taylor's series about some *a priori* estimate of the orbit which is defined by *a priori* values for the initial conditions and the dynamical and measurement model parameters [*Tapley*, 1973]. The accuracy of this linear estimate is dependent on the accuracy of the nominal values of the parameters. The closer the *a priori* estimate is to the true value, the more accurate the new estimate will be. Otherwise, the process must be iterated. It is particularly important that the satellite orbit be reasonably close to the

true orbit, so that the partial derivatives required for the parameter estimation are accurate.

Thus, it was most efficient to converge the individual Lageos-1 and Lageos-3 orbits separately in order to obtain good quality preliminary orbits. The parameters estimated in this orbit determination procedure were the initial state for the three-year integration, the satellite solar reflectivity, and 15-day values for the empirical along-track acceleration ("drag"). The magnitude of the Earth Yarkovsky effect was not estimated, but was empirically adjusted based on the average magnitude of the estimated drag. Since it is estimated that there is approximately 1 pm/s^2 of drag on Lageos, and one would expect a similar level of drag on Lageos-3, the magnitude of the Earth Yarkovsky effect for each satellite was modified during the preliminary orbit fits to obtain an average value of the estimated drag of approximately -1 pm/s^2. Since the simulated drag was allowed to vary as much as 50% from this value, the adjusted Earth Yarkovsky acceleration could be in error by as much as 15%. While *Rubincam* [1988] does not provide an error estimate for his model, the level of agreement with the engineering data and with the drag observed in the Lageos orbit indicates that the error in his model is unlikely to be larger than this. The only other parameters which were estimated were the gravitational coefficient, GM, and the frequency-independent solid Earth tide parameter, k_2, when the magnitude of the residuals from the preliminary orbit solutions indicated that the nominal values of these parameters contained an unacceptable level of error.

The resulting orbits generally fit the simulated range data to the 30 to 50 cm level. Experience with Lageos indicates that this level of agreement with the observations is generally adequate for reliable solutions for dynamical model parameters without the necessity of iterating. Improved results might have been obtained if the solutions had been iterated further, but the process is time-consuming, and there was insufficient time available in this investigation to pursue this possibility.

The rms of the resulting fits by station for Case 3 are summarized in Table 5. The quantity referred to as the data error rms is the contribution of the station-dependent observation errors

(range, troposphere and timing biases and white noise). The difference between the data error and the fit rms reflects the contribution of the kinematical and dynamical model errors. It is not surprising that the Lageos-3 fit is worse than Lageos-1, since the gravity model errors in the simulation were based on the GEM-T1 gravity model solution covariance [*Marsh et al.*, 1988]. That solution contained data from Lageos and thus would be expected to fit Lageos-1 data well. There were no satellites similar to Lageos-3 in the solution, hence the less accurate fit to Lageos-3.

After the preliminary orbits had been obtained, information equations could be generated for the parameters to be estimated or considered. The total set of parameters included in the estimation and consider analysis is summarized in Table 6. The parameters can be broadly divided into satellite independent parameters (parameters common to the modeling for both satellites) and satellite dependent parameters. The common parameters included the non-zonal coefficients of the geopotential up to degree and order 7, the zonal coefficients to degree 20, GM, the dynamical tide parameter k_2, the secular zonal rates, the coefficients for 34 ocean tide constituents (degrees 2 through 6 for all prograde tides in GEM-T1 plus selected additional tides). All of the albedo and emissivity parameters in the UTOPIA Earth radiation pressure model were included, which consists of zonals of degree 0, 1 and 2 plus an annual variation in the first-degree zonal. The cartesian coordinates of all eight stations were included also in the parameter set. The satellite dependent parameter set consisted of the initial satellite position and velocity, 15-day empirical drag coefficients, the solar radiation reflectivity parameter, the Earth radiation reflectivity parameters for optical and infrared wavelengths, and the Earth and solar Yarkovsky parameters.

Solution Results and Error Analysis

Many preliminary solutions were performed in order to gauge the sensitivity of the estimate of L to the set of parameters included in the estimation process. The main variation between the test solutions was the number of tidal coefficients estimated. The strategy usually employed in the

Lageos long-arc solutions is to estimate enough tide coefficients so that most of the dynamical modeling errors can be absorbed, making some of the less well-determined tides effectively "garbage cans" for the residual orbit error. However, this process must be applied with care or too much non-tidal signal will be absorbed, with the subsequent degradation in the estimate of other parameters of interest. Thus, the choice of estimated parameters requires a careful balance between too many and too few parameters. The variations in L as the set of estimated tide parameters was changed were very consistent with the estimated uncertainty in L, indicating that in the actual experiment, the results should not be too sensitive to the set of tide parameters chosen for estimation. It should be noted that there was no *a priori* information or constraint on any of the parameters in the solution.

The final set of estimated and considered parameters is summarized in Table 7. Only a few zonals and zonal rates were estimated, leaving the remainder of the geopotential field for consider error analysis using the standard deviations from the GEM-T1 solution covariance. GM and k_2 were also estimated. The station coordinates for all eight stations were estimated, although one station longitude was held fixed to avoid the singularity that occurs if the orbit and all station coordinates are estimated. The set of tides chosen for estimation consisted of all the degree 2 and 3 coefficients for the prograde tides, and the degree 4 and 5 coefficients for selected diurnal and semidiurnal tides. The uncertainties in the remaining tides were assumed to be the 2, 6 and 15 mm caps of the simulation for the semidiurnal, diurnal and long-period tides, respectively. This level of consider error, although much more conservative than the error introduced into the simulation, was employed to compensate partly for the inability to consider the effect of the stochastic geopotential variations or the retrograde tides. Both of these errors had been included in the simulation, but the nature of the stochastic geopotential variations prevents parameterization, and the partial derivatives for the retrograde tides were unavailable in the version of UTOPIA employed for the simulation.

The satellite dependent parameters estimated were the initial state, the solar reflectivity coefficient, and 15-day empirical drag coefficients. The Earth radiation pressure albedo and emissivity coefficients and the satellite optical and infrared reflectivities were all considered with an error of 0.03. The Earth Yarkovsky effect was considered at 1 pm/s^2, or about the 15% level. The solar Yarkovsky effect, which had an error of 15 to 75 pm/s^2 in the simulation, was considered at the 30 pm/s^2 level in the error analysis, equivalent to the conservative assumption that the best model that will eventually be developed for this effect will be only about 50% accurate.

The results of the six blind solutions are summarized in Table 8, where the difference between the CSR estimate and the true value of L is listed. The scatter of the simulation solutions was 8%, and the mean of the differences between the estimate and true value of L was zero. In comparison, a covariance analysis for each case, based on considering the effect of errors in the non-estimated parameters similar to those included in the simulation, indicated that the 1-σ uncertainty in the estimate of L varied between 5 and 7%. The results are displayed graphically in Figure 17, where each solution is shown with respect to the true value and the size of the 95% confidence interval as predicted by the consider-covariance analysis. The covariance analysis could not consider the effect of the stochastic error sources and would be expected to predict a smaller uncertainty; otherwise, the agreement between the simulation results and the covariance analysis is remarkably good. The combination of the six simulations, supported by consistent results from the consider error analysis, indicate that the Lense-Thirring precession should be measurable at the 8% accuracy level. That only one simulation solution out of the six deviated by as much as 15% is entirely consistent with this error assessment.

The simulation results include the effects of all modeled errors, but they do not allow one to quantify the contribution of the individual sources of error. Thus, the covariance analysis is necessary in order to identify the error sources which are the major limitations in the accuracy of the

Lense-Thirring precession measurement. The error in the gravitational model is the primary contributor to the overall error. The constant errors in the mean values of the Earth's geopotential and tide model are expected to contribute about 4 to 5%. The effect of errors in the even zonal harmonics are proportional to the size of the Lageos-3 orbit injection errors, with a conservative assessment of 3% for each 0.1° error in the inclination. The unmodeled thermal forces were found to cause a little less than a 3% uncertainty, while the contribution of the errors in the model for the Earth radiation pressure (reflected optical and reradiated infrared) was approximately 1%. The uncertainty due to the remaining parameters was generally negligible. The various stochastic errors not amenable to the consider analysis, particularly the seasonal variations in the geopotential, are conservatively estimated to contribute an additional 5%.

The quality and consistency of the dual-satellite solution can be further evaluated by comparing the true value with the estimated value for some of the more significant dynamical parameters. In Table 9, which summarizes the various solutions, it can be seen that the recovered values are in good agreement with the true values. The level of error is generally consistent with the current assessment of the errors in these parameters, although the errors are, in some cases, smaller than currently obtained. The reduced errors very likely represents the increased strength of the Lageos-1/Lageos-3 combination. It can also be seen in Table 9 that the estimates for $\dot{J}_2$ and $\dot{J}_3$ are worse for Cases 1 through 4 than for Cases 5 or 6, yet the accuracy of the Lease-Thirring parameter is not affected. This result highlights the advantage of choosing an inclination for Lageos-3 supplementary to Lageos-1. Accurate knowledge of the zonals and their variations is not required for the accurate measurement of the Lease-Thirring precession, a characteristic which is shared by no other satellite configuration.

An alternative method of assigning an uncertainty to the estimated value of the Lense-Thirring parameter is a simplified procedure referred to as a modified worst-case analysis [*Ashby et al.*,

University of Colorado, manuscript in preparation, 1988], which consists of multiplying the formal uncertainty of a parameter by the square-root of the number of observations. This approach allows one to estimate the error in a parameter if all the systematic errors had the worst possible time dependence for that particular parameter. The formal uncertainty, estimating only the satellite dependent parameters, was 0.00063. There were approximately 100,000 normal points in the three-year arc, leading to a worst-case uncertainty for L of approximately 0.2. Since it is highly pessimistic to assume that all of the errors have the worst possible time dependence, we may consider the worst-case uncertainty of 20% to reflect a 3-σ error estimate, which compares well with a 3-σ error of 24% from the simulation and 21% from the covariance analysis. This result, while not as rigorous as a full error analysis, lends additional support to the results of the simulation and consider-covariance analysis.

Post-Solution Residual Analysis

Extensive analysis was performed on the post-solution residuals of Case 3 in order to evaluate the fidelity of the adopted error models. A complete analysis of all six cases was not possible in the available time allocated for this study. Although Case 3 was selected arbitrarily, it is typical of the cases considered and any conclusions based on this sample should be applicable to the other cases as well. The residuals from Case 3 are compared to the residuals from a fit to actual Lageos laser ranges from eight high-precision stations during the interval of January 1, 1986, to January 1, 1988.

In the post-solution residual analysis, the values of all of the dynamical and kinematical parameters which had been estimated in the combined solution were included in new three-year orbit fits to the simulated data. The only parameters estimated in these fits were the initial state and the empirical drag coefficients, since experience has indicated that the estimation of these parameters in post-solution fits is essential. This is primarily due to the nonlinear convergence properties of the orbit determination problem, in which several iterations are generally required to obtain a final

estimate of the initial conditions and the along-track forces. The resulting fit for Case 3 is summarized in Table 10.

The post-solution laser range residuals can be represented in two ways. The residual analysis method usually used at CSR consists of mapping the range residuals in each 5-day interval into an estimate of the mean error for each orbital element (3- or 6-day intervals are also used). This is essentially equivalent to comparing the long-arc orbit to short-arc fits, except that the orbit element differences are computed from an analytical approximation rather than actually converging a larger number of 5-day fits. The former procedure is considerably more efficient, and tests have indicated no significant differences in the results. Analysis of the residual errors in terms of orbital elements is very useful, since it provides insight into the nature and magnitude of the modeling errors which remain in the long-arc orbit. For example, errors in even-degree ocean tide model coefficients tend to appear as errors in the inclination and node. Alternatively, the effect of odd-degree tide coefficient errors appear in the eccentricity and perigee residuals.

The orbital element residual analysis technique, although very useful, is limited to investigating variations in the residuals with periods greater than 10 days because of the 5-day averaging interval used. In order to obtain information about shorter period modeling deficiencies (up to a few cycles per orbital revolution), an alternative method is employed. In this approach, an estimate of a bias and the along-track orbit error, in terms of an apparent bias in the time of closest approach, is estimated from the range residuals for each station pass. After removing the biases and a second-order polynomial from the residuals, the remainder is nearly Gaussian noise, and the rms is a good estimate of the data precision.

In the following analyses, the 5-day orbital element residuals from the actual Lageos data are plotted and compared to the corresponding residuals from the simulated Lageos-1 and Lageos-3 data. The spectrum of the orbital element residuals and the apparent time-biases are also compared

to illustrate the fidelity of the error models used in the simulation.

Table 10 summarizes the statistics of the residuals for the real Lageos data and the simulated data for Case 3. The actual orbital element residuals are plotted for comparison in Figures 18 through 22. It can be seen in Table 10 that the overall statistics of the simulated data are similar to the actual data statistics. In particular, the quantity called postprocess noise is nearly identical, indicating comparable high frequency gravity error, measurement error and station location error in both the simulated and real data. The other quantities generally have a higher rms for the simulated data than for the real data, even though the same parameters were estimated in the actual Lageos orbit fit and the dual-satellite solution. This is not surprising, because the parameters estimated in a single satellite solution will accommodate the various errors much better than a solution which includes two satellites with different orbit parameters. Many of the effects have different signatures for the two satellites, and a model parameter cannot act as a "garbage can" for errors if its signature does not match both satellites.

This is precisely the reason why many satellites are required in the determination of an accurate gravity field model. When more satellites are involved in a solution, the estimated parameters in the gravity field model are recovered more accurately; they are less able to absorb other model errors, which generally have conflicting signatures for the different satellites. The errors will remain, instead, in the residuals, as evidenced by Table 10. Thus, while it is not possible to produce residuals from Lageos exactly analogous to the simulated Lageos-1/Lageos-3 residuals, Figures 18 through 22 indicate that a significant level of modeling error has been included in the simulation.

By the reasoning given above, the spectra of the orbital element residuals shown in Figures 23 through 26 cannot be expected to match exactly. The comparison is valuable, however, in indicating that the error spectrum of the simulated data is generally as complex as the real data, and the magnitudes of the residual errors are usually significantly larger than those seen in the real data.

Although the spectra are plotted as a function of frequency, the various peaks are labeled in terms of period (in days) for convenience.

The spectra of the orbital element residuals are useful in analyzing the long period errors, but for short period errors, it is necessary to examine the spectra of the time biases. These spectra are noisier, since each time-bias solution contains at most 50 ranges, while the 5-day orbit element solutions may contain over 500 ranges. In Figure 27, the spectra of the time-biases from the simulated residuals in the region of 6 to 60 days are compared to the spectrum of the real Lageos time-biases. Figure 28 is a similar comparison for periods less than 6 days. The peaks are labeled in terms of period (days) in Figure 27 and in terms of frequency (cycles per day) in Figure 28. It can be seen that the spectra of the time biases from the simulated data are generally as complex as the actual data, and the magnitudes are similar.

The statistics of the real and the simulated range residuals are summarized in Tables 11, 12 and 13. The overall values for the orbit fit rms, The rms after removing the bias and time-bias, and the rms after also removing a quadratic polynomial (the true data precision) are all in remarkably good agreement. Except that the statistics of the simulated data are the same for each station, it would be difficult to distinguish between the real and simulated data based on these tables. Similarly, the statistics of the pass-by-pass biases and time-biases indicate good consistency between the real and simulated data residuals.

The results of the various comparisons indicate that, taking into consideration the fact that the Lageos residuals are naturally smaller since a single-satellite solution can accommodate more error than a dual-satellite solution, the power and spectrum of the simulated residuals are quite similar to the real Lageos residuals, and the error model used in the simulation has generated realistic, but generally conservative, levels of modeling error.

V. ORBIT INJECTION REQUIREMENTS FOR LAGEOS-3

A separate study has been conducted to determine the range of errors in the orbit parameters of the Lageos-3 satellite which can be tolerated and still obtain a successful measurement of the Lense-Thirring precession [*Casotto*, 1989]. Because this issue has been identified to be particularly crucial in light of the known (or unknown) performance characteristics of some of the possible launch vehicles, it was studied in more detail than was possible in a limited set of simulations. The critical orbital elements are the semimajor axis, inclination and eccentricity. There is no dependence on the initial value of the other orbital angles (node, perigee and mean anomaly) since these angles all go through large changes over the three-year period. For example, the Lageos node will have precessed through one full revolution with respect to inertial space by the end of the three-year mission. The analysis considered all possible combinations of semimajor axis, inclination and eccentricity errors using an approach called the method of equal influences, and the full GEM-T1 covariance for the even zonals was used. The results indicate that each 0.1° error in inclination and 15 km error in semimajor axis causes an uncertainty in the measurement of the Lense-Thirring precession of about 3%. Since the other sources of error depend less on the cancellation effect of the supplementary inclinations, this would be the dominating source of error if the inclination error were to exceed 0.5°.

The range of allowable eccentricity values is so large that it is not a consideration, and the range of the allowable semimajor axis error is also not particularly restricting, so that the result of 3% per 0.1° error in inclination is conservative. For example, if there were no significant error in the eccentricity or semimajor axis of the Lageos-3 orbit, the same 0.1° error in inclination would result in an uncertainty of approximately 1.7% in the Lense-Thirring measurement. The errors in the GEM-T1 gravity model are also considered to be pessimistic with respect to the quality of the gravity models that are likely to be available in the future. The GEM-T2 gravity model, which is a significant improvement over GEM-T1, is already available [*Marsh et al.*, 1989]. There is always

the possibility, however, that the covariance matrices from the gravity model solutions are somewhat optimistic. Furthermore, because of variations in the mass distribution of the Earth, a gravity model determined during one decade may not be entirely accurate during the next. Thus, a degree of conservatism in the assumed errors in the geopotential model is retained by using the GEM-T1 predicted errors.

VII. SUMMARY AND DISCUSSION

A preliminary analysis of the measurement of the Lense-Thirring precession using two Lageos satellites in supplementary orbits indicated that the measurement should have an uncertainty of approximately 10% [*Ciufolini*, 1989]. In that study, a fairly large number of error sources were considered, but the analysis used a rather simplistic approach which compared the effect of a given force model error on the node of the satellite orbits with the size of the Lense-Thirring precession. Although the analysis is useful in a qualitative sense and can be used to identify error sources which are likely to be significant, the approach cannot be used to accurately quantify the uncertainty in the Lense-Thirring measurement, since the orbit determination problem falls in the domain of general nonlinear parameter estimation. Geometric arguments cannot include the complex nonlinear interaction that takes place between the various estimated quantities and the satellite orbit during the orbit and parameter determination process. The orbit plane is only an imaginary construct, useful for perturbation analyses, and as a consequence, the concept of "measuring the absolute inclination" of a satellite orbit is vague and ill-defined. To conclude that the "absolute inclination" of the Lageos orbit can or cannot be "measured" to a specified accuracy is to make a statement that cannot be verified in any real sense.

The estimation approach used in the CSR simulation and covariance analysis is rigorous and naturally includes all interactions between the various error sources. It is not necessary to consider the measurement as the determination of two large numbers (the magnitude of the Lageos-1 and

Lageos-3 node rates) computed separately, based on observations from an unsteady intermediate structure (the Earth), and subtracted with a precision of a part in 10^8. Parameterizing the Lense-Thirring effect and the many potential sources of error in the context of a dual-satellite, least-squares estimation problem is the only method that can rigorously and quantitatively determine the real uncertainty in the result. This method is limited only by the fidelity of the error model and completeness of the parameterization. Concerns about the accuracy of the results must be addressed in the context of deficiencies in assumptions used for the model errors. The ability of laser ranging observations of Lageos to accurately measure a dynamically defined quantity cannot be based on the vague assertion that centimeter-level ranges are not adequate. Given a realistic and complete error model, if a quantity affects the dynamic motion, it will be measurable to some accuracy level, and that accuracy level will be determined through the complex interaction of the data distribution, the measurement errors, the observation modeling errors and the force modeling errors.

For the experiment proposed here, the dominant error sources have been identified as the geopotential, ocean tides, and the thermal thrust forces due to solar heating. The whole of the non-zonal geopotential and ocean tide error is estimated to contribute no more than 5%, while the thermal thrust forces contribute approximately 3% total for both satellites. The combination of all other random and stochastic errors is conservatively estimated to contribute another 5%. Earth radiation pressure is not insignificant, but still contributes only about 1% to the error. If the inclination of the Lageos-3 orbit departs from the desired 70.2°, the results are degraded, with the total error approaching 10% for an inclination error of 0.2° for the level of geopotential error assumed for this investigation.

This error budget, summarized in Table 14, is considered to be conservative for a number of reasons. The dynamical and measurement model errors adopted were generally conservative, resulting in residuals for the simulated data which look like, but have larger magnitude, than the

actual data. The errors in the gravity models that will be available in the future are likely to be significantly smaller than those adopted in this analysis, which were based on GEM-T1. In fact, GEM-T2 and TEG-1 are models which show substantial improvement over GEM-T1 [*Marsh et al.*, 1989; *Tapley et al.*, 1988b]. The effect of stochastic and seasonal variations in the low-degree geopotential harmonics can be reduced by the estimation of annual values for these parameters. The effect of ocean tide errors can also be reduced by including additional years of tracking data in the measurement, so that the long-period variations average better. The recent progress in modeling the thermal drag forces on Lageos indicates that much of this effect may be modelable, removing a significant error source from the measurement. Furthermore, with the improved understanding of the thermal forces acting on Lageos, it should be possible to choose an optimal spin-axis orientation for Lageos-3 to minimize the thermal drag forces, and reduce or remove this area of uncertainty in the force modeling. While there is no control over the Lageos spin-axis orientation, the orientation chosen for Lageos-3 in the simulation was considered to be a worst-case. The magnitude of the thermal drag was near its maximum value, but the spin-axis was sufficiently far from a polar alignment to cause significant periodic variations as well. Insertion of Lageos-3 into orbit so that its spin-axis is in the equator would significantly reduce both the Earth and solar thermal forces.

An important concern in this analysis is whether any significant error source has been ignored. It could be argued, for example, that the errors assumed for the thermal thrusts are optimistic, since the existing model does not completely model the observed variations in Lageos drag. However, even assuming that the thermal forces were 100% larger than considered here and that the solar heating component cannot be modeled, an assumption that appears unlikely based on the existing analysis, the error estimate increases from 8% to only 10%. In order to affect the error estimate of the Lense-Thirring measurement significantly, root-sum-squaring an additional 12% to increase the error estimate to the 15% level, for example, would require forces whose effects are four times larger than

the thermal forces, yet these large effects must be indistinguishable somehow in the current Lageos residuals. While there are certainly significant systematic errors remaining in the Lageos residuals, they can generally be explained using known physical effects, such as the year-to-year fluctuations in the seasonal changes of the Earth's gravity field. These errors have been included in the analysis leading to the 8% overall error estimate. The thermal forces on the Lageos satellite represent essentially the limit of the forces that can be affecting the satellite significantly. *Ciufolini* [1989] has examined a wide variety of lesser forces and found that the maximum effects of those not already considered in this analysis were generally less than a few tenths of a percent. Since reasonable limits on the existing forces have been determined and used in this simulation, the existence of a large, unsuspected force with a new physical mechanism must be considered a very unlikely event. A similar argument applies to possible measurement errors which must be large enough, have just the right time dependence, and must be common to all stations over the three-year period. While such effects are impossible to rule out, they must be considered to be remote possibilities and should not be included in a 1-σ error estimate. It would appear that the 3-σ error estimate (or 99% confidence interval) of 24% would adequately include the effect of such unlikely errors.

VII. CONCLUSION

Given a sufficiently accurate launch vehicle and a moderate effort to track Lageos and Lageos-3 during a three-year mission, the Lense-Thirring precession of the two satellite orbit planes should be detectable with a high degree of confidence. Uncertainties in every aspect of the modeling were considered in order to have confidence that the error models adopted in the CSR simulation were complete and realistic. In addition to a pessimistic level of observational error in the simulated ranges, errors were included in nutation, precession, Earth orientation, plate motion, station locations, gravitational forces and nongravitational forces. The simulation accounted for over 1500 individual error sources. The tracking scenario was pessimistic as well, assuming only eight stations

which obtained approximately 50,000 normal points for each satellite during the three-year mission.

The results indicate that a three-year mission using laser ranging to a pair of Lageos-type satellites, in inclinations of 109.8° and 70.2°, can determine the Lense-Thirring precession to an accuracy of 8%. This estimate is based both on a comprehensive consider-covariance analysis and the results of a limited Monte-Carlo analysis in which six simulated data sets were processed without knowledge of the truth value for the Lense-Thirring parameter or any of the other error sources.

REFERENCES

Afonso, G., F. Barlier, C. Berger, F. Mignard, and J. J. Walch, Reassessment of the charge and neutral drag of Lageos and its geophysical implications, *J. Geophys. Res.*, *90*(B11), 9381, 1985.

Anselmo, L., B. Bertotti, P. Farinella, A. Millani, and A. M. Nobili, Orbital perturbations due to radiation pressure for a spacecraft of complex shape, *Celest. Mech.*, *29*, 27, 1983.

Box, G. E. P., and G. M. Jenkins, *Time Series Analysis: Forecasting and Control*, Holden-Day, San Francisco, 23–84, 1970.

Burns, J. A., P. L. Lamy, and S. Sater, Radiation forces on small particles in the solar system, *Icarus*, *40*, 1, 1979.

Cartwright, D. E., and R. J. Tayler, New computations of the tide-generating potential, *Geophys. J. R. Astron. Soc.*, *23*, 45–74, 1971.

Casotto, S., Orbit injection error analysis for the proposed Lageos-3 mission, *Tech. Mem. 89-01*, Center for Space Research, The University of Texas at Austin, Austin, Texas 78712, 1989.

Center for Space Research, The University of Texas at Austin, Semiannual Report for NASA Grant No. NAGW-1330, December 30, 1988.

Center for Space Research, The University of Texas at Austin, Annual Report for NASA Grant No. NAGW-1330, May 3, 1989.

Chao, B. F., Excitation of the Earth's polar motion due to mass variations in major hydrological reservoirs, *J. Geophys. Res.*, *93*(B11), 13811, 1988.

Cheng, M. K., R. J. Eanes, C. K. Shum, B. E. Schutz, and B. D. Tapley, Temporal variations in low degree zonal harmonics from Starlette orbit analysis, *Geophys. Res. Lett.*, *16*(5), 393, 1989.

Christodoulidis, D. C., D. E. Smith, R. G. Williamson, and S. M. Klosko, Observed tidal braking in the Earth/Moon/Sun system, *J. Geophys. Res.*, *93*(B6), 6216, 1988.

Ciufolini, I., Measurement of the Lense-Thirring drag on high-altitude, laser-ranged artificial satellites, *Phys. Rev. Let.*, *56*, 278, 1986.

Ciufolini, I., The Lageos Lense-Thirring precession and the Lageos nongravitational nodal perturbations-I, *Celest. Mech.*, *40*, 19, 1987.

Ciufolini, I., Lageos-3, in proceedings of NASA Workshop on Relativity and Gravitation Experiments in Space, Annapolis, Maryland, June 28–30, 1988.

Ciufolini, I., A comprehensive introduction to the Lageos gravitomagnetic experiment, *Int. Journal of Modern Physics A*, *4*, 3083, 1989.

De Sitter, W., On Einstein's theory of gravitation and its astronomical consequences, *Mon. Not. Roy. Astron. Soc.*, *77*, 155, 1916.

Drozyner, A., Unmodeled effects in satellite motion, part I: Theoretical description, artificial satellites, *Planetary Geodesy*, *11*(23), 1988.

Eanes, R. J., B. D. Tapley, and B. E. Schutz, Earth and ocean tide effects on Lageos and Starlette, *Proceedings of the Ninth International Symposium on Earth Tide*, J. T. Kuo, Ed., E. Schweizerbart'sche Verlagsbuchhandlung, 1983.

Farinella, P., A. M. Nobili, F. Barlier, and F. Mignard, Effects of thermal thrust on the node and inclination of Lageos, submitted to *Astron. Astrophys., Main Journal, Section 11*, 1989.

Gutierrez, R., and C. R. Wilson, Seasonal air and water mass redistribution effects on Lageos and Starlette, *Rev. Geophys. Space Phys., 21*(8), 1657, 1987.

Haley, D., Solar radiation pressure calculations in the GEODYN program, NASA Goddard Space Flight Center, *Planetary Sciences Department Report No. 008-73*, August 1973.

Herring, T. A., Very long baseline interferometry and its contributions to geodynamics, *Space Geodesy and Geodynamics*, A. J. Anderson and A. Cazenave, Eds., Academic Press, 169–196, 1986.

Herring, T. A., Resolutions to IAU nutations working group, personal communication to D. McCarthy, July 14, 1988.

Huang, C., J. C. Ries, B. D. Tapley, and M. M. Watkins, Relativistic effects for near-Earth satellite orbit determination, submitted to *Celest. Mech.*, 1989.

Kaula, W. M., *Theory of Satellite Geodesy*, Blaisdell Publishing Co., Waltham, Mass., 1966.

Knocke, P. C., and J. C. Ries, Earth radiation pressure effects on satellites, *Tech. Mem. 87-01*, Center for Space Research, The University of Texas at Austin, Austin, Texas 78712, September 1987.

Knocke, P. C., Earth radiation pressure effects on satellites, *CSR-89-1*, Center for Space Research, The University of Texas at Austin, Austin, Texas 78712, January 1989.

Lense, J., and H. Thirring, ber die Einfluss der Eigenrotation der Zentralkrper auf die Bewegung der Planeten und Monde nach der Einsteinschen Gravitationstheorie, *Phys. Zeitschr., 19*, 156, 1918; English translation by B. Mashhoon et al., *Gen. Relativ. Gravit., 16*, 711, 1984.

Lochry, R. R., The perturbative effects of diffuse radiations from the Earth and Moon on close satellites, Dept. of Engineering, University of California, Los Angeles, Ph.D. dissertation, 1966.

Marsh, J. G., F. J. Lerch, B. H. Putney, D. C. Christodoulidis, D. E. Smith, T. L. Felsentreger, B. V. Sanchez, S. M. Klosko, E. C. Pavlis, T. V. Martin, J. W. Robbins, R. G. Williamson, O. L. Colombo, D. D. Rowlands, W. F. Eddy, N. L. Chandler, K. E. Rachlin, G. B. Patel, S. Bhati,

and D. S. Chinn, A new gravitational model for the Earth from satellite tracking data: GEM-T1, *J. Geophys. Res.*, *93*(B6), 6169, 1988.

Marsh, J. G., F. J. Lerch, and Gravity Modeling Team, Earth gravity model computation at Goddard Space Flight Center, presented at the Spring Meeting of the American Geophysical Union, Baltimore, Maryland, 1989.

Marini, J. W., and C. W. Murray, Jr., Correction of laser range tracking data for atmospheric refraction at elevations above 10 degrees, *Rep. X-591-73-351*, Goddard Space Flight Center, Greenbelt, Maryland, November 1973.

McCarthy, J. J., and T. V. Martin, A computer efficient model of Earth albedo satellite effects, NASA Goddard Space Flight Center, *Planetary Sciences Department Report No. 012-77*, June 1977.

Mecherikunnel, A. T., R. B. Lee, III, H. L. Kyle, and E. R. Major, Intercomparison of solar total irradiance data from recent spacecraft measurements, *J. Geophys. Res.*, *93*(D8), 9503, 1988.

Minster, J. B., and T. H. Jordan, Present-day plate motions, *J. Geophys. Res.*, *83*(B11), 5331, 1978.

Minster, J. B., and T. H. Jordan, Vector constraints on western U.S. deformation from space geodesy, neotectonics, and plate motions, *J. Geophys. Res.*, *92*(B6), 4798, 1987.

NASA/Goddard Space Flight Center, Report on MATLAS, MTLRS1, and MTLRS2 collocation at Matera, Greenbelt, Maryland 20771, September 1988.

Newhall, X X, E. M. Standish, and J. G. Williams, DE 102, a numerically integrated ephemeris of the Moon and planets spanning forty-four centuries, *Astron. Astrophys.*, *125*, 150, 1983.

Ries, J. C., C. Huang, and M. M. Watkins, Effect of General Relativity on a near-Earth satellite in the geocentric and barycentric reference frames, *Phys. Rev. Lett.*, *61*, 903, 1988.

Ries, J. C., R. J. Eanes, C. Huang, B. E. Schutz, C. K. Shum, B. D. Tapley, M. Watkins, and D. N. Yuan, Determination of the gravitational coefficient of the Earth from near-Earth satellites,

Geophys. Res. Lett., 16(4), 271, 1989.

Rubincam, D. P., Atmospheric drag as the cause of the secular decrease in the semimajor axis of Lageos's orbit, *Geophys. Res. Lett., 7*(6), 468, 1980.

Rubincam, D. P., On the secular decrease in the semimajor axis of Lageos's orbit, *Celest. Mech., 26*(4), 361, 1982.

Rubincam, D. P., Postglacial rebound observed by Lageos and the effect viscosity of the lower mantle, *J. Geophys. Res., 89*, 1077, 1984.

Rubincam, D. P., and N. R. Weiss, The orbit of Lageos and solar eclipses, *J. Geophys. Res., 90*(B11), 9399, 1985.

Rubincam, D. P., Lageos orbit decay due to infrared radiation from the Earth, *J. Geophys. Res., 92*(B2), 1287, 1987.

Rubincam, D. P., P. Knocke, V. R. Taylor, and S. Blackwell, Earth anisotropic reflection and the orbit of Lageos, *J. Geophys. Res., 92*(B11), 11662, 1987.

Rubincam, D. P., Yarkovsky thermal drag on Lageos, *J. Geophys. Res., 93*(B11), 13805, 1988.

Scharroo, R., K. F. Wakker, R. Noomen, B. A. C. Ambrosius, and H. Leenman, On the along-track acceleration of Lageos, presented at the 4th WEGENER-MEDLAS Conference, Scheveningen, June 7–9, 1989.

Schwiderski, E. W., On charting global ocean tides, *Rev. Geophys. Space Phys., 18*, 243–268, 1980.

Sehnal, L., Effects of the terrestrial infrared radiation pressure on the motion of an artificial satellite, *Celest. Mech., 25*, 169, 1981.

Shapiro, I. I., C. C. Counselman, III, and R. W. King, Verification of the principle of equivalence for massive bodies, *Phys. Rev. Let., 36*, 555, 1976.

Shapiro, I. I., R. D. Reasenberg, J. F. Chandler, and R. W. Babcock, Measurement of the de Sitter precession of the Moon: A relativistic three-body effect, *Phys. Rev. Let., 61*, 2643, 1988.

Slabinski, V. J., Lageos acceleration due to intermittent solar heating during eclipse periods, in proceedings of 19th Regular Meeting of Division on Dynamical Astronomy – American Astronomical Society, Gaithersburg, Maryland, July 25–26, 1988.

Smith, D. E., and P. J. Dunn, Long term evolution of the Lageos orbit, *Geophys. Res. Lett.*, *7*(6), 437, 1980.

Soffel, M., R. Wirrer, J. Schastox, H. Ruder, and M. Scheider, Relativistic effects in the motion of artificial satellites: The oblateness of the central body I, *Celest. Mech.*, *42*(81), 1988.

Stephens, G. L., G. G. Campbell, and T. H. Vonder Haar, Earth radiation budgets, *J. Geophys. Res.*, *86*(C10), 9739, 1981.

Sullivan, L. J., Infrared coherent radar, SPIE, *CO2 Laser Devices and Applications*, 227, 1980.

Tapley, B. D, Statistical orbit determination theory, *Recent Advances in Dynamical Astronomy*, D. Reidel Publishing Co., 396–425, 1973.

Tapley, B. D., B. E. Schutz, R. J. Eanes, and M. M. Watkins, Analysis of a twelve-year Lageos long arc, *Eos Trans. AGU*, *69*(16), 1988a.

Tapley, B. D., C. K. Shum, D. N. Yuan, J. C. Ries, and B. E. Schutz, An improved model for the Earth's gravity field, TEG-1, in proceedings of the Chapman Conference on Progress in Determination of the Earth's Gravity Field, Ft. Lauderdale, Florida, 1988b.

Wahr, J. M., Body Tides on an Elliptical, Rotating, Elastic and Oceanless Earth, *Geophys J. R. Astron. Soc.*, *64*,677, 1981.

Watkins, M. M., R. J. Eanes, B. D. Tapley, and B. E. Schutz, Baselines and plate motion from Lageos 11.7-year-long arc (LLA 8801), presented at the 13th NASA Crustal Dynamics Project Meeting, Jet Propulsion Laboratory, Pasadena, March 22–24, 1988.

Weinberg, S., *Gravitation and Cosmology: Principles and Application of the General Theory of Relativity*, John Wiley and Sons, New York, 230–241, 1972.

Will, C. M., *Theory and Experiment in Gravitational Physics*, Cambridge University Press, Cambridge, Massachusetts, 208–213, 1981.

Willson, R. C., Accurate solar 'constant' determination by cavity pyroheliometers, *J. Geophys. Res.*, *83*(C8), 4003, 1978.

Willson, R. C., and H. S. Hudson, Solar luminosity variations in solar cycle 21, *Nature, 332*, 810, 1988.

Yoder, C. F., J. G. Williams, J. O. Dickey, B. E. Schutz, R. J. Eanes, and B. D. Tapley, Secular variations of Earth's gravitational harmonic J_2 coefficients from Lageos and nontidal acceleration of Earth rotation, *Nature, 303*, 757, 1983.

Table 1: Tracking scenario

- Eight globally distributed stations selected from among existing sites
- Laser range data generated at 3-minute intervals when satellites were in view of station during scheduled tracking shift
- Single 8-hour tracking shift (not optimized for either satellite)
- Four stations track only 5 days a week
- Resulting passes randomly decimated (75% of all passes were eliminated)
- Combination of decimation and fixed tracking schedule caused stations to 'disappear' for periods of days or weeks, simulating weather outages and downtime

Table 2: Measurement model errors

- 5 cm random errors in station coordinates
- 1 mas random noise in 5 day values of x_p, y_p, UT1
- 1 cm/yr random error in all plate velocities
- Random precession and nutation errors:
  - 0.1 mas/yr random error in precession
  - 1.0 mas noise in 5 day values
  - 0.1 mas random errors in long period components
  - 0.05 mas random errors in short period components
- 5% random errors in individual station tide corrections
- Observation errors:
  - 1 cm random measurement noise
  - 2 cm stochastic range biases
  - 2 microsecond stochastic time tag errors
  - 0.2% stochastic troposphere biases

Note: All errors are 1-σ.

Table 3: Dynamical model errors

- *GM* error of 0.001 km^3/sec^2
- Geopotential errors derived from GEM-T1 covariance
- $\dot{J}_2$ and $\dot{J}_3$ errors of 10×10^{-12}/yr
- 20, 30 and 40% errors in semidiurnal, diurnal and long period tides, respectively, with maximum errors of 2 mm, 6mm, and 15mm.
- Stochastic seasonally variations in low-degree gravity coefficients
- 3% dynamical solid Earth tide (k_2)
- Radiation pressure errors:
  - Errors of 0.01 in solar, optical and infrared reflectivities
  - 5 km error Earth shadow radius
  - 0.03 in all Earth albedo and emissivity coefficients (equivalent to 3% of total available Earth radiation at the satellite)
- 'Drag' model error was composed of a combination of three error sources:
  - 10-30% error in Earth Yarkovsky
  - 100% error in solar Yarkovsky
  - Stochastic drag with a mean of about -1 pm/s^2, an rms about the mean of 1 pm/s^2; and a correlation time of approximately 1–2 days

Note: All errors are 1-σ.

Table 4a: Comparison of predicted Earth radiation pressure effect on Lageos node

	$\Delta\Omega$ (mas/yr) optical only	$\Delta\Omega$ (mas/yr) infrared only
UTOPIA (average of 1980 and 1982) *	-0.45	-2.4
Rubincam and Weiss [1985]	+0.57	
Sehnal [1981]		-36.8 †

* Node rates determined from 1-year arcs are not necessarily equal to long-term average.

† This value appears to be a miscalculation and too large by at least a factor of 10.

Table 4b: Comparison of Earth radiation pressure effect on Lageos-1 and Lageos-3

	Optical $\Delta\Omega$ (mas/yr)		Infrared $\Delta\Omega$ (mas/yr)		Total $\Delta\Omega$ (mas/yr)
	J_0	total	J_2	total	
Lageos-1 *	-4.0	-0.9	-2.2	-1.9	-2.8
Lageos-3 *	+3.3	+0.9	+2.2	+2.2	+3.1
Net effect †		0.0		+0.3	+0.3

* Node rates determined from 1-year arcs are not necessarily equal to long-term average.

† Net effect on sum of Lageos-1 and Lageos-3 nodes, assuming identical size, mass and reflectivity.

Table 5: Simulated data results for a typical case (blind data Case 3)

Station ID	Lageos-1 # obs	Lageos-3 # obs	Lageos-1 data fit *	Lageos-3 data fit *	Data error *
7907	4952	6116	38	56	2.1
7051	5856	6186	38	52	2.5
7597	7560	4652	39	56	1.9
7210	4386	5139	37	51	2.3
7064	6167	7669	37	62	2.5
7840	7565	7853	35	54	2.3
7837	6306	6329	34	57	2.4
7090	5071	4920	34	60	2.4
TOTALS	47863	48864	36	56	2.3

* RMS in cm

Notes:

1) Fit RMS were obtained after estimating initial conditions, solar reflectivity, and 15-day empirical drag (where necessary, GM and k_2, were estimated also).

2) Data error RMS indicates observation error introduced into simulated data, consisting of 1 cm noise, 2 cm stochastic range biases, 0.2% stochastic troposphere biases,and 2 microsecond stochastic timing biases (all 1-σ errors). The difference between the data error and the data fit indicates the effect of the dynamical and observational model errors prior to the simultaneous adjustment of the various parameters in the LT solution.

Table 6: Parameter set available for analysis

- 7×7 geopotential + zonals through degree 20
- GM, k_2, $\dot{J}_2$ and $\dot{J}_3$
- 34 ocean tide constituents (degrees 2-6) (GEM-T1 +)
- J_0, J_1, J_2 model for Earth albedo and emissivity + amplitude of annual variation of J_1
- Station coordinates (all 8 stations)
- Satellite parameters:
  - Initial position and velocity
  - 15-day empirical drag
  - solar radiation pressure reflectivity
  - Earth radiation reflectivities (optical and infrared)
  - Earth and solar Yarkovsky parameters

606 Total Parameters

Table 7: Solution and consider parameter set

- Geopotential: $J_2, J_3, J_4, J_5, \dot{J}_2$ and $\dot{J}_3$ estimated, remainder of the 7×7 geopotential and zonals to degree 20 considered using GEM-T1 covariance. GM and k_2 also estimated.
- Ocean tides: Degrees 2 and 3 estimated for all constituents. Degrees 4 and 5 estimated also for diurnal and semidiurnal tides: (*PI1, P1, S1, K1, K1±, PSI1, PHI1, T2, R2, S2, K2, 271a*). Remainder considered using 2, 6, and 15 mm errors for semi-diurnal, diurnal and long period tides.
- Mean station coordinates estimated.
- Satellite position and velocity, 15-day empirical drag, and solar radiation pressure reflectivity estimated.
- Earth radiation reflectivity for optical and infrared considered at 0.03.
- Earth albedo and emissivity parameters considered at 0.03, 0.01 for annual variability.
- Earth Yarkovsky estimated during UTOPIA runs by examining average drag; remaining error of ~1 pm/s^2 was a considered error. Solar Yarkovsky error of 30 pm/s^2 considered.

Table 8: Results of Lense-Thirring simulation blind analysis

Case	True Value of L-T Scale	UT/CSR Solution	Solution Difference	Estimated Uncertainty
1	0.55	0.47	0.08	0.06*
2	1.38	1.32	0.06	0.06
3	0.08	0.02	0.06	0.05
4	0.86	0.83	0.03	0.07
5	1.83	1.98	-0.15	0.07
6	0.94	1.02	-0.08	0.07

Mean of difference = 0.0 RMS of difference = 0.08

* 0.06 can interpreted as 6% of the nominal General Relativity prediction of 1.0

Table 9: Parameter recovery results from combined Lageos-1/Lageos-3 solution

Parameter	Case 1	Case 2	Case 3	Case 4	Case 5	Case 6	comment
Lense-Thirring	0.55	1.38	0.08	0.86	1.83	0.94	estimate
	0.47	1.32	0.02	0.83	1.98	1.02	true value
	0.06	0.06	0.05	0.07	0.07	0.07	sigma
	0.08	0.06	0.06	0.03	-0.15	-0.08	error
Error in semimajor axis (km)	3	15	3	15	3	15	Lageos-3
Error in inclination (deg)	0.01	0.01	0.03	0.03	0.1	0.1	injection error
GM (km^3/s^2)	398660.4316	398600.4414	398600.4406	398600.4398	398600.4398	398600.4409	estimate
	398600.4314	398600.4410	398600.4407	398600.4401	398600.4398	398600.4413	true value
k_2	0.299	0.295	0.295	0.288	0.289	0.288	estimate
	0.295	0.290	0.290	0.280	0.280	0.280	true value
J_2 ($\times 10^{-6}$)	484.16829	484.16813	484.16781	484.16854	484.16884	484.16901	estimate
	484.16907	484.16898	484.16907	484.16907	484.16898	484.16906	true value
J_3 ($\times 10^{-6}$)	0.96136	0.9601	0.9588	0.9584	0.9574	0.9574	estimate
	0.95777	0.9576	0.9578	0.9578	0.9576	0.9578	true value
$\dot{J}_2$ ($\times 10^{-12}$/yr)	-8.5	-6.8	-19.4	-21.6	-36.5	-11.6	estimate
	-20	-15	-20	-30	-35	-10	true value
$\dot{J}_3$ ($\times 10^{-12}$/yr)	-13.6	5.5	0.59	-17.6	-19.9	-2.3	estimate
	-25	0	5	-15	-20	-5	true value
Lageos-1 solar reflectivity	0.1159	0.1107	0.1275	0.1214	0.1347	0.1340	estimate
	0.1299	0.1192	0.1319	0.1278	0.1340	0.1234	true value
Lageos-3 solar reflectivity	0.1195	0.1256	0.1236	0.1235	0.1177	0.1344	estimate
	0.1258	0.1260	0.1259	0.1250	0.1193	0.1287	true value

Table 10: Simultaneous solution post-fit summary for Case 3

Parameter	RMS of orbit element residuals: Lageos (1986–1988)	Simulated Lageos-1	Simulated Lageos-3
a (mm)	0.6	0.6	0.7
e (billionths)	1.9	5.9	6.4
i (mas)	0.9	1.4	1.8
Ω (mas)	1.6	2.0	2.2
ω (mas)	59	291	283
rms fit (cm)	5.6 *	9.7 †	9.9 †
postprocess rms (cm) §	4.3	4.2	4.7

* Residuals after adjustment of parameters for Lageos only

† Residuals after simultaneous adjustment of common and local parameters

§ Post-fit residual analysis removing 5-day mean orbit element errors; measurement errors station coordinate errors and short period force model errors are the limiting factors.

Table 11a: Summary of range residual analysis for Lageos (1986–1988)

	Station	Passes	Obs	Raw RMS	Bias/Time-bias RMS	Poly RMS
7210	HOLLAS	455	3894	5.5	1.5	1.2
7109	QUINC2	885	10982	4.0	0.8	0.6
7110	MNPEAK	1045	11515	4.3	1.0	0.7
7105	GRF105	765	7634	3.8	0.8	0.5
7090	YARAG	755	8608	4.0	0.9	0.6
7839	GRAZ	459	4282	4.8	1.4	1.2
7840	RGO	900	8485	4.6	2.0	1.7
7122	MAZTLN	524	5617	4.5	1.1	0.7
	TOTALS	5788	61017	4.3	1.2	0.9

Table 11b: Multiple pass observation bias and time-bias solutions for Lageos (1986–1988)

	Station	Passes	Bias RMS (cm)	Time-bias RMS (microsec)
7210	HOLLAS	413	3.6	19.1
7109	QUINC2	874	2.4	15.5
7110	MNPEAK	1023	3.0	19.2
7105	GRF105	743	2.3	17.6
7090	YARAG	736	2.7	17.4
7839	GRAZ	454	3.4	18.7
7840	RGO	862	3.2	18.0
7122	MAZTLN	511	2.9	23.4

Notes:
1) Raw RMS = RMS of residuals before any pass parameters are estimated and removed but after the removal of long period orbit errors.

2) Bias/Time Bias RMS = RMS of residuals after most of orbit and station errors are removed in the form of a bias and an along-track error (in terms of an apparent timing bias at the point of closest approach).

3) Poly RMS = RMS of residuals after a second-order polynomial has also been removed. This is an estimate of the true noise of the data.

4) RMS of bias and time-bias solutions is the scatter of all the pass solutions about the average bias and time-bias for each station. This is a measure of the level of short-period orbit errors as well as biases in troposphere or station coordinate. Passes for which there was inadequate separation between the bias and time bias solutions are not included.

Table 12a: Summary of range residual analysis for Lageos-1 (Case 3)

	Station	Passes	Obs	Raw RMS	Bias/Time-bias RMS	Poly RMS
7210	HOLLAS	389	4383	3.7	1.1	0.9
7051	QUINCY	475	5852	3.8	1.1	0.9
7837	SHAHAI	580	6297	5.4	1.0	0.9
7064	GRF064	496	6162	3.5	1.1	0.9
7090	YARAG	467	5066	4.1	1.2	0.9
7597	WET597	580	7549	4.1	1.1	0.9
7840	RGO	578	7559	4.0	1.2	0.9
7907	ARELAS	420	4947	4.5	1.1	0.9
	TOTALS	3985	47815	4.2	1.1	0.9

Table 12b: Multiple pass observation bias and time-bias solutions for Lageos-1

	Station	Passes	Bias RMS (cm)	Time-bias RMS (microsec)
7210	HOLLAS	374	2.9	14.8
7051	QUINCY	461	2.9	14.6
7837	SHAHAI	564	3.5	25.4
7064	GRF064	486	2.4	14.1
7090	YARAG	438	2.8	18.9
7597	WET597	566	2.5	17.6
7840	RGO	562	2.8	15.6
7907	ARELAS	405	3.5	20.0

Notes:
1) Raw RMS = RMS of residuals before any pass parameters are estimated and removed but after the removal of long period orbit errors.

2) Bias/Time Bias RMS = RMS of residuals after most of orbit and station errors are removed in the form of a bias and an along-track error (in terms of an apparent timing bias at the point of closest approach).

3) Poly RMS = RMS of residuals after a second-order polynomial has also been removed. This is an estimate of the true noise of the data.

4) RMS of bias and time-bias solutions is the scatter of all the pass solutions about the average bias and time-bias for each station. This is a measure of the level of short-period orbit errors as well as biases in troposphere or station coordinate. Passes for which there was inadequate separation between the bias and time bias solutions are not included.

Table 13a: Summary of range residual analysis for Lageos-3 (Case 3)

	Station	Passes	Obs	Raw RMS	Bias/Time-bias RMS	Poly RMS
7210	HOLLAS	353	4650	4.3	1.1	0.9
7051	QUINCY	437	6109	4.1	1.1	0.9
7837	SHAHAI	488	6316	5.6	1.1	0.9
7064	GRF064	439	6184	3.7	1.0	0.9
7090	YARAG	407	5133	4.5	1.3	0.9
7597	WET597	536	7665	4.8	1.2	0.9
7840	RGO	534	7846	4.8	1.2	0.9
7907	ARELAS	374	4915	5.4	1.1	0.9
	TOTALS	3568	48818	4.7	1.2	0.9

Table 13b: Multiple pass observation bias and time-bias solutions for Lageos-3

	Station	Passes	Bias RMS (cm)	Time-bias RMS (microsec)
7210	HOLLAS	339	2.4	23.1
7051	QUINCY	428	2.5	20.6
7837	SHAHAI	478	3.4	29.4
7064	GRF064	424	2.5	19.2
7090	YARAG	389	2.8	26.9
7597	WET597	520	3.0	23.3
7840	RGO	521	2.8	22.2
7907	ARELAS	360	3.3	33.7

Notes:
1) Raw RMS = RMS of residuals before any pass parameters are estimated and removed but after the removal of long period orbit errors.

2) Bias/Time Bias RMS = RMS of residuals after most of orbit and station errors are removed in the form of a bias and an along-track error (in terms of an apparent timing bias at the point of closest approach).

3) Poly RMS = RMS of residuals after a second-order polynomial has also been removed. This is an estimate of the true noise of the data.

4) RMS of bias and time-bias solutions is the scatter of all the pass solutions about the average bias and time-bias for each station. This is a measure of the level of short-period orbit errors as well as biases in troposphere or station coordinate. Passes for which there was inadequate separation between the bias and time bias solutions are not included.

Table 14: Estimated error budget for Lense-Thirring measurement

Geopotential (other than even zonals) + tides	5%
Earth radiation pressure	1%
Uncertainty in other relativistic effects [1]	1%
Earth- and solar-induced thermal forces [2]	3%
Even zonal geopotential (per 0.1° inclination injection error) [3]	3%
Other errors (such as random and stochastic errors included in simulation but not in covariance analysis) [4]	5%

	RSS Error
assuming 0.1° injection error or less	8%
assuming 0.2° injection error	10%
assuming 0.3° injection error	12%

Notes:

1) The only significant uncertainties are in the amount of geodesic (or de Sitter) precession and in the exact value of the PPN parameter γ.

2) The effect of the solar heating was based on the conservative assumption that no modeling is possible.

3) The result of 3% error per 0.1° inclination injection error assumes an equal influence of error in the semimajor axis and eccentricity, but the bounds on the semimajor axis and eccentricity injection errors are less demanding than the bounds on inclination. As a result, the predicted effect on the Lense-Thirring estimate is considered to be conservative.

4) Consider-covariance analysis results were augmented by an additional 5% to account for the effect of time-correlated stochastic errors (such as the seasonal variations in the geopotential, drag, and observation biases), which were included in the simulation, but could not be included explicitly in the covariance analysis.

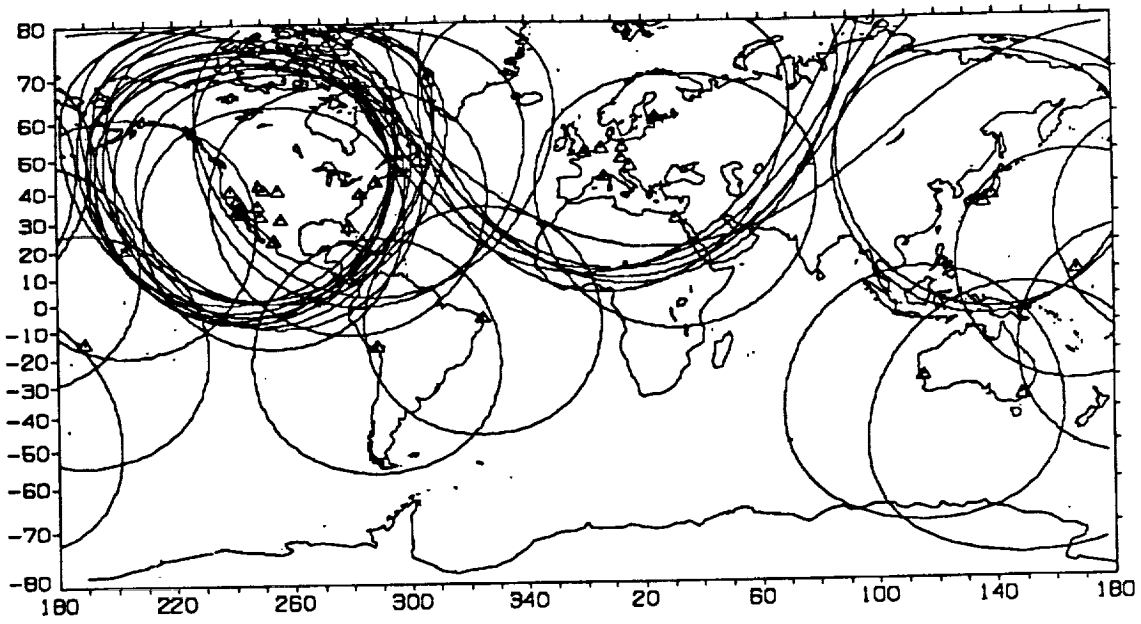

Figure 1. Laser ranging tracking network for Lageos

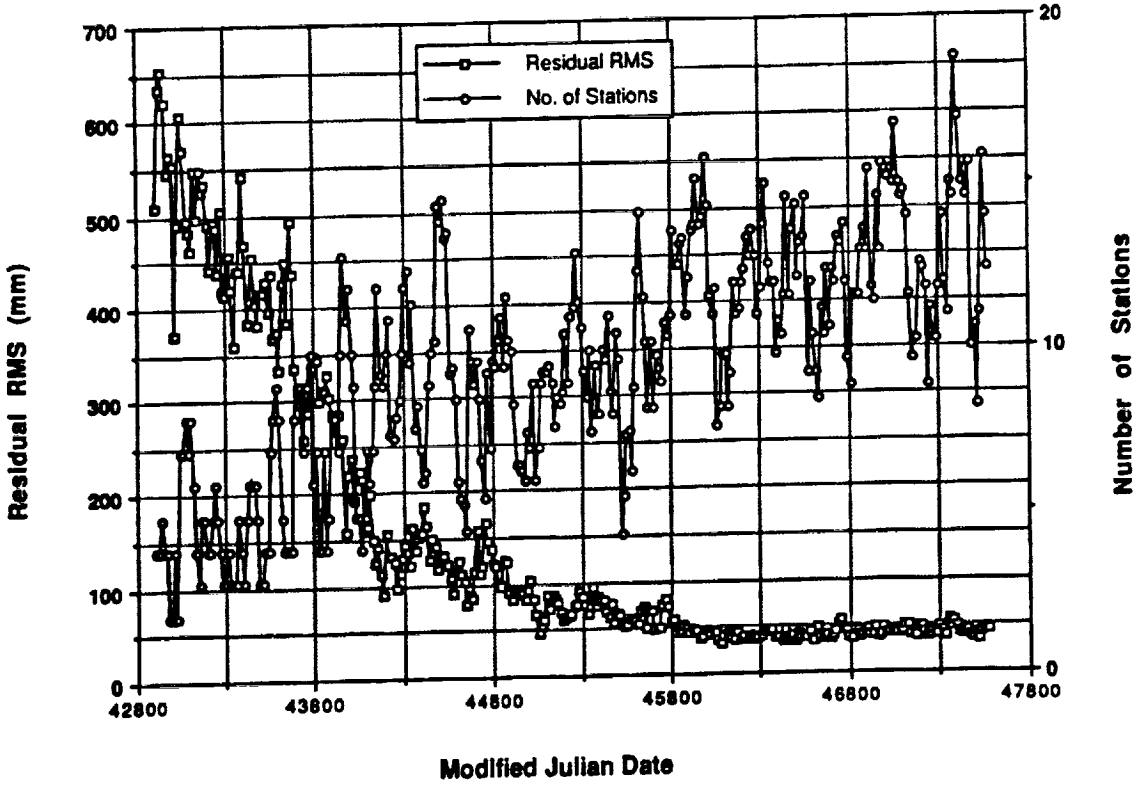

Figure 2. Number of stations and post-fit RMS in 15-day bins for Lageos long-arc

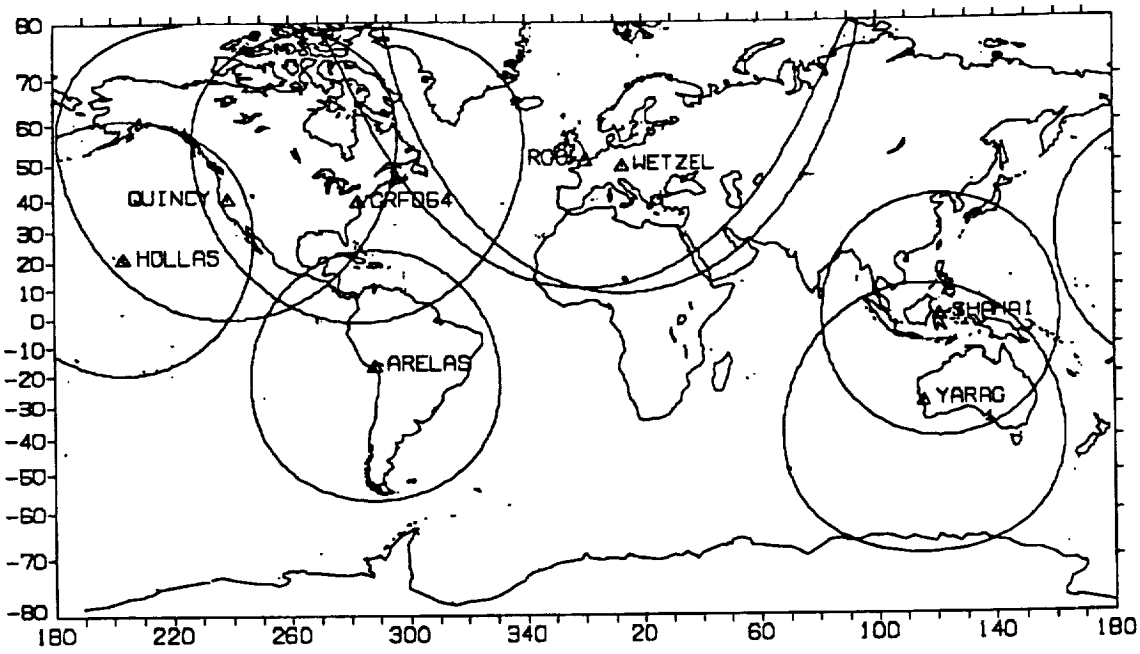

Figure 3. Tracking network for simulated laser ranging

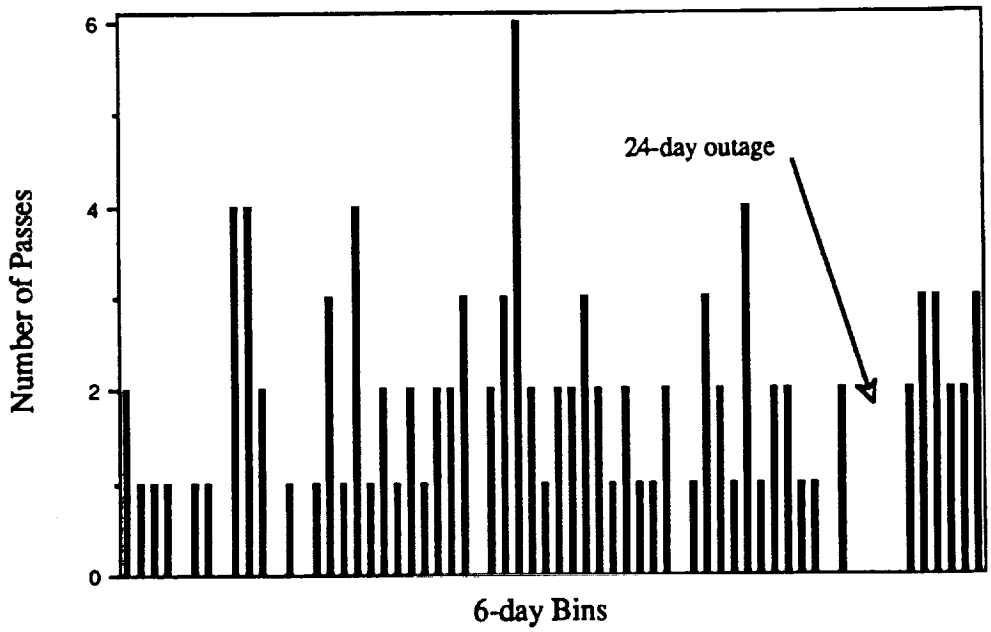

Figure 4. Typical tracking data distribution for Hollas

C-2

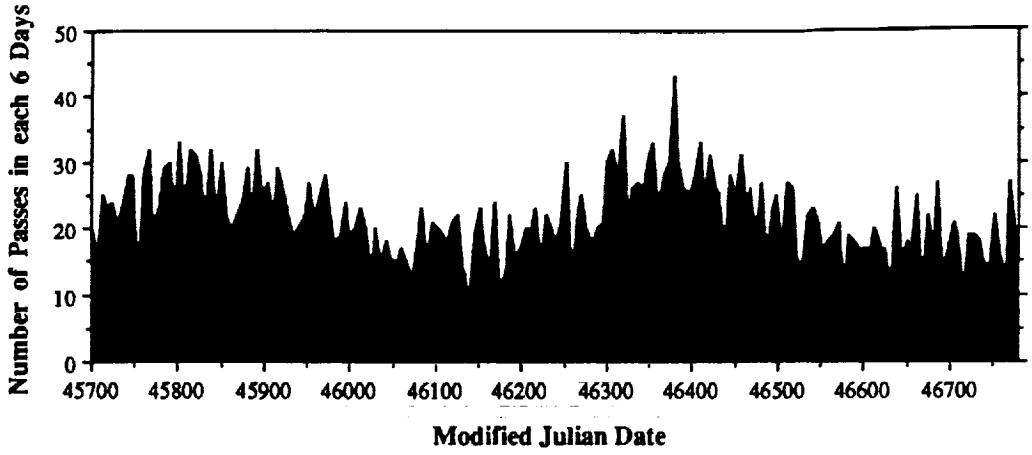

Figure 5a. Histogram of simulated Lageos-1 tracking data

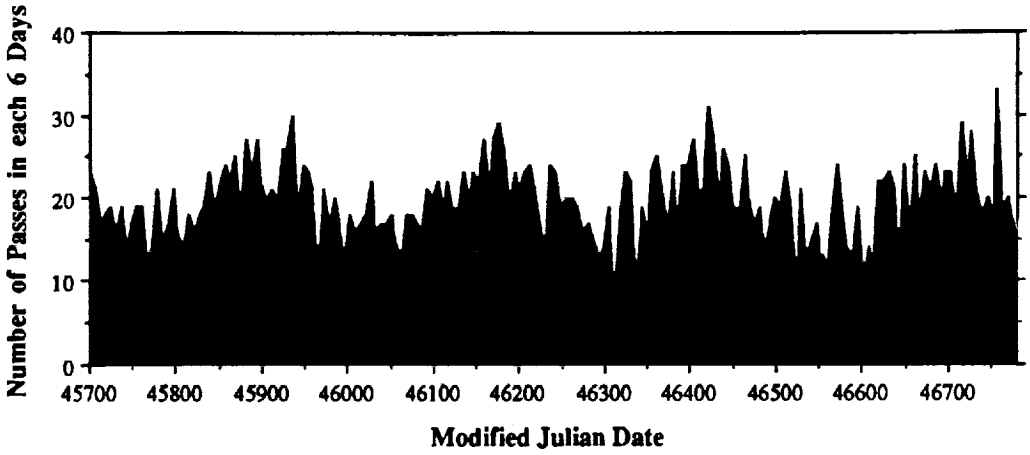

Figure 5b. Histogram of simulated Lageos-3 tracking data

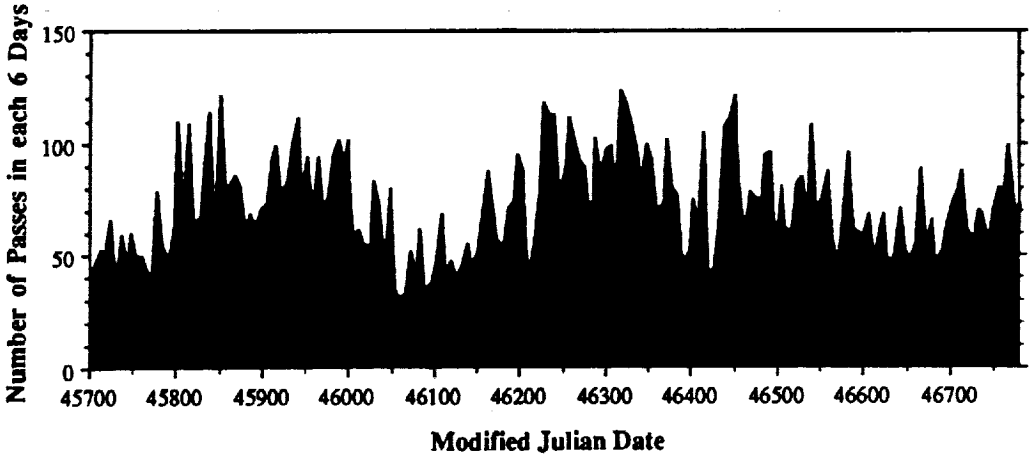

Figure 5c. Histogram of actual Lageos tracking data

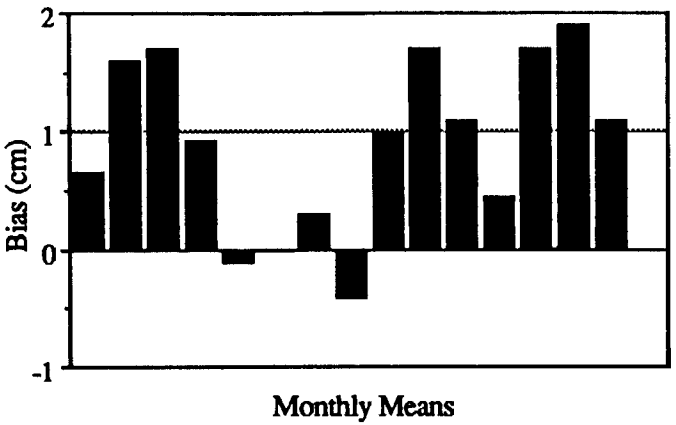

Figure 6a. Estimated range biases for MOBLAS-7

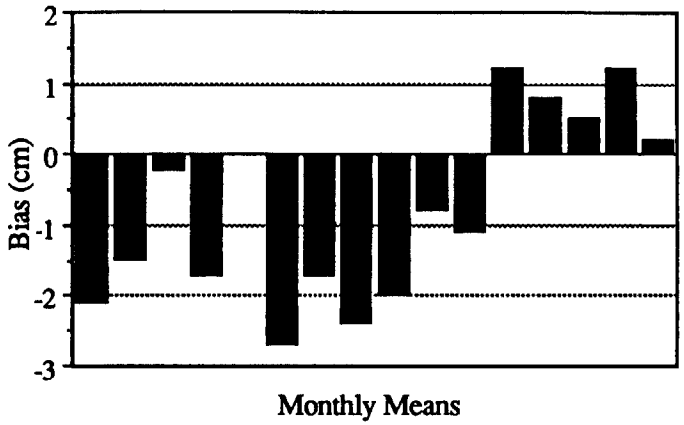

Figure 6b. Estimated range biases for RGO

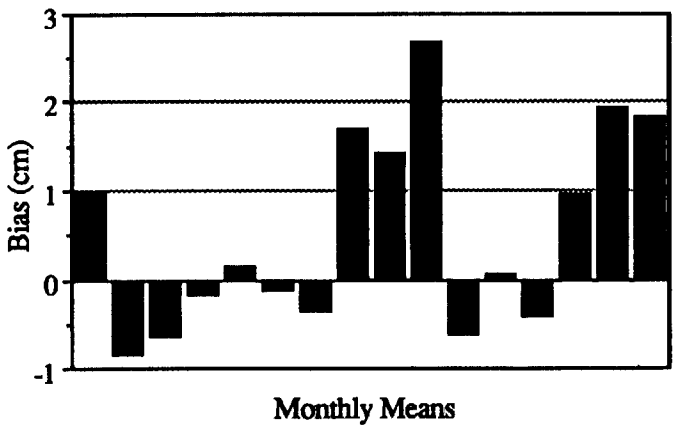

Figure 6c. Typical simulated range biases

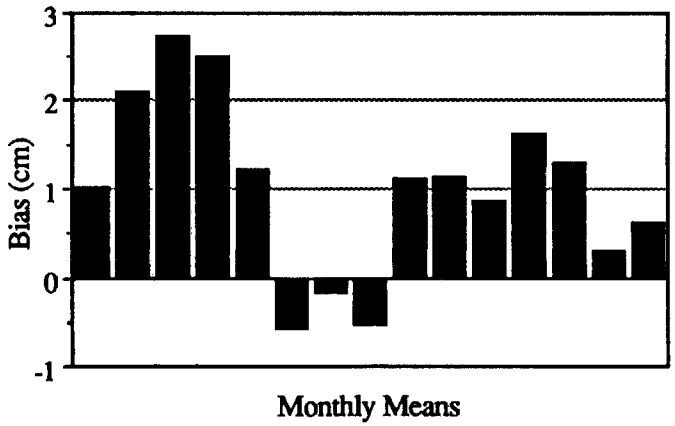

Figure 6d. Typical simulated range biases

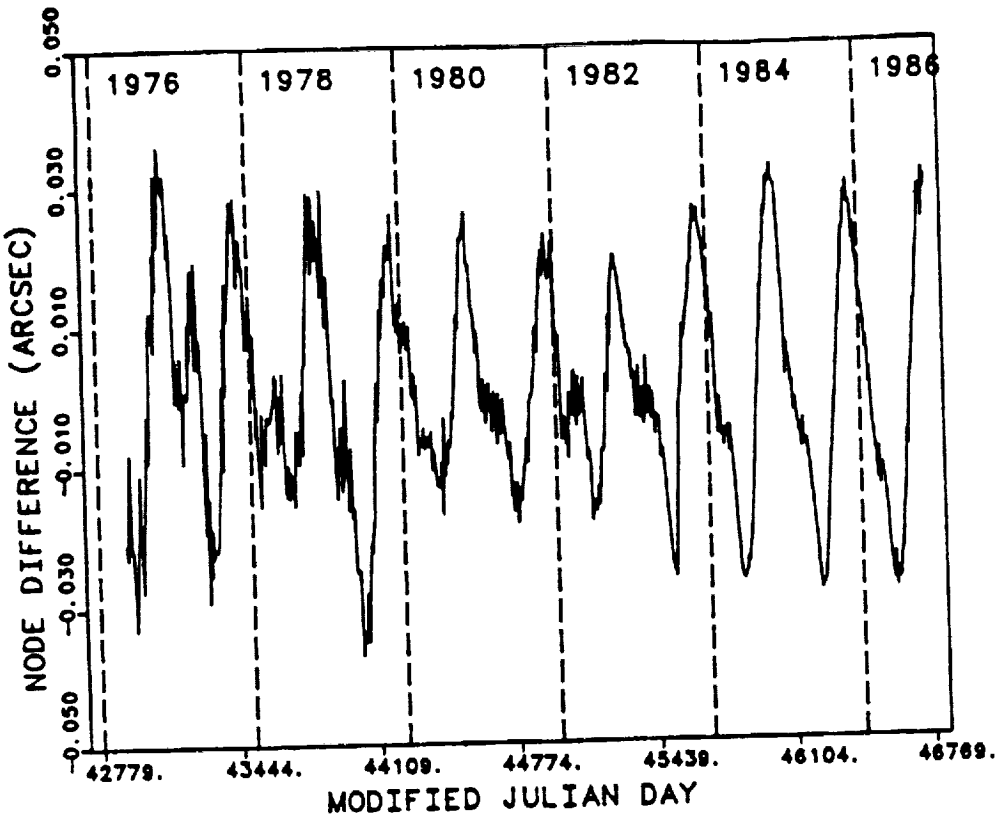

Figure 7a. Lageos 11-year orbit node residual time history showing seasonal variation

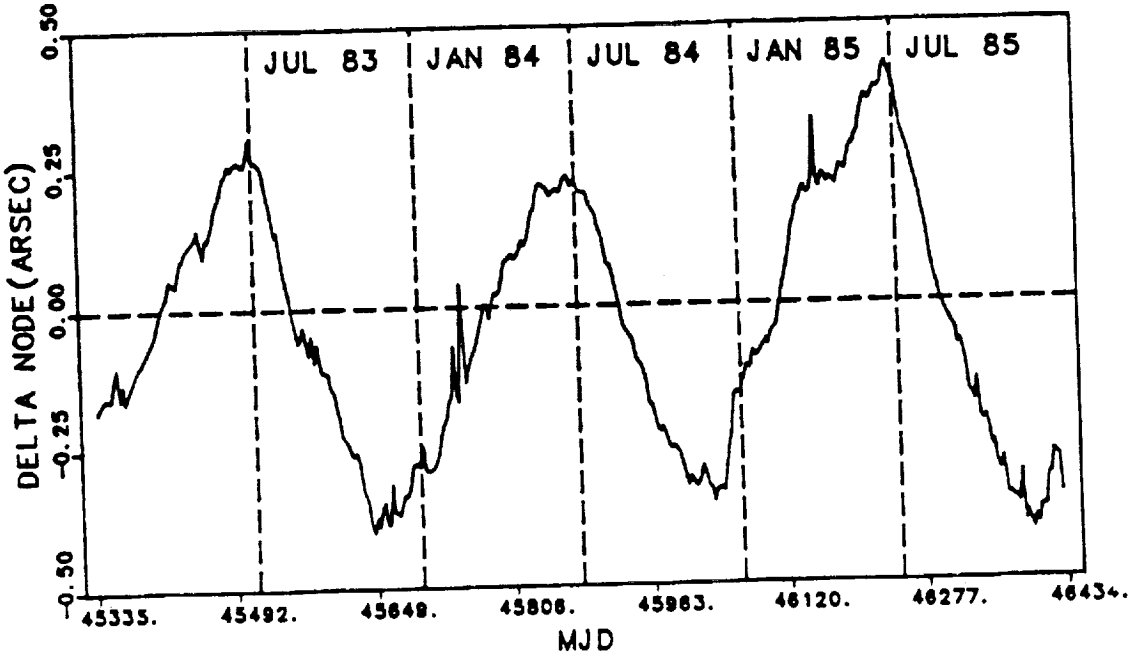

Figure 7b. Starlette 3-year orbit node residual time history showing seasonal variation

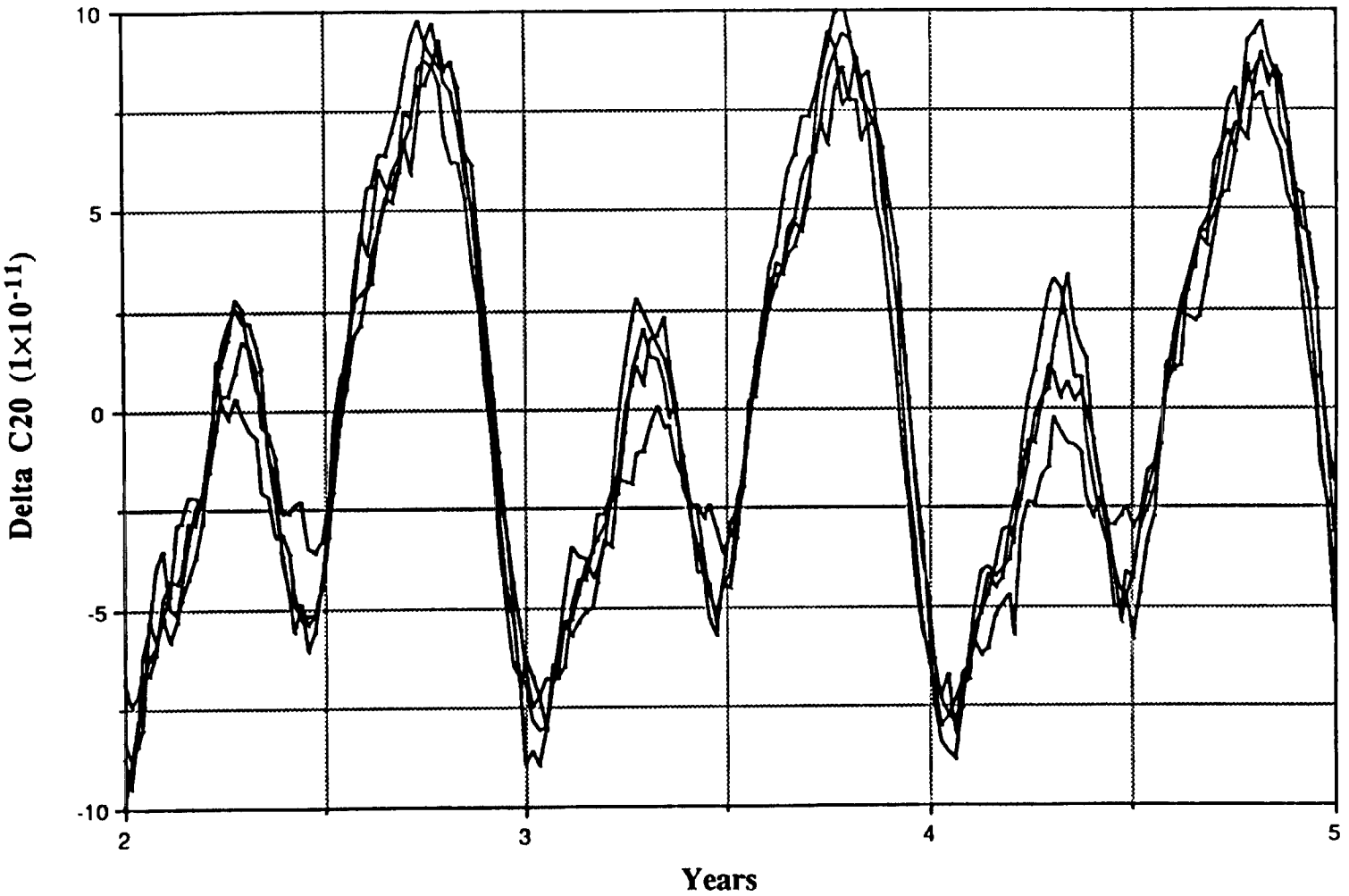

Figure 8. Four realizations of stochastic variations of C20

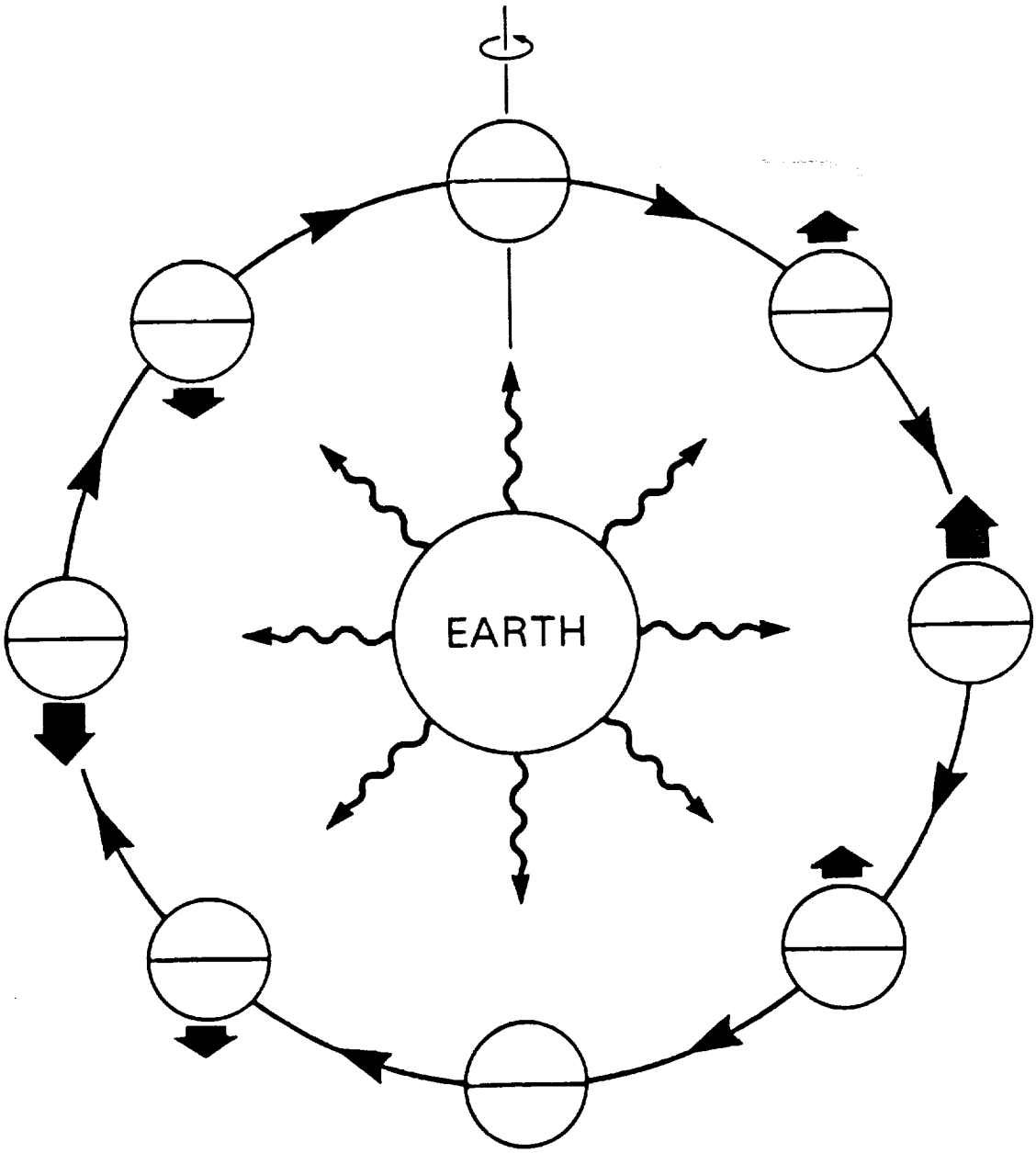

Figure 9. Schematic diagram of effect of infrared heating of Lageos. The thermal lag angle is taken to be 90° to illustrate that there is an along-track acceleration due to the Earth's infrared radiation (wavy arrows) but the actual angle is closer to 55°. (Figure taken from Rubincam [1987a])

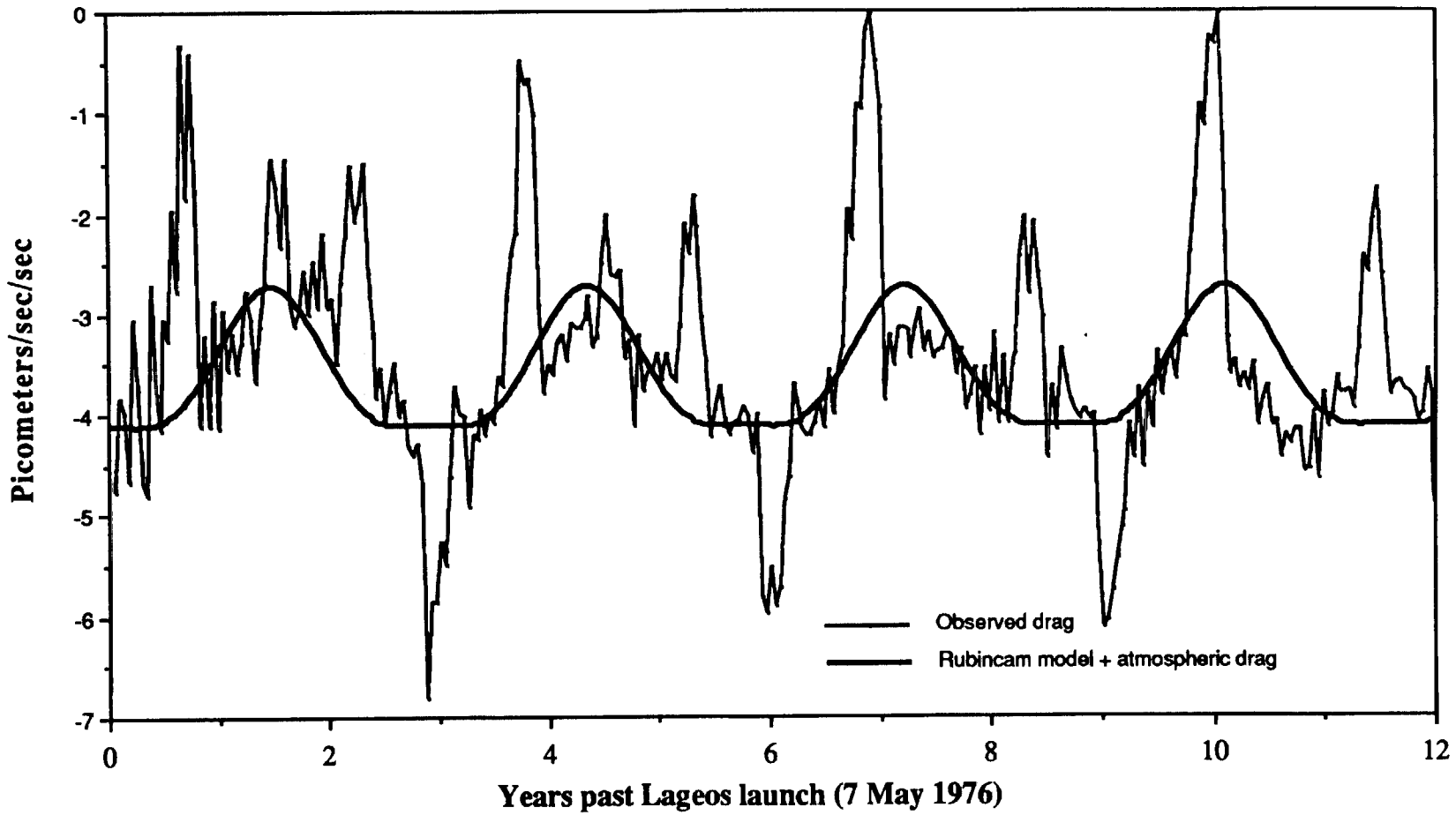

Figure 10. Earth Yarkovsky model compared to Lageos 'drag' estimates at 15-day intervals

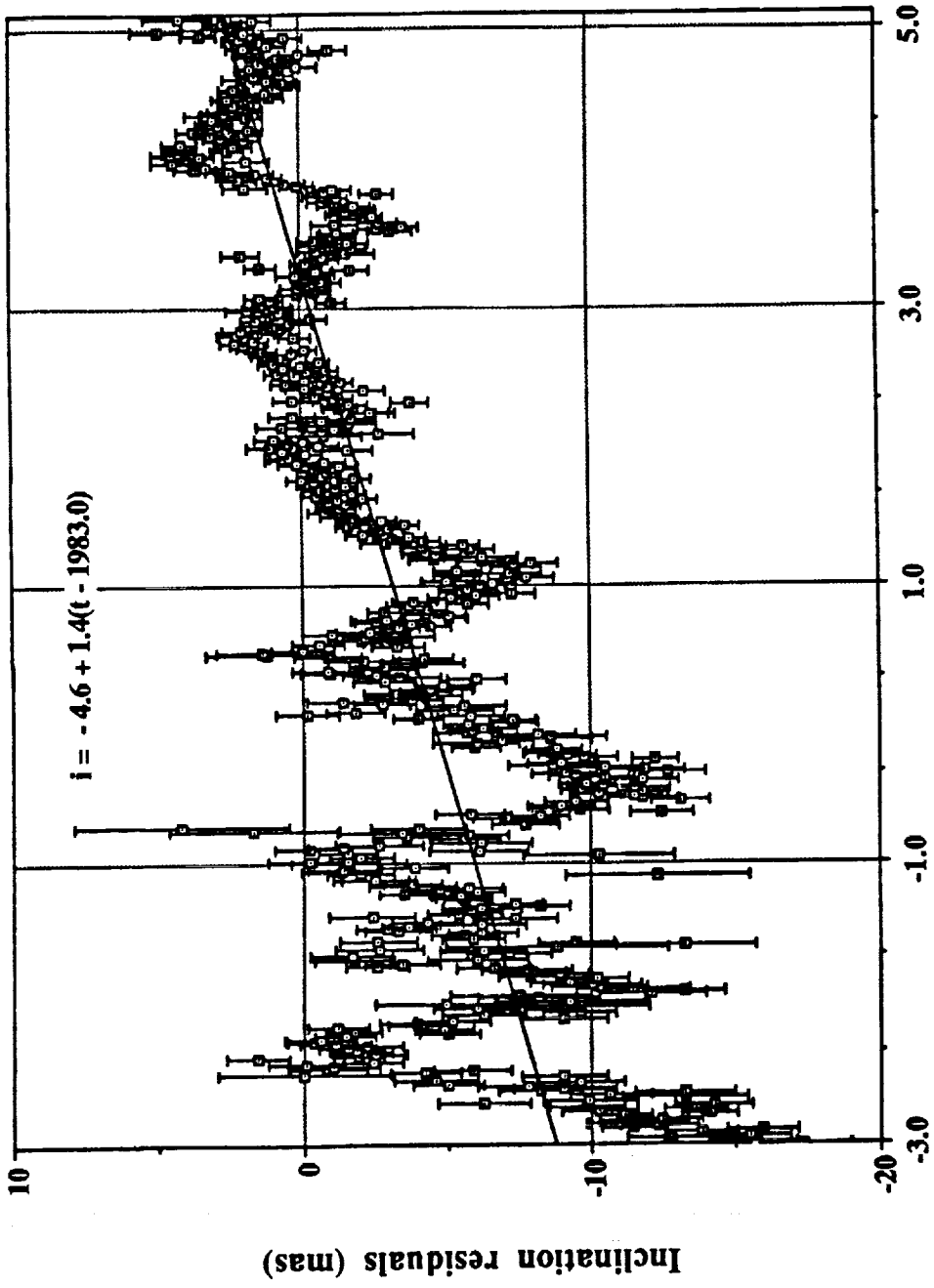

Figure 11. Inclination residuals from Lageos long-arc 8808 (1980—1988)

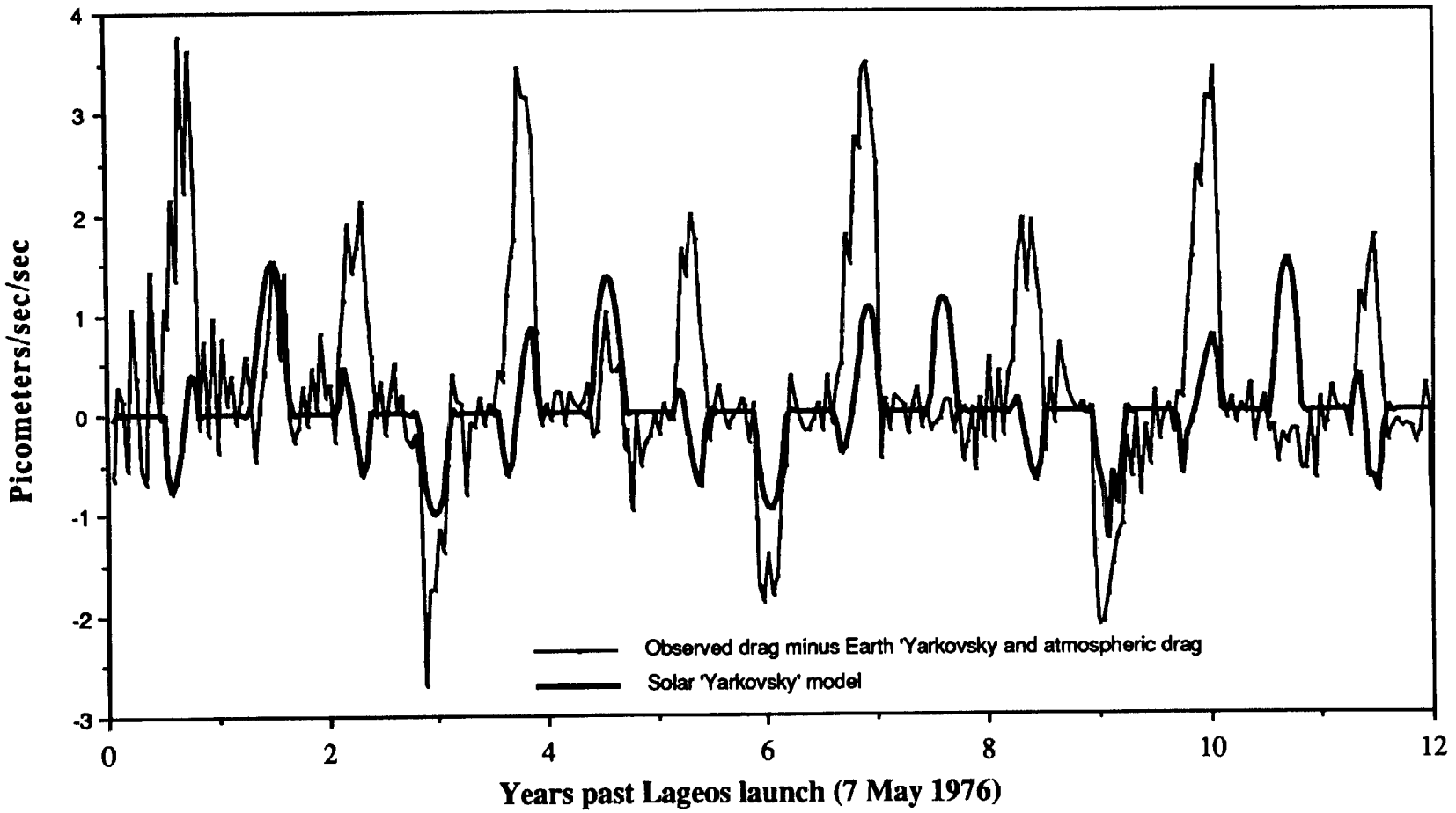

Figure 12. Solar Yarkovsky model compared to Lageos 'drag' estimates at 15-day intervals. Models for Earth Yarkovsky and atmospheric drag removed from observed drag.

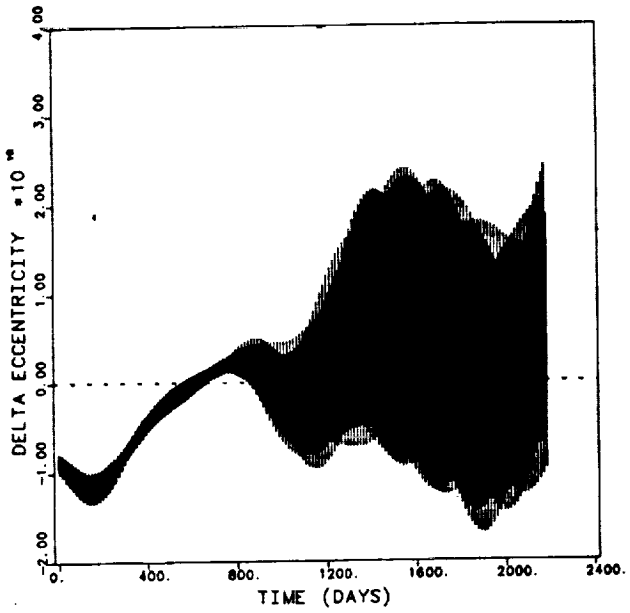

Figure 13 a. Effect of Earth Yarkovsky on Lageos-1 Orbit Eccentricity

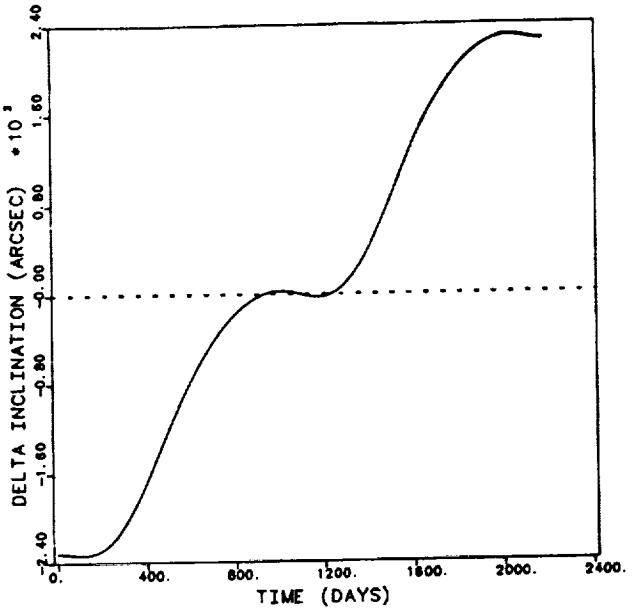

Figure 13b. Effect of Earth Yarkovsky on Lageos-1 Orbit Inclination

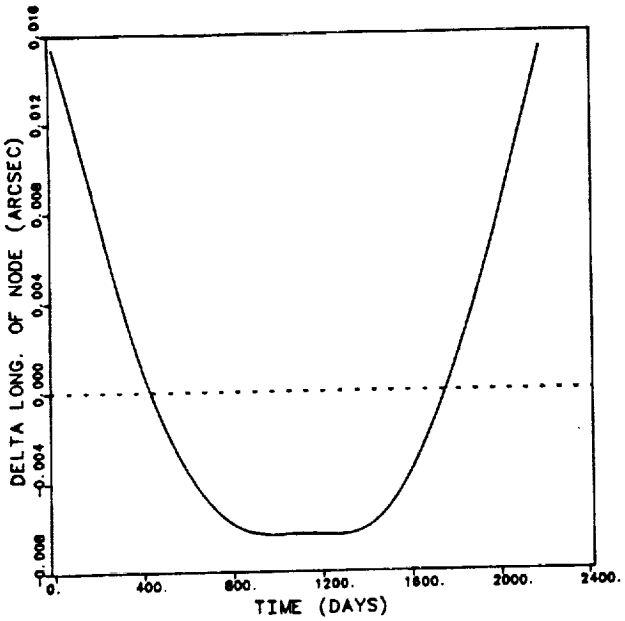

Figure 13c. Effect of Earth Yarkovsky on Lageos-1 Orbit Node

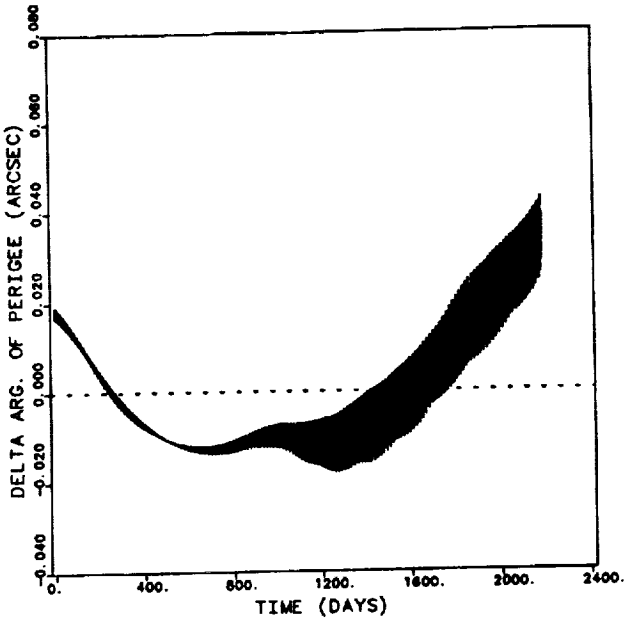

Figure 13d. Effect of Earth Yarkovsky on Lageos-1 Orbit Perigee

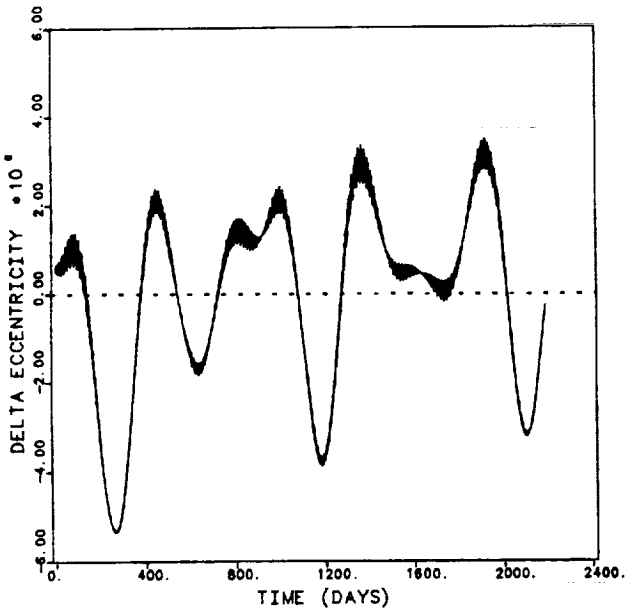

Figure 14a. Effect of Solar Yarkovsky on Lageos-1 Orbit Eccentricity

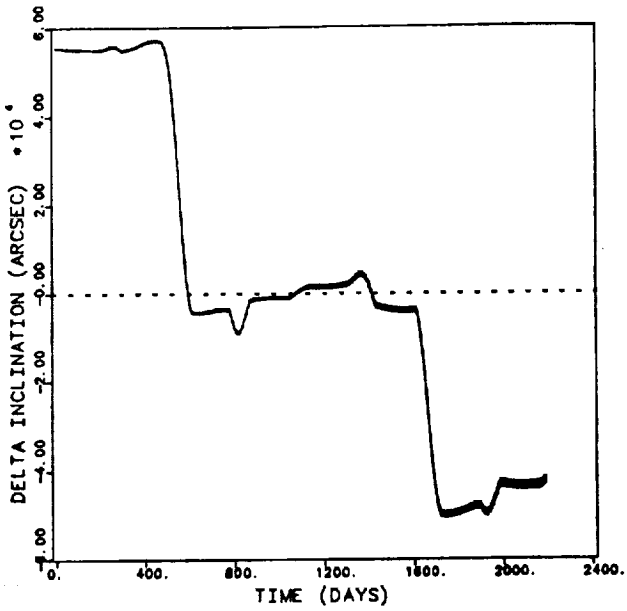

Figure 14b. Effect of Solar Yarkovsky on Lageos-1 Orbit Inclination

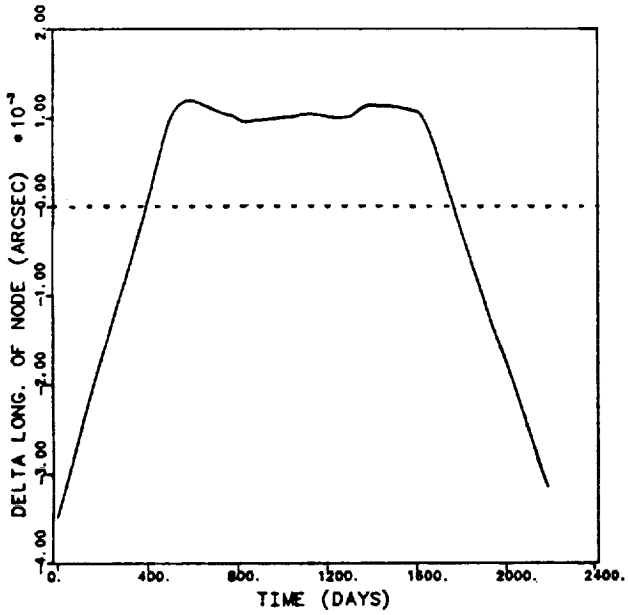

Figure 14c. Effect of Solar Yarkovsky on Lageos-1 Orbit Node

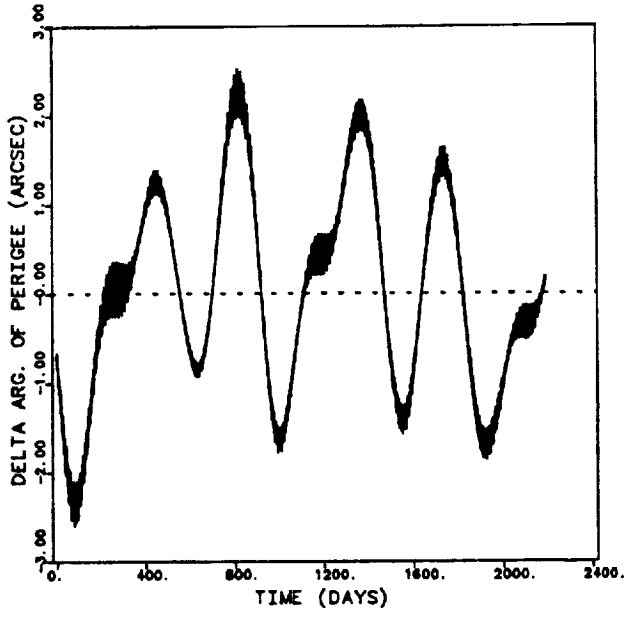

Figure 14d. Effect of Solar Yarkovsky on Lageos-1 Orbit Perigee

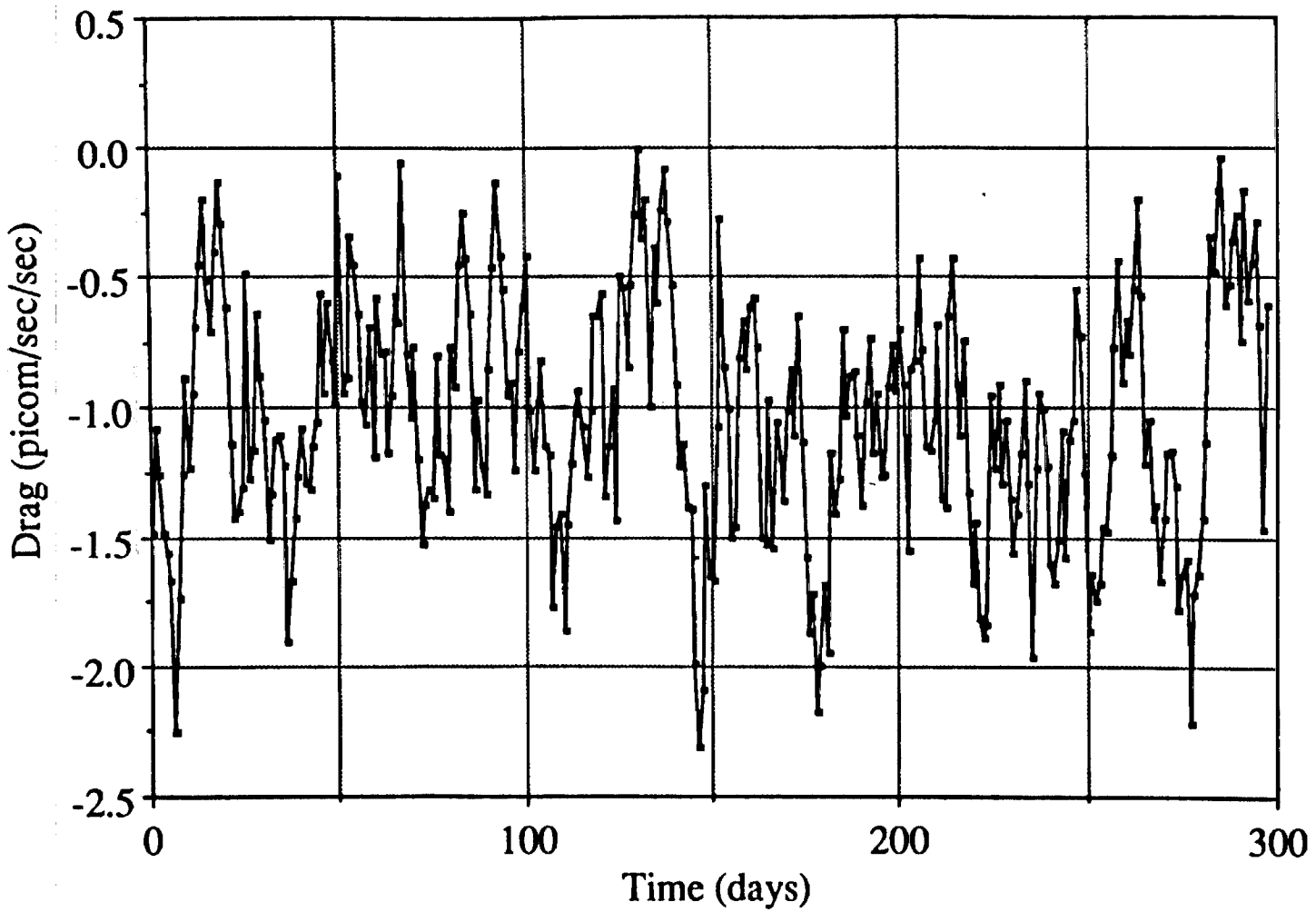

Figure 15. Typical daily samples of simulated stochastic drag

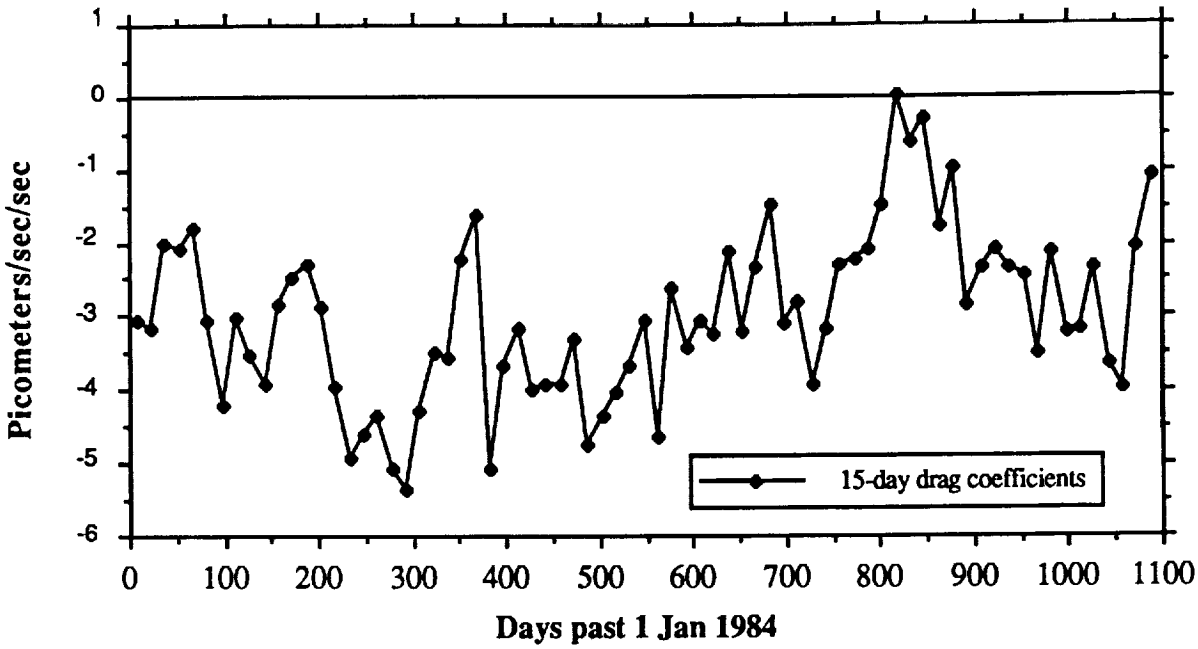

Figure 16a. 15-day empirical drag estimates from Lageos-1 simulated data generated by the combination of Earth Yarkovsky, solar Yarkovsky and atmospheric drag

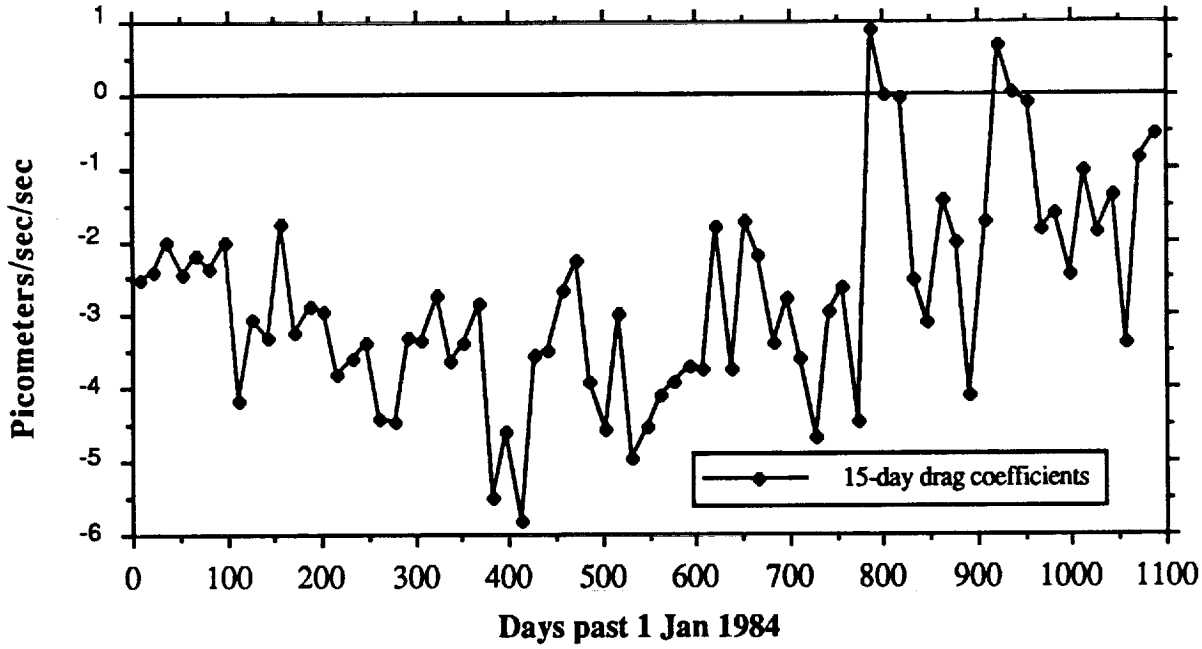

Figure 16b. 15-day empirical drag estimates from Lageos-3 simulated data generated by the combination of Earth Yarkovsky, solar Yarkovsky and atmospheric drag

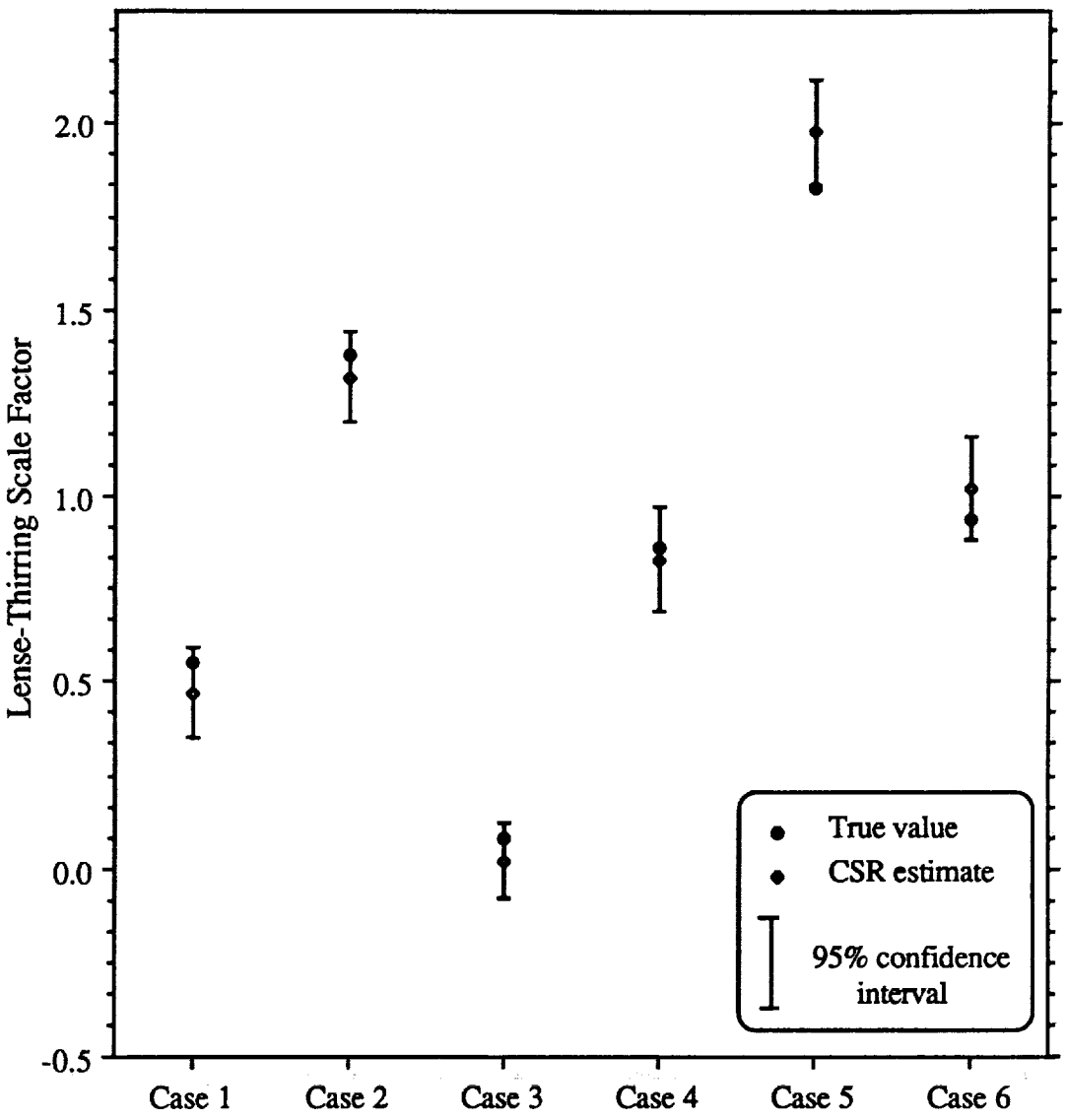

Figure 17. Lense-Thirring blind simulation results

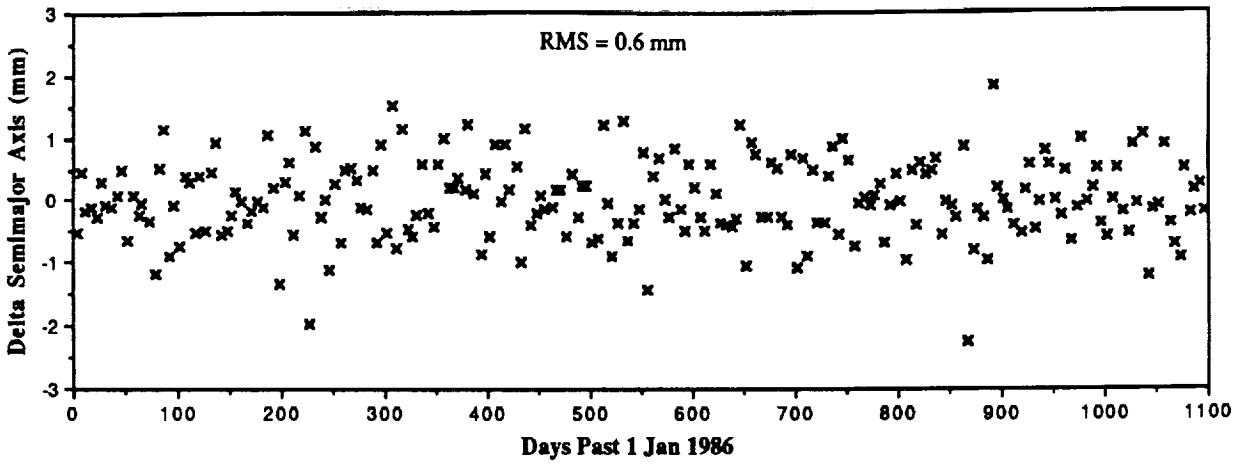

Figure 18a. Residual semimajor axis errors in Lageos long-arc (1986—1988)

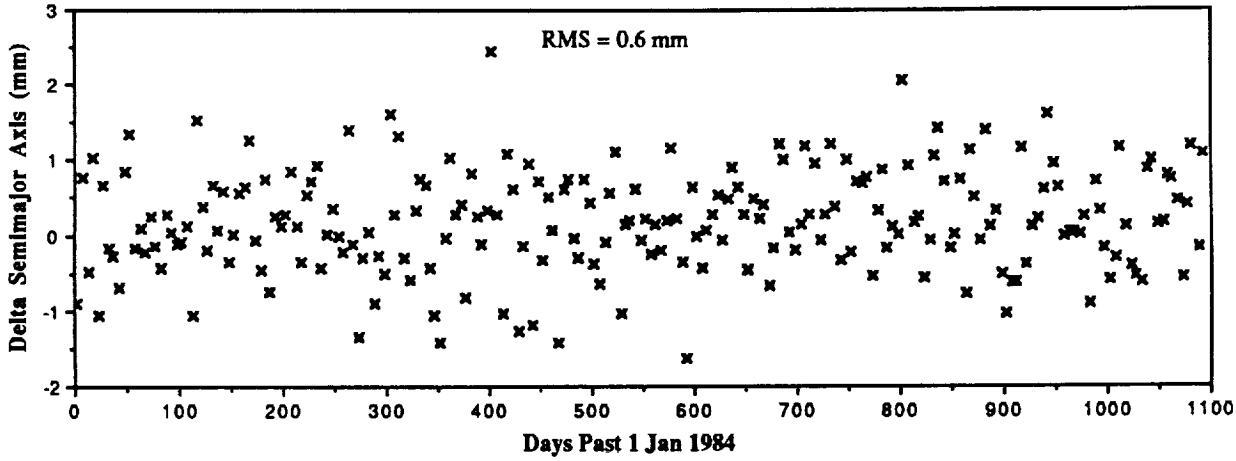

Figure 18b. Residual Lageos-1 semimajor axis errors for simulation Case 3

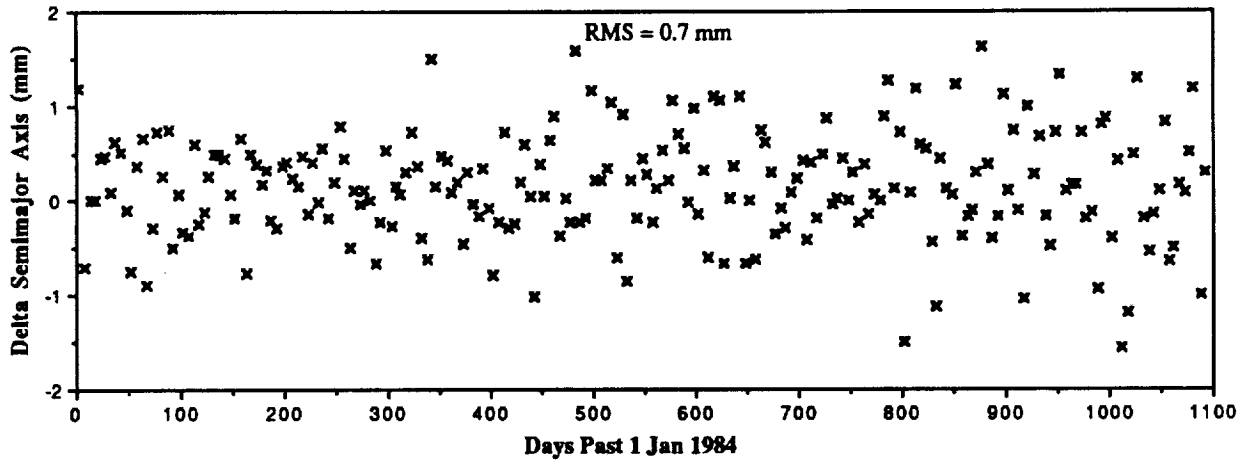

Figure 18c. Residual Lageos-3 semimajor axis errors for simulation Case 3

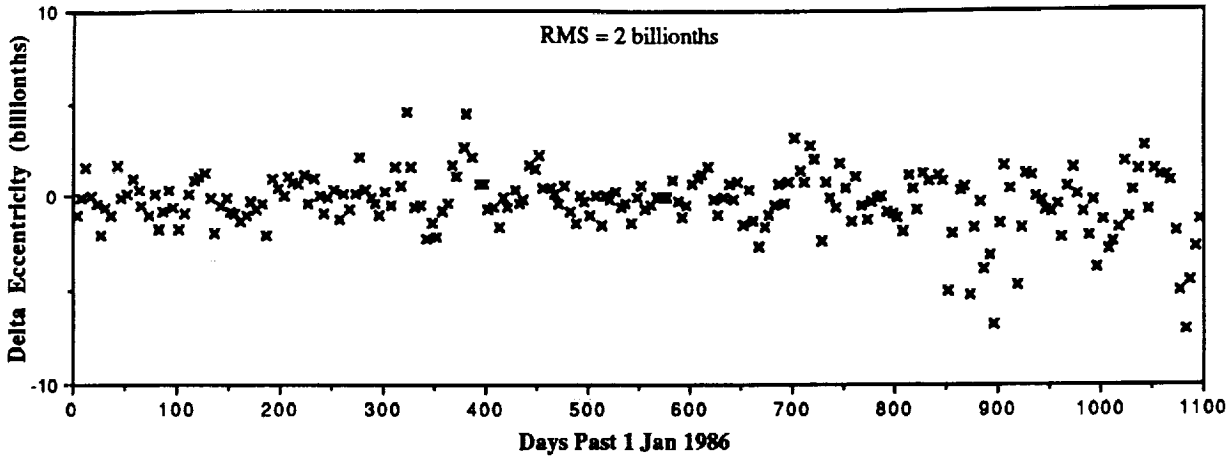

Figure 19a. Residual eccentricity errors in Lageos long-arc (1986—1988)

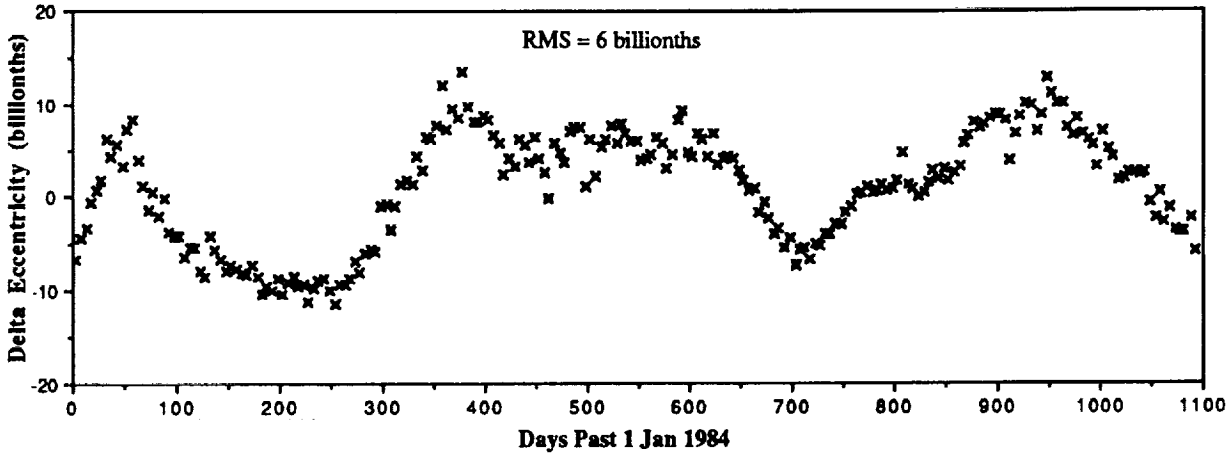

Figure 19b. Residual Lageos-1 eccentricity errors for simulation Case 3

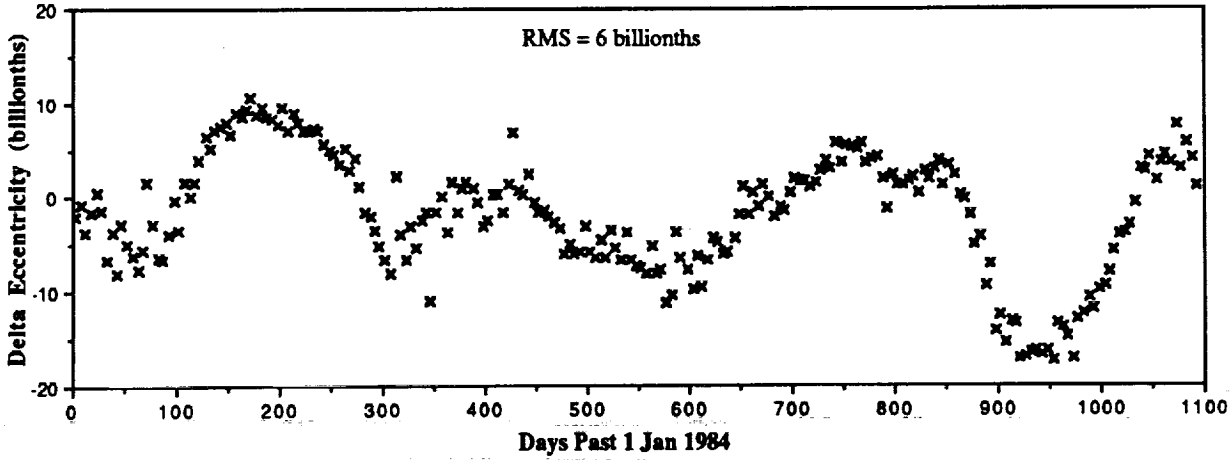

Figure 19c. Residual Lageos-3 eccentricity errors for simulation Case 3

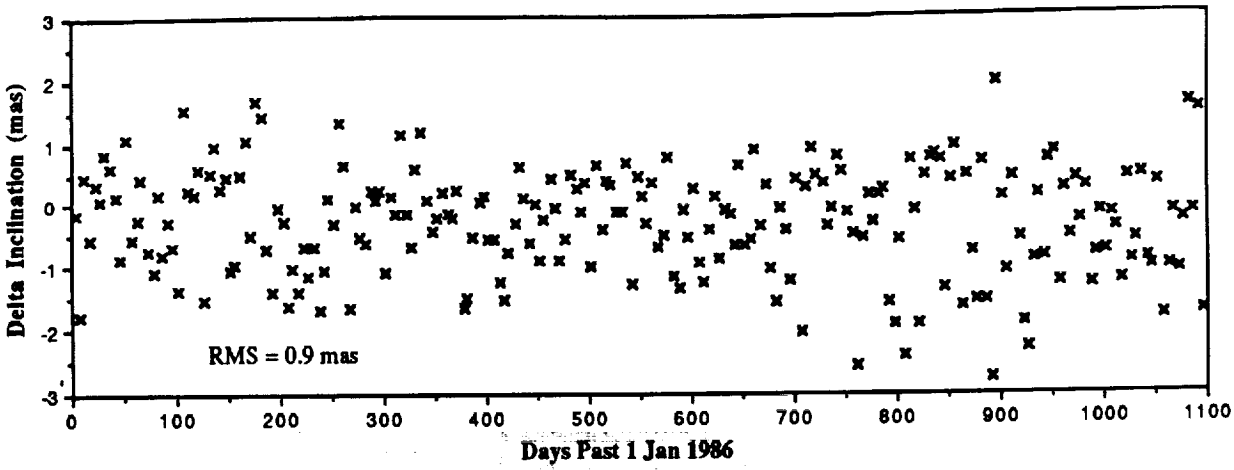

Figure 20a. Residual inclination errors in Lageos long-arc (1986—1988)

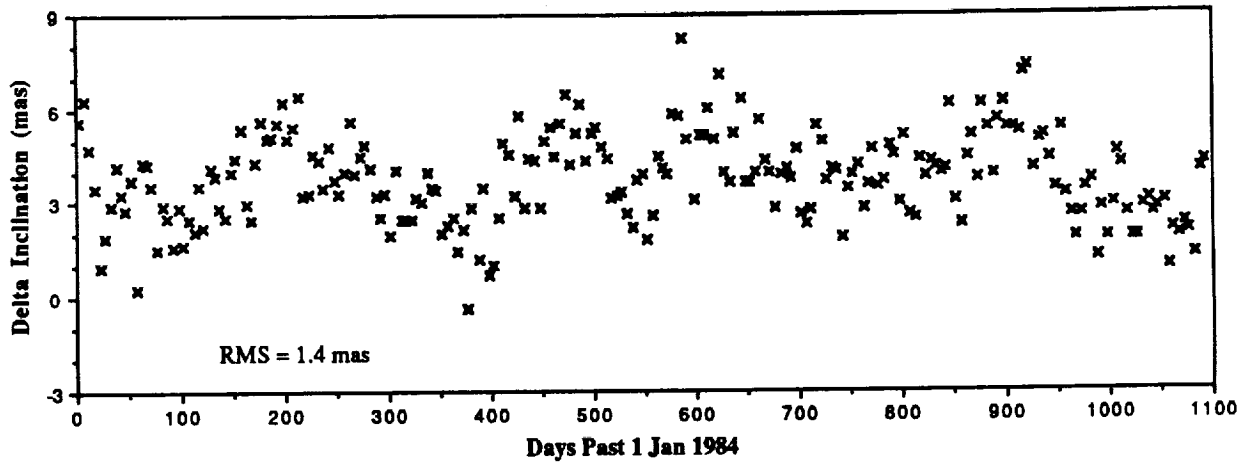

Figure 20b. Residual Lageos-1 inclination errors for simulation Case 3

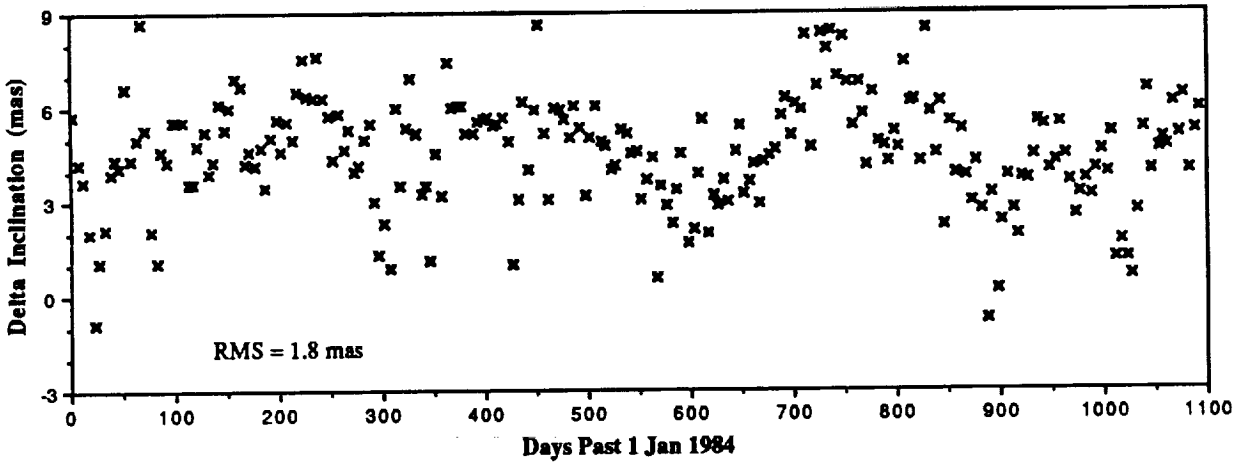

Figure 20c. Residual Lageos-3 inclination errors for simulation Case 3

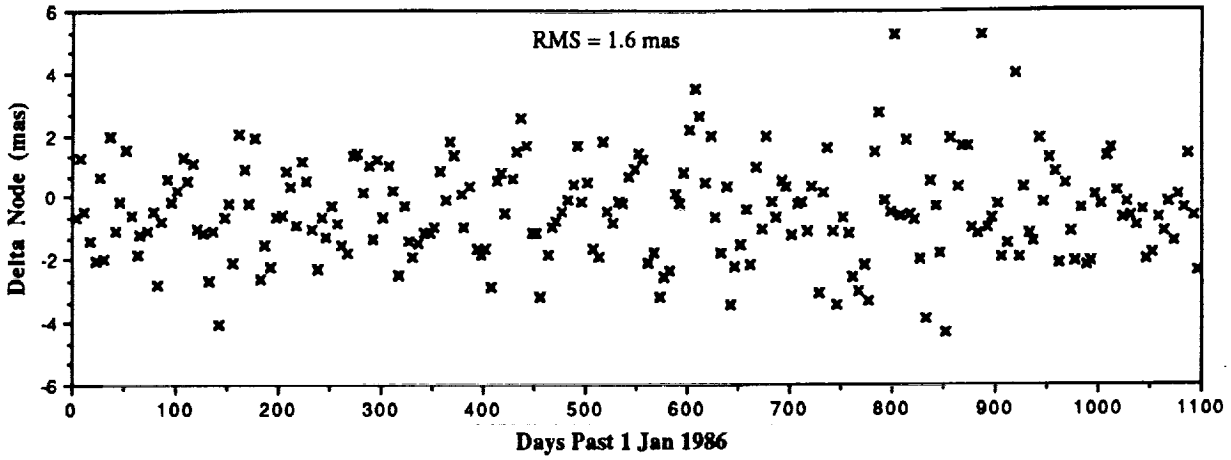

Figure 21a. Residual node errors in Lageos long-arc (1986—1988)

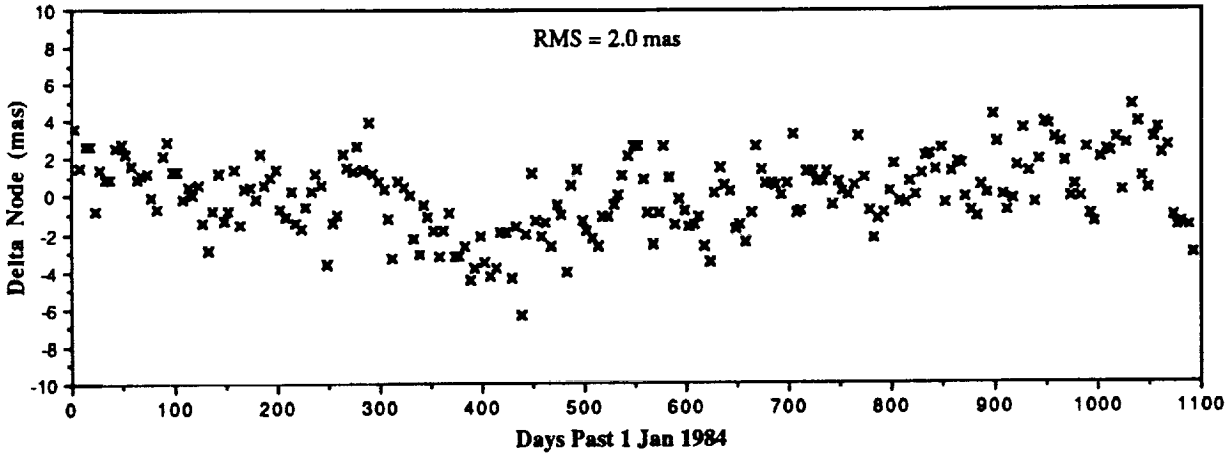

Figure 21b. Residual Lageos-1 node errors for simulation Case 3

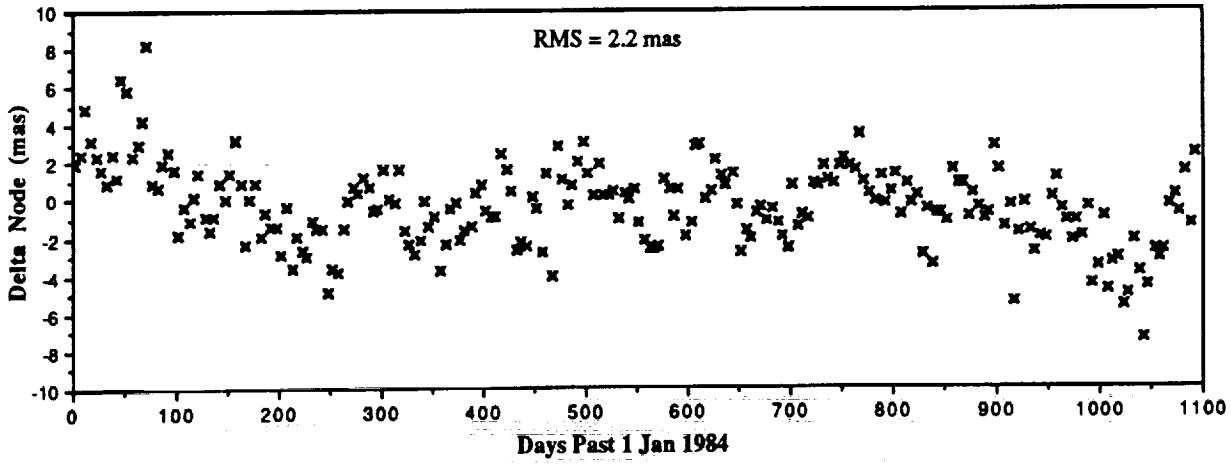

Figure 21c. Residual Lageos-3 node errors for simulation Case 3

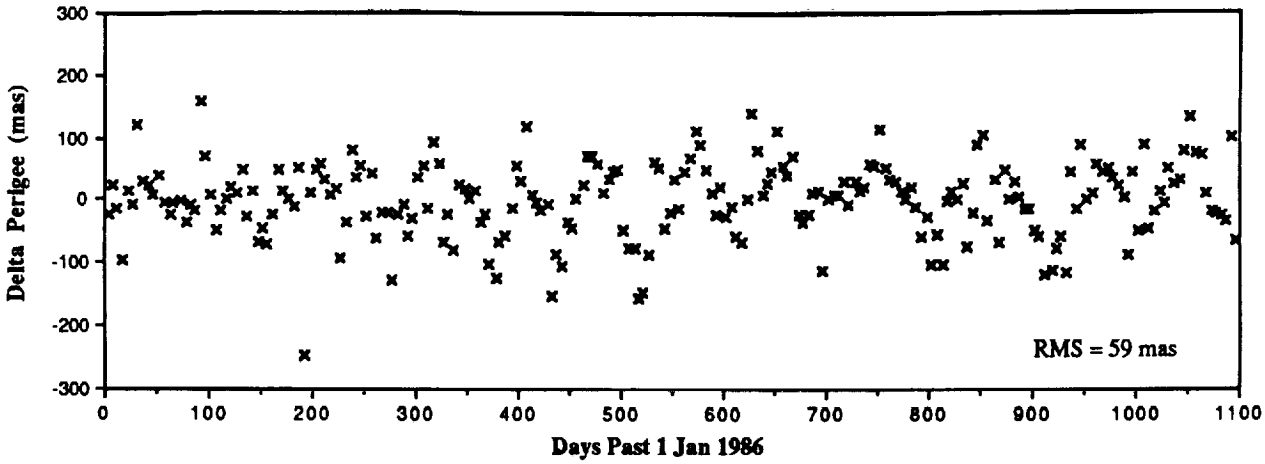

Figure 22a. Residual argument of perigee errors in Lageos long-arc (1986—1988)

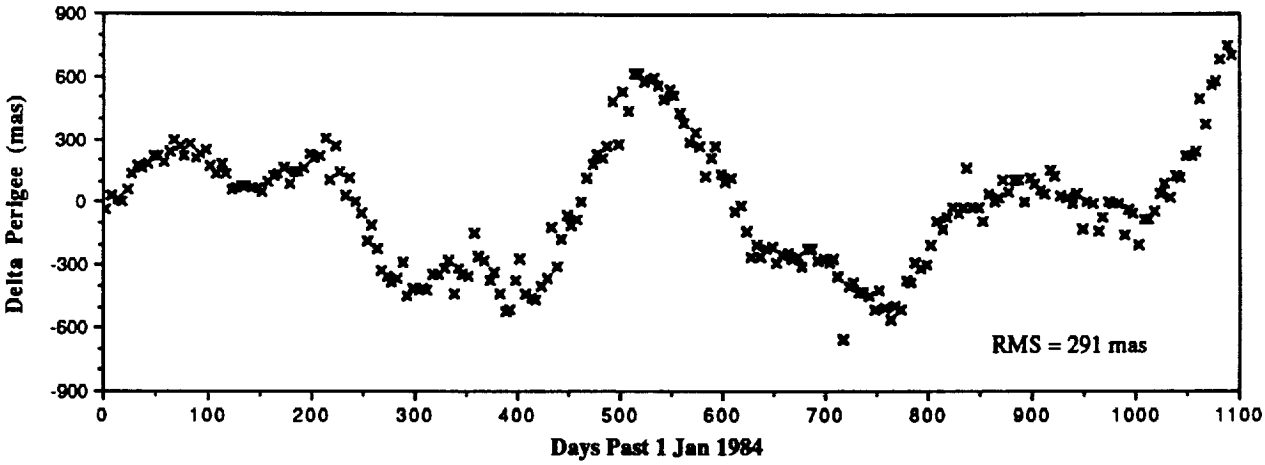

Figure 22b. Residual Lageos-1 argument of perigee errors for simulation Case 3

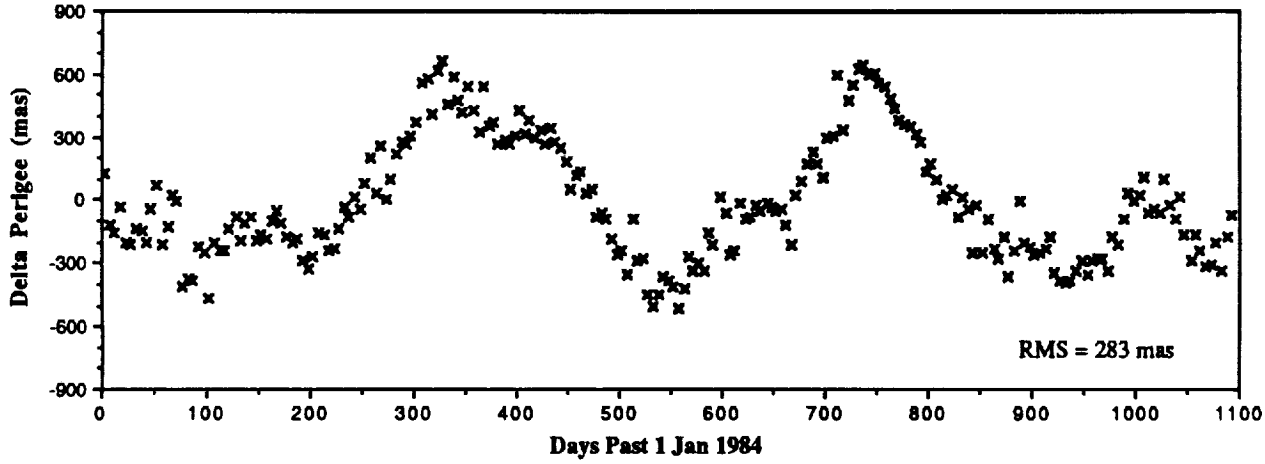

Figure 22c. Residual Lageos-3 argument of perigee errors for simulation Case 3

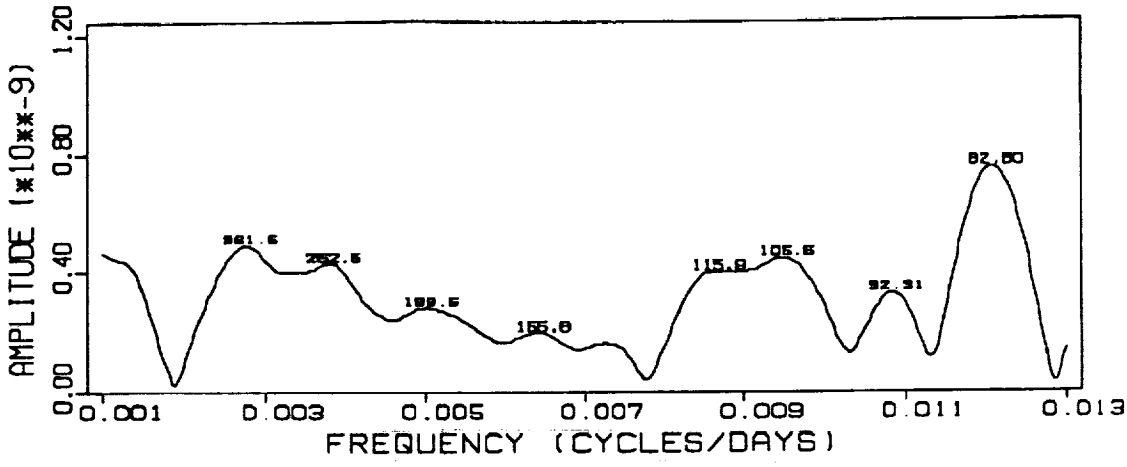

Figure 23a. Periodigram of Lageos eccentricity residuals (1986–1988)

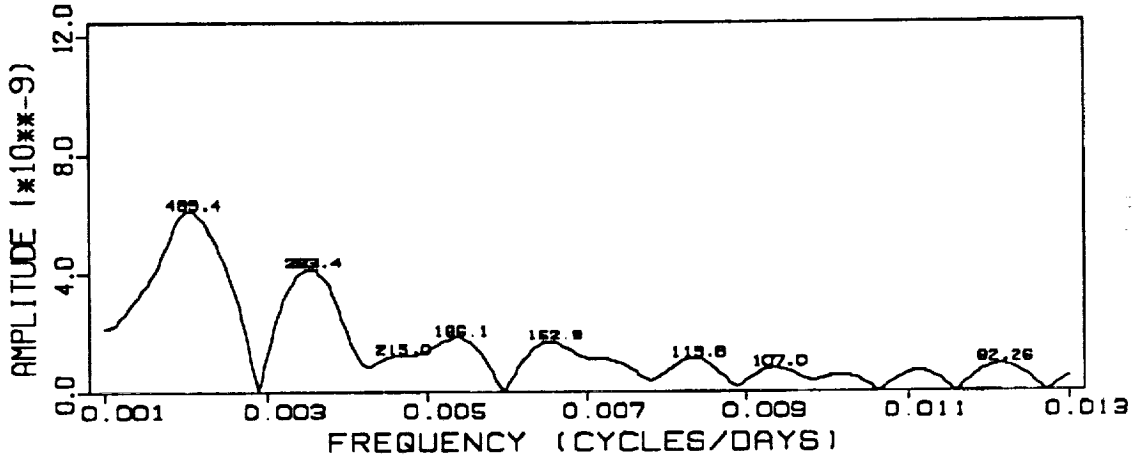

Figure 23b. Periodigram of Lageos-1 eccentricity residuals

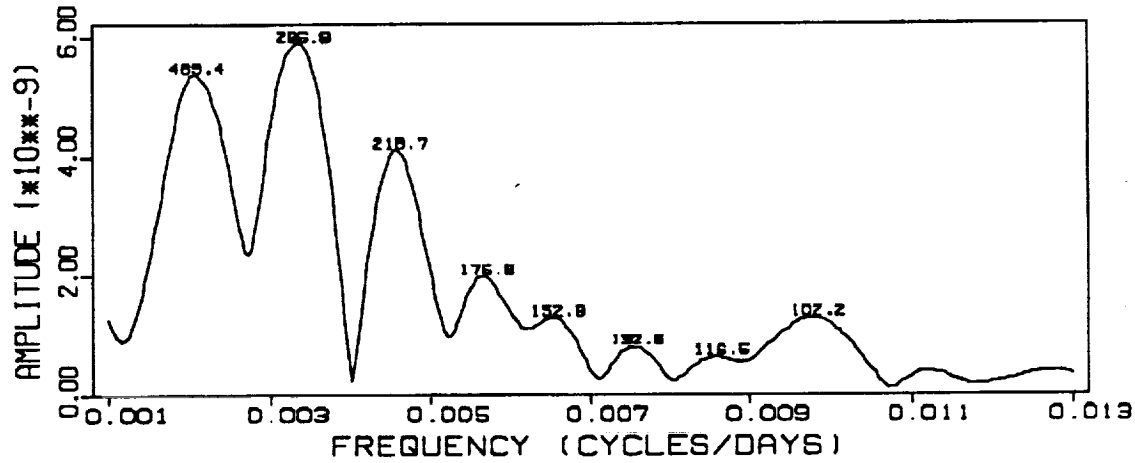

Figure 23c. Periodigram of Lageos-3 eccentricity residuals

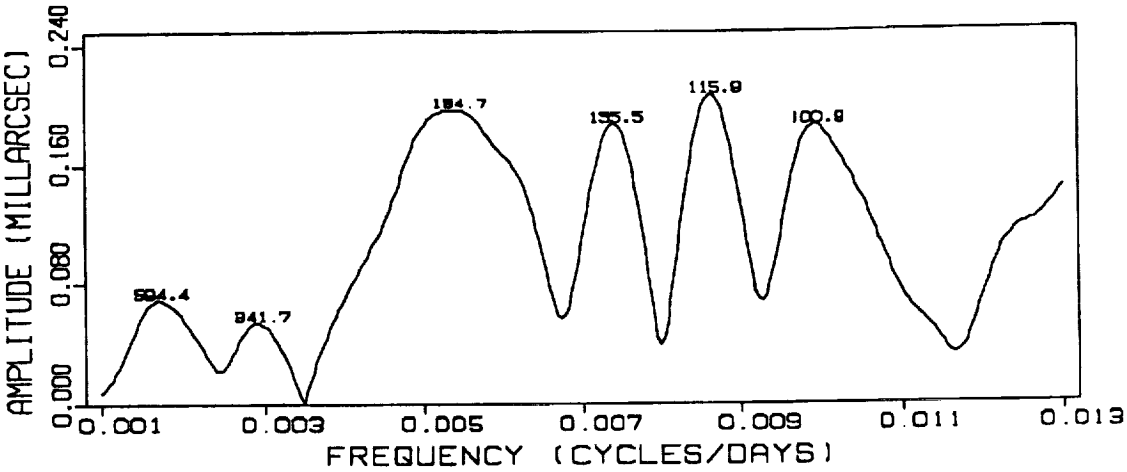

Figure 24a. Periodigram of Lageos inclination residuals (1986–1988)

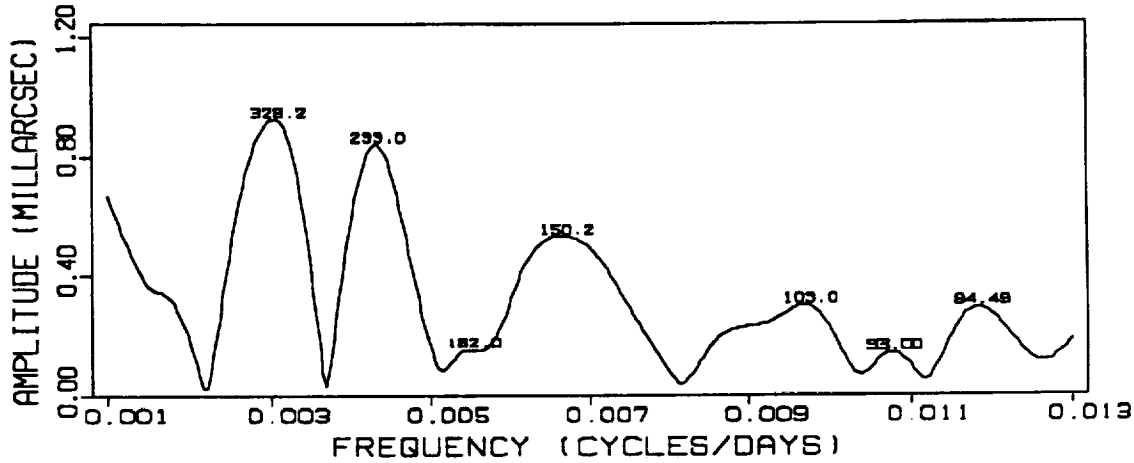

Figure 24b. Periodigram of Lageos-1 inclination residuals

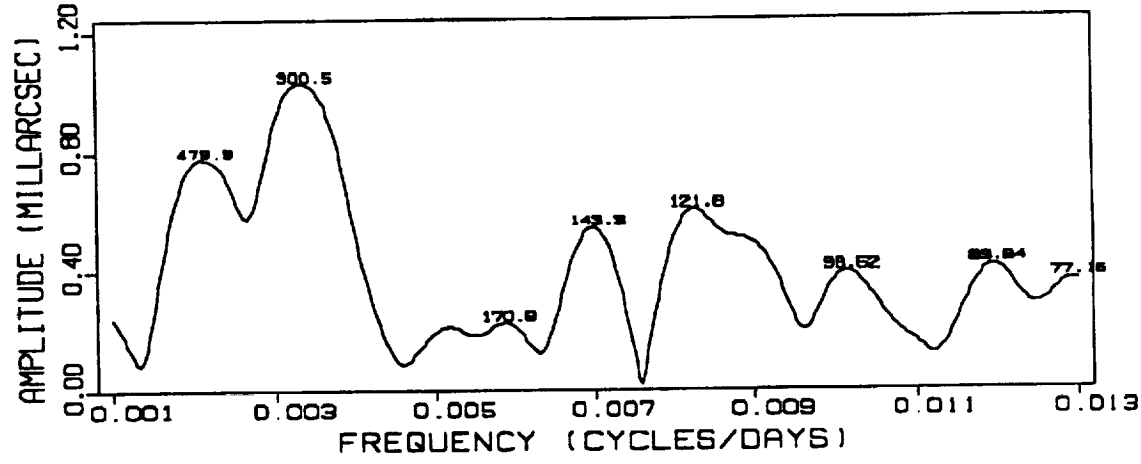

Figure 24c. Periodigram of Lageos-3 inclination residuals

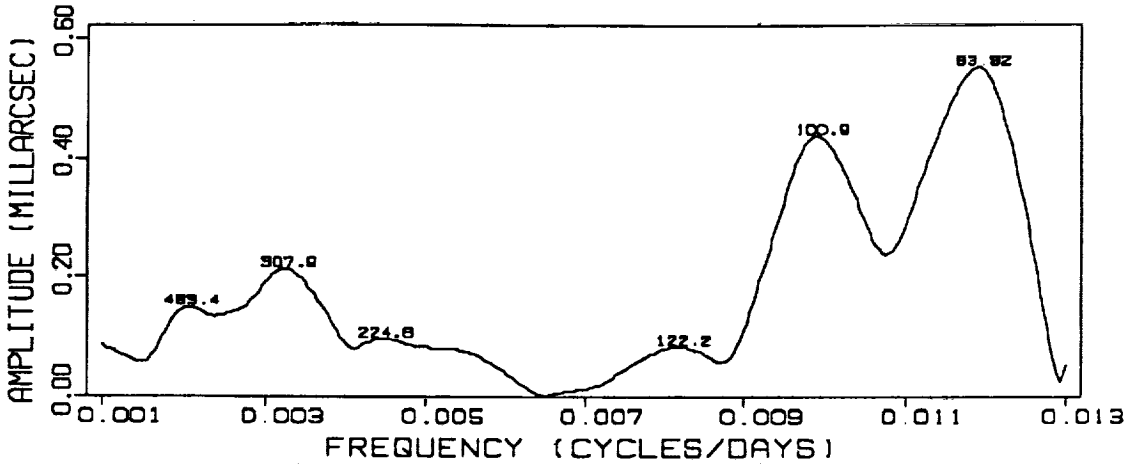

Figure 25a. Periodigram of Lageos node residuals (1986–1988)

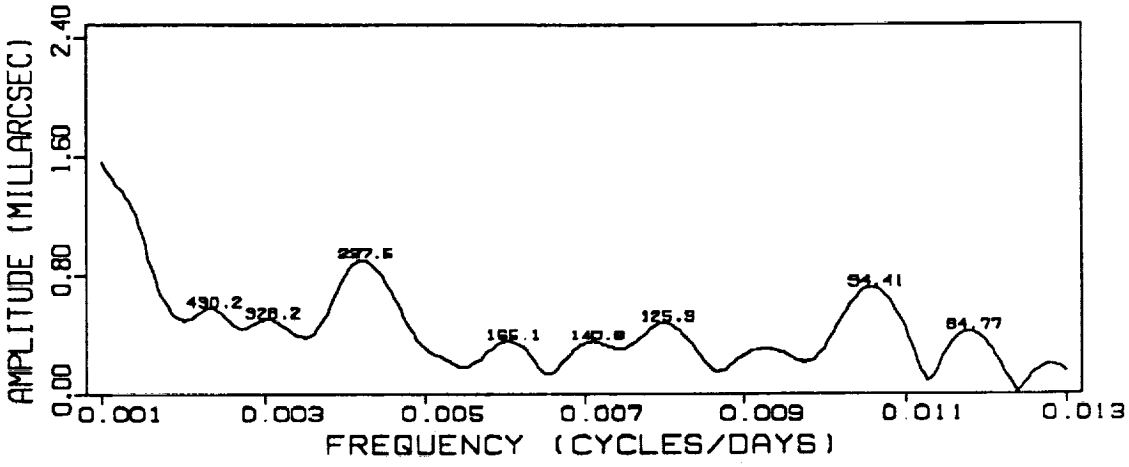

Figure 25b. Periodigram of Lageos-1 node residuals

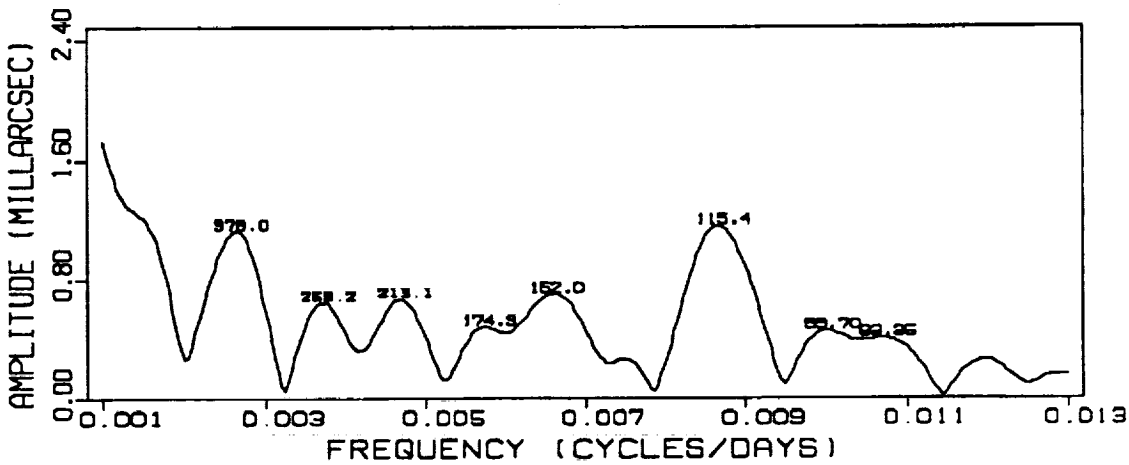

Figure 25c. Periodigram of Lageos-3 node residuals

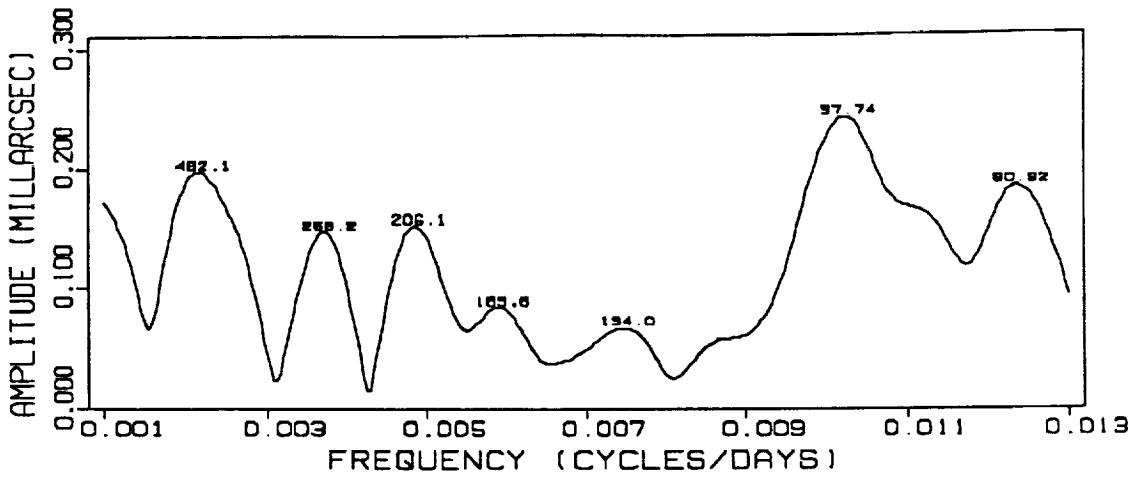

Figure 26a. Periodigram of Lageos perigee residuals (1986–1988)

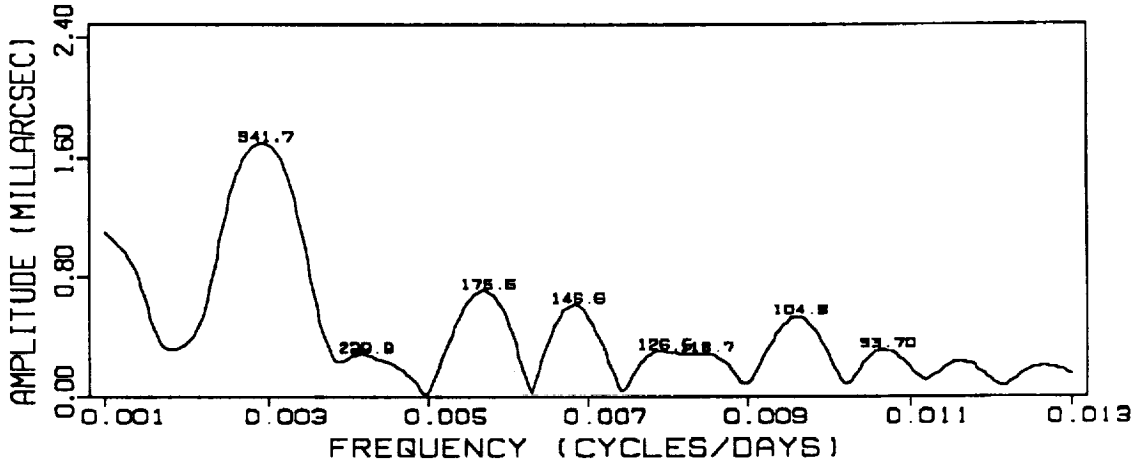

Figure 26b. Periodigram of Lageos-1 perigee residuals

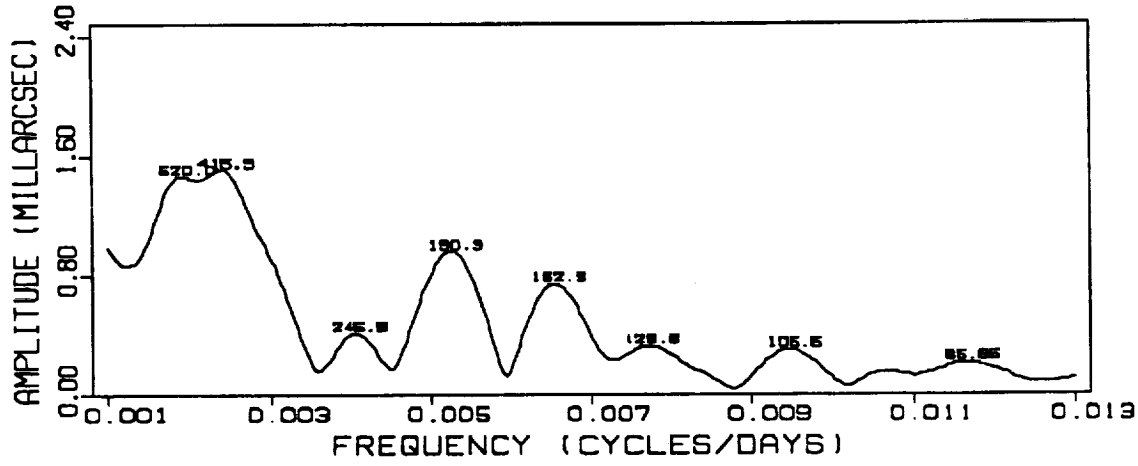

Figure 26c. Periodigram of Lageos-3 perigee residuals

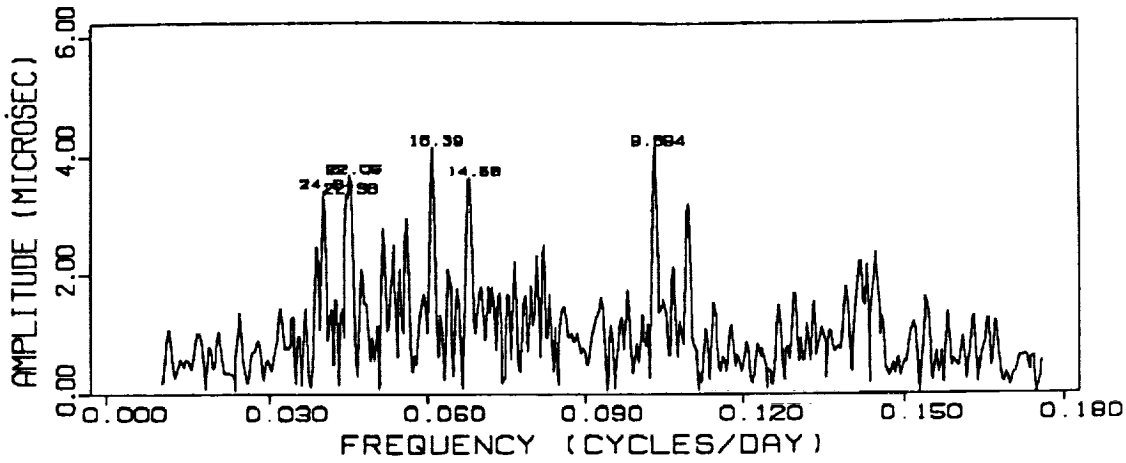

Figure 27a. Periodigram of estimated time biases in Lageos residuals (1986–1988) (periods > 6 days)

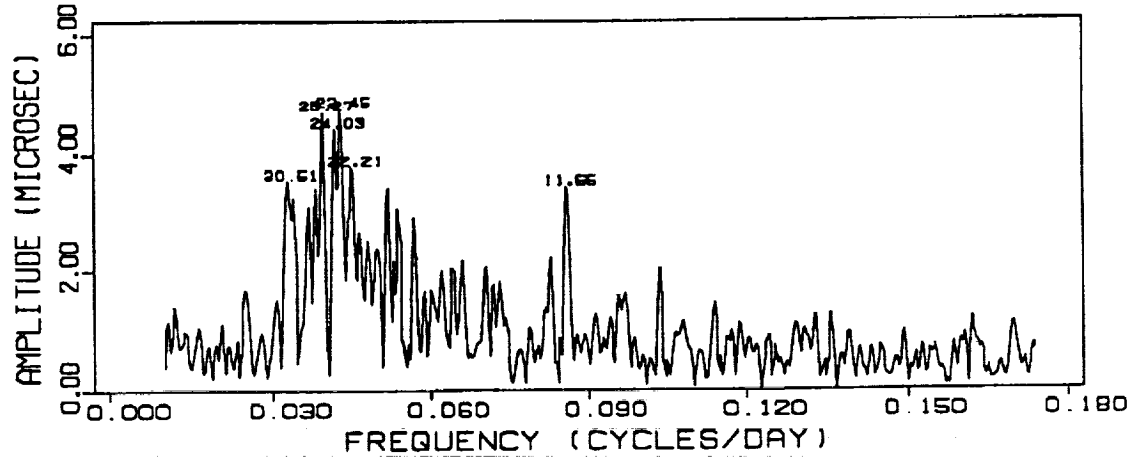

Figure 27b. Periodigram of estimated time biases in Lageos-1 residuals (periods > 6 days)

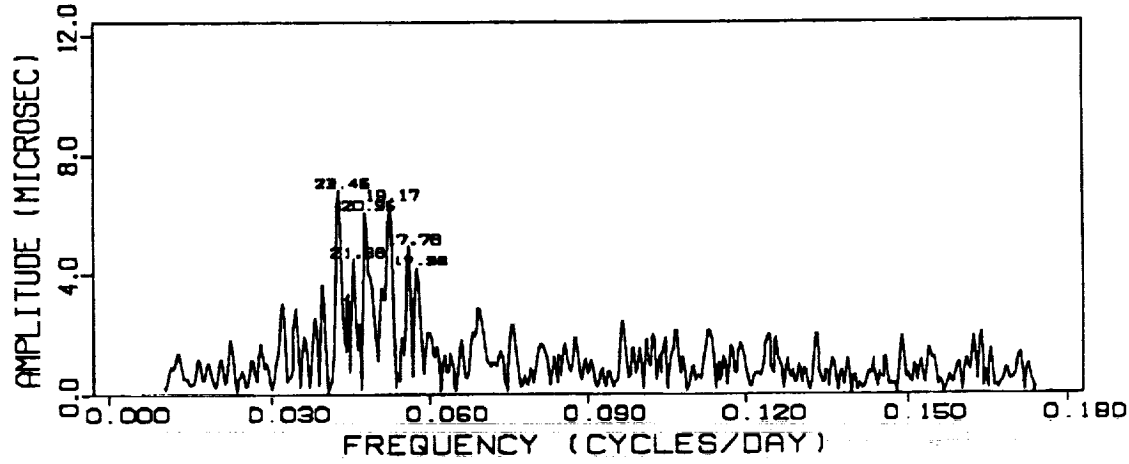

Figure 27c. Periodigram of estimated time biases in Lageos-3 residuals (periods > 6 days)

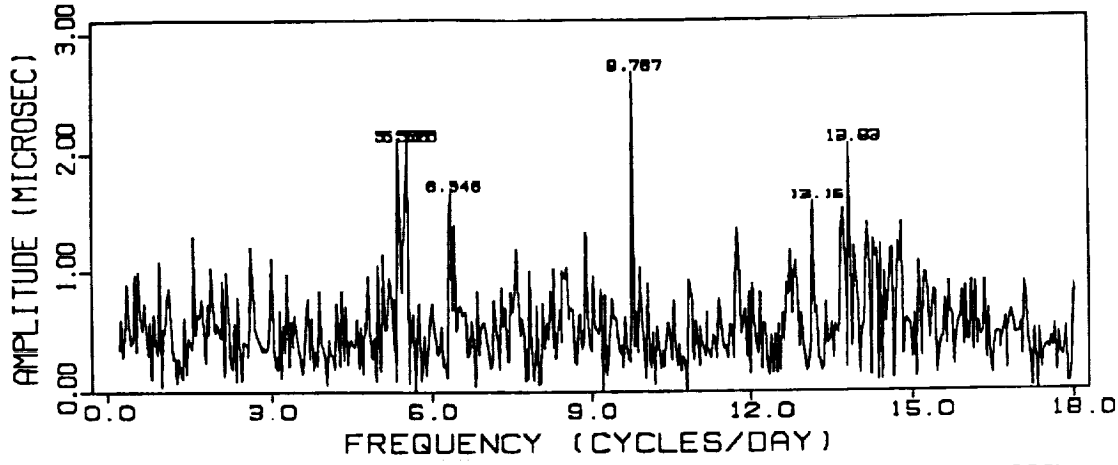

Figure 28a. Periodigram of estimated time biases in Lageos residuals (1986–1988) (periods < 6 days)

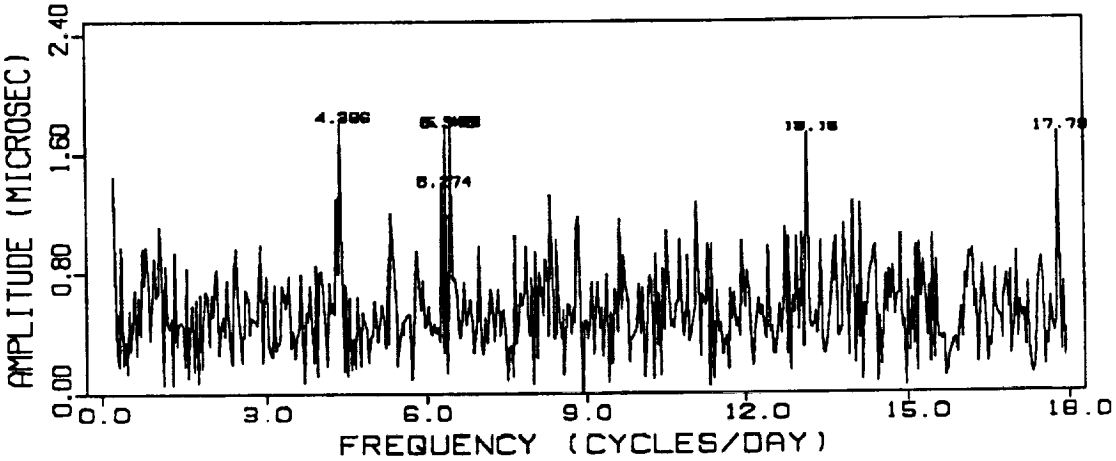

Figure 28b. Periodigram of estimated time biases in Lageos-1 residuals (periods < 6 days)

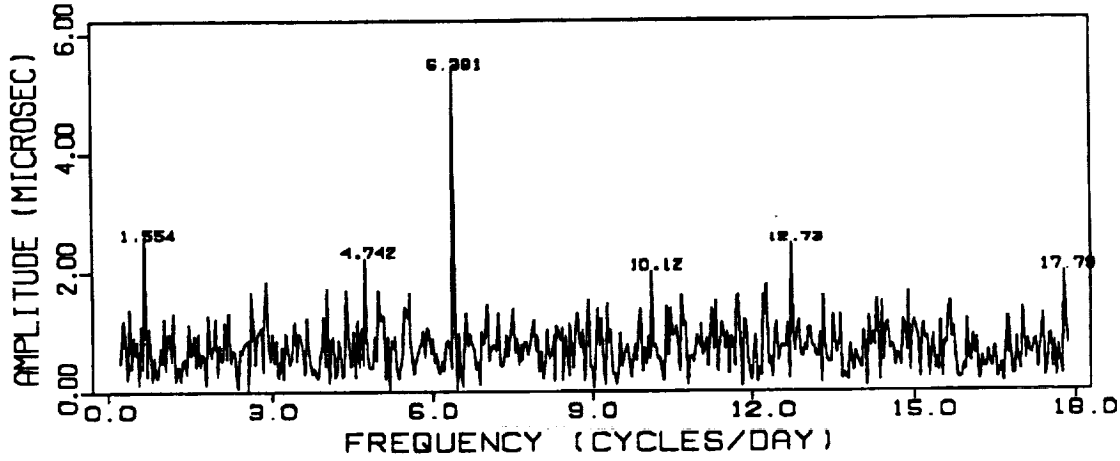

Figure 28c. Periodigram of estimated time biases in Lageos-3 residuals (periods < 6 days)

APPENDIX A-2

Orbit Injection Error Analysis for the Proposed Lageos-3 Mission

by

Stefano Casotto

Orbit Injection Error Analysis for the Proposed Lageos III Mission

Stefano Casotto

Center for Space Research

The University of Texas at Austin, Austin, Texas

Abstract. An analysis is presented of the orbital injection errors for the Lageos III satellite mission. Several methods are introduced for the solution of the Inverse Problem in the Theory of Errors. The novelty of the present approach is the use of the full geopotential covariance matrix in the expression of the orbit injection errors. The GEM-T1 covariance matrix is used in the computations. It is found that the most stringent constraint is on inclination, whose nominal value must be realized within approximately 0.2 degrees for the recovery of the Lense-Thirring precession to be successful.

1. The Lageos III Experiment

The Lageos III experiment is designed to measure the Lense-Thirring precession $\dot{\Omega}^*_{L-T}$ of the orbital plane of a satellite as predicted by Einstein's General Theory of Relativity. The Lense-Thirring precession only depends on the orbital semi-major axis and eccentricity and on the angular momentum of the central body (Lense and Thirring, 1918). For a satellite at Lageos altitude, $\dot{\Omega}^*_{L-T} \approx 31$ milliarcsec/year. The impossibility of separating such a small effect from the Newtonian precession of about 126 deg/year becomes apparent when one considers that the uncertainty in the classical precession due to the standard error in the value of the quadrupole moment of the Earth is estimated to be ≈174 milliarcsec/year based on GEM-T1 (Marsh *et al.*, 1988).

To overcome this difficulty Ciufolini (1986) proposed the use of two satellites in a configuration that effectively reduces the uncertainty in the nodal precession caused by the errors in the zonal harmonic coefficients of the gravity field of the Earth.

The theorem from Celestial Mechanics that provides the basis for the Lageos III experiment is introduced below.

1.1 The Precession of Satellites with Supplementary Inclinations

It is well known that the J_2 harmonic of the geopotential field causes a secular variation of the longitude of the node of a satellite orbit which depends on the cosine of the orbital inclination. That the same kind of modulation also characterizes the secular motion of the node when all the multipole moments of the geopotential are taken into account is less obvious.

We want to prove that two satellites with equal semi-major axes and eccentricities and supplementary inclinations have equal and opposite nodal precession rates. Since a formal proof is not easily found in the literature, one is presented here.

According to the Newtonian Theory of Gravitation the secular motion of the node is caused by the even zonal harmonics J_{2k}, $k = 1,2, \ldots$, of the central body and is given by one of Laplace's Planetary Equations (Brouwer and Clemence, 1961)

$$\dot{\Omega}(a,e,i,\mathbf{J}) = \frac{1}{na^2(1-e^2)^{1/2}\sin i}\frac{\partial R_s}{\partial i}, \tag{1}$$

where $\mathbf{J}$ is the (infinite dimensional) vector of the even zonal harmonics and the secular disturbing function R_s can be expressed as

$$R_s = -\frac{\mu}{a}\sum_{k=1}^{\infty}\left(\frac{a_e}{a}\right)^{2k} F_{(2k)0k}(i)\, G_{(2k)k0}(e)\, J_{2k} \tag{2}$$

in terms of the inclination functions $F_{lmp}(i)$ and the eccentricity functions $G_{lpq}(e)$ (Kaula, 1966; Caputo, 1967).

In order to find the dependence of $\dot{\Omega}$ on the inclination we only need the expression for the inclination function appearing in (2). Kaula (1966) and Caputo (1967) derive the general expression for $F_{lmp}(i)$, which can be specialized to

$$F_{(2k)0k}(i) = \sum_{t=0}^{k}\frac{(-1)^t(2k-t)!!}{2^{2k-t}t!\,[(k-t)!]^2}\sin^{2(k-t)}i. \tag{3}$$

Substituting this expression into the perturbing function (2), taking the partial with respect to inclination and using the result in (1), we find that the motion of the node is given by

$$\dot{\Omega}(a,e,i,\mathrm{J}) = \frac{D(a,e,i,\mathrm{J})}{na^2(1-e^2)^{1/2}} \cos i \tag{4}$$

where the function

$$D(a,e,i,\mathrm{J}) = \frac{\mu}{a} \sum_{k=1}^{\infty} \left(\frac{a_e}{a}\right)^{2k} J_{2k}\, G_{(2k)k0}(e) \sum_{t=0}^{k} \frac{(-1)^t (k-t)[2(2k-t)-1]!!}{2^{2k-t-1} t!\,[(k-t)!]^2} \sin^{2(k-t-1)} i \tag{5}$$

can easily be seen to have the property:

$$D(a,e,i,\mathrm{J}) = D(a,e,\pi-i,\mathrm{J}). \tag{6}$$

It then follows from (4) that the secular motion of the node has the property

$$\dot{\Omega}(a,e,i,\mathrm{J}) = -\dot{\Omega}(a,e,\pi-i,\mathrm{J}), \tag{7}$$

which proves the theorem.

1.2 The Residual Motion of the Mean Node

The best way to see how the theorem introduced above helps in reducing the error in the classical precession of the node is through the introduction of the *mean* node of a two-satellites configuration, defined as the *spatial* average of the nodes of the two satellites (not to be confused with the *average* node which conventionally indicates a *time* average).

If we now indicate with $\dot{\Omega}^I = \dot{\Omega}(a^I, e^I, i^I, \mathrm{J})$ and $\dot{\Omega}^{III} = \dot{\Omega}(a^{III}, e^{III}, i^{III}, \mathrm{J})$ the nodal precessions of Lageos I and Lageos III respectively, then the classical motion $\dot{\Omega}^*$ of the mean node is given by

$$\dot{\Omega}^* = \frac{1}{2}(\dot{\Omega}^I + \dot{\Omega}^{III}) \tag{8}$$

If the two sets of relevant orbital elements only differ in that the inclinations are supplementary, eqs. (7) and (8) show that the newtonian motion of their mean node is zero.

However, the mean node is also subject to the Lense-Thirring precession. This can now effectively be separated because, as will be shown in the next sections, the error in the classical

motion of the mean node is of second order in the standard errors ΔJ of the even zonal harmonics and the standard errors $\Delta a, \Delta e, \Delta i$ of the orbit elements of the second satellite relative to its nominal values.

The orbital elements of Lageos III can be expressed in terms of the elements of Lageos I as follows

$$\begin{aligned} a^{III} &= a^{I} + \Delta a \\ e^{III} &= e^{I} + \Delta e \\ i^{III} &= \pi - i^{I} + \Delta i \end{aligned} \tag{9}$$

where $\Delta a, \Delta e, \Delta i$ are the orbit injection errors of Lageos III.

Substituting (9) into (8) and expanding to first order we get the residual classical motion of the mean node

$$\dot{\Omega}^{*} = \frac{1}{2}\,\Delta\dot{\Omega}(a^{I}, e^{I}, \pi - i^{I}, J), \tag{10}$$

where

$$\Delta\dot{\Omega}(a,e,i,J) = \frac{\partial\dot{\Omega}}{\partial a}\Delta a + \frac{\partial\dot{\Omega}}{\partial e}\Delta e + \frac{\partial\dot{\Omega}}{\partial i}\Delta i \tag{11}$$

The partials in (11) can be easily computed from (4) and (5). The magnitude of the residual precession $\dot{\Omega}^{*}$ is seen to be of first order in the orbit injection errors.

A successful experiment requires that the magnitude of the residual precession be known with an error of 10%, or ≈3 milliarcsec/year, in order to have high confidence that the Lense-Thirring precession has been observed. Since there are many other error sources to be considered, it is desirable to keep the contribution from orbit injection errors small. Thus for this analysis a criterion of 3%, or ≈1 milliarcsec/year, is adopted in order to establish the orbit injection error tolerance for Lageos III.

2. *Orbit Injection Error Analysis*

2.1 Uncertainty in the Residual Motion of the Mean Node

The uncertainty in the value of the residual precession (10) of the mean node is mainly due to errors ΔJ in the even zonal harmonics of the geopotential, and to a negligible extent to the uncertainty in the orbital parameters of Lageos I. We can therefore write that the error in $\dot{\Omega}^*$ is given by

$$\Delta\dot{\Omega}^* = \frac{\partial\dot{\Omega}^*}{\partial J}\Delta J, \tag{12}$$

where the vector of partials is given by

$$\frac{\partial\dot{\Omega}^*}{\partial J} = \frac{1}{2}\left(\frac{\partial^2\dot{\Omega}}{\partial a\partial J}\Delta a + \frac{\partial^2\dot{\Omega}}{\partial e\partial J}\Delta e + \frac{\partial^2\dot{\Omega}}{\partial i\partial J}\Delta i\right) \tag{13}$$

Equation (12) expresses the fact that the error in the residual motion of the mean node is of mixed second order in $\Delta J, \Delta a, \Delta e, \Delta i$.

The values of the second partials in (13) are shown in Table 1 for the first 14 even zonal harmonic coefficients.

n	$\frac{\partial^2\dot{\Omega}}{\partial a\partial J_n}$	$\frac{\partial^2\dot{\Omega}}{\partial e\partial J_n}$	$\frac{\partial^2\dot{\Omega}}{\partial i\partial J_n}$
2	.2651918616E+09	-.1636381245E+09	-.7495930711E+09
4	.2071033701E+09	-.2236274716E+09	-.9867064123E+08
6	.7250662102E+08	-.1148193218E+09	.1533258189E+09
8	.7626665012E+07	-.1603424227E+08	.1098118095E+09
10	-.6041665073E+07	.1587939535E+08	.3856354086E+08
12	-.4168202102E+07	.1316352997E+08	.6321912181E+07
14	-.1441783036E+07	.5320337075E+07	-.1302456918E+07
16	-.2682388852E+06	.1132910910E+07	-.1352577907E+07
18	.1805487432E+05	-.8590093390E+05	-.5278565170E+06
20	.3553240017E+05	-.1880562787E+06	-.1184768056E+06
22	.1516367641E+05	-.8836718616E+05	-.4817560266E+04
24	.3774497061E+04	-.2401591242E+05	.9031036604E+04
26	.3538437145E+03	-.2440730477E+04	.4667651009E+04
28	-.1803288872E+03	.1340332113E+04	.1334580865E+04

Table 1. Second Partial Derivatives of Nodal Precession Rate: Units are [mas/year/km], [mas/year/100], [1/year/60000]

2.2 The Inverse Problem in the Theory of Errors

The normal use of equation (12) is in the context of error propagation, where the error in the residual motion is found in terms of the orbital injection errors. In the present case, however, the situation is reversed, since we need to determine (bounds for) the Lageos III orbital injection errors on the basis of the a priori error for the residual motion. The difficulty lies in the fact that we have only one equation to work with, and therefore the solution is not unique. This problem is called the Inverse Problem in the Theory of Errors, and the only place in the literature where it was found to be treated is Shchigolev (1965), where the Method of Equal Influences is proposed to find a solution in terms of limiting absolute errors. We will introduce this method in the next section.

2.2.1 Maximum Error Analysis

The propagation of the maximum error is the crudest, and most restrictive, method in the theory of errors. However, it gives us the opportunity to introduce the concept of *equal influences*, upon which we will elaborate later.

Propagation of maximum error leads to rewrite (12) in the form

$$\Delta\dot{\Omega}^* = \frac{1}{2}\left|\frac{\partial^2\dot{\Omega}}{\partial a\partial \mathbf{J}}\right|\Delta a\Delta\mathbf{J} + \frac{1}{2}\left|\frac{\partial^2\dot{\Omega}}{\partial e\partial \mathbf{J}}\right|\Delta e\Delta\mathbf{J} + \frac{1}{2}\left|\frac{\partial^2\dot{\Omega}}{\partial i\partial \mathbf{J}}\right|\Delta i\Delta\mathbf{J} \qquad (14)$$

where the vertical bars around the vectors of partials indicate that the absolute values of the components is to be taken, and where (13) has been used.

According to the method of equal influences, the three terms on the r.h.s. of (14) are then assumed to have equal (positive) values. A justification of this assumption is not easily given, but its similarity to the Bayesian point of view in the Theory of Probability may easily be appreciated, along with all the ensuing controversies.

Then it follows that

$$\Delta a = \frac{2}{3}\left[\sum_{k=1}^{14}\left|\frac{\partial^2\dot{\Omega}}{\partial a \partial J_{2k}}\right|\Delta J_{2k}\right]^{-1}$$
$$\Delta e = \frac{2}{3}\left[\sum_{k=1}^{14}\left|\frac{\partial^2\dot{\Omega}}{\partial a \partial J_{2k}}\right|\Delta J_{2k}\right]^{-1} \qquad (15)$$
$$\Delta i = \frac{2}{3}\left[\sum_{k=1}^{14}\left|\frac{\partial^2\dot{\Omega}}{\partial a \partial J_{2k}}\right|\Delta J_{2k}\right]^{-1}$$

Using the values from Table 1 and identifying the errors ΔJ_l with the standard deviations of the GEM-T1 coefficients shown in Table 2, we obtain

$$\begin{aligned} |\Delta a| &\le 1.32 \ \text{km} \\ |\Delta e| &\le 0.01 \\ |\Delta i| &\le 0.01 \ \text{deg} \end{aligned} \qquad (16)$$

An alternative method is to take as zero two of the three obital injection errors, as was done by Casotto and Ciufolini (1987). Then it is possible to solve for the only remaining error and the bounds thus found are exactly three times as large as those in (16).

2.2.2 Covariance Analysis

The orbital injection errors should be correctly regarded as random variables. Their characterization is therefore given in terms of the first two moments of their frequency distributions, or their means and covariances, respectively. Such a characterization is complete in the case of normal distributions. As is usual, all means will be assumed to be zero. Further, we can consider the errors appearing on the r.h.s. of (12) as divided into two mutually independent sets of random variables $\{\Delta\mathbf{J}\}$ and $\{\Delta a, \Delta e, \Delta i\}$. This follows from the assumption that the orbit injection errors only depend on the satellite launching apparatus, and not on the gravity field of the Earth.

In order to find the second order statistics of the random variables, we first take the square of both sides of equaton (12)

$$4\,(\Delta\dot{\Omega}^*)^2 = \left[\frac{\partial\dot{\Omega}^*}{\partial\mathbf{J}}\right]\Delta\mathbf{J}\,\Delta\mathbf{J}^{\mathrm{T}}\left[\frac{\partial\dot{\Omega}^*}{\partial\mathbf{J}}\right]^{\mathrm{T}} \qquad (17)$$

If for compactness we now define the vectors

$$\begin{aligned}\dot{\Omega}_{aJ} &\equiv \frac{\partial^2 \dot{\Omega}}{\partial a \partial J} \\ \dot{\Omega}_{eJ} &\equiv \frac{\partial^2 \dot{\Omega}}{\partial e \partial J} \\ \dot{\Omega}_{iJ} &\equiv \frac{\partial^2 \dot{\Omega}}{\partial i \partial J}\end{aligned} \tag{18}$$

we can expand (17) in the form

$$\begin{aligned}4\,(\Delta\dot{\Omega}^*)^2 = &\dot{\Omega}_{aJ}\,\Delta J \Delta J^T\,\dot{\Omega}_{aJ}^T\,(\Delta a)^2 \\ &+ \dot{\Omega}_{eJ}\,\Delta J \Delta J^T\,\dot{\Omega}_{eJ}^T\,(\Delta e)^2 \\ &+ \dot{\Omega}_{iJ}\,\Delta J \Delta J^T\,\dot{\Omega}_{iJ}^T\,(\Delta i)^2 \\ &+ 2\,\dot{\Omega}_{aJ}\,\Delta J \Delta J^T\,\dot{\Omega}_{eJ}^T\,\Delta a \Delta e \\ &+ 2\,\dot{\Omega}_{aJ}\,\Delta J \Delta J^T\,\dot{\Omega}_{iJ}^T\,\Delta a \Delta i \\ &+ 2\,\dot{\Omega}_{eJ}\,\Delta J \Delta J^T\,\dot{\Omega}_{iJ}^T\,\Delta e \Delta i\end{aligned} \tag{19}$$

We can now apply the expectation operator $E[.]$ with respect to both sets of random variables identified above and use their independence to obtain

$$\begin{aligned}4\,\sigma_{\dot{\Omega}^*}^2 = &\dot{\Omega}_{aJ}\,\mathbf{P}\,\dot{\Omega}_{aJ}^T\,\sigma_a^2 \\ &+ \dot{\Omega}_{eJ}\,\mathbf{P}\,\dot{\Omega}_{eJ}^T\,\sigma_e^2 \\ &+ \dot{\Omega}_{iJ}\,\mathbf{P}\,\dot{\Omega}_{iJ}^T\,\sigma_i^2 \\ &+ 2\rho_{a_e}\,\dot{\Omega}_{aJ}\,\mathbf{P}\,\dot{\Omega}_{eJ}^T\,\sigma_a\sigma_e \\ &+ 2\rho_{ai}\,\dot{\Omega}_{aJ}\,\mathbf{P}\,\dot{\Omega}_{iJ}^T\,\sigma_a\sigma_i \\ &+ 2\rho_{ei}\,\dot{\Omega}_{eJ}\,\mathbf{P}\,\dot{\Omega}_{iJ}^T\,\sigma_e\sigma_e,\end{aligned} \tag{20}$$

where the covariance matrix $\mathbf{P} = E[\Delta J \Delta J^T]$ of the even zonal harmonic coefficients appears, and the covariance σ_{xy} between two random variables Δx and Δy, where x and y stand for any of a, e, i, has been rewritten in terms of the total correlation coefficient ρ_{xy} and the variances σ_x and σ_y. The elements of $\mathbf{P}$ up to degree 28 are displayed in Table 2.

Several things should be noted about the error equation (20). In the first place, equation (20) defines a quadric surface in $\sigma_a, \sigma_e, \sigma_i$ -space. Since the nature of a quadric is determined by the eigenvalues of the associated matrix, inspection of (20) reveals that the type of quadric, for a

l_1 l_2	$\sigma_{l_1 l_2}$	l_1 l_2	$\sigma_{l_1 l_2}$
2 2	.16354743386413E-18	10 16	-.99725614288160E-17
2 4	-.44255031142273E-18	10 18	.97926100170970E-17
2 6	.57372102475274E-18	10 20	-.11697079004533E-16
2 8	-.82943963924300E-18	10 22	.11064906979244E-16
2 10	.69297539737869E-18	10 24	-.10859783701640E-16
2 12	-.74864689655563E-18	10 26	.92689314290929E-17
2 14	.43322746149793E-18	10 28	-.48567493496756E-17
2 16	-.77739696176188E-18	12 12	.12282073009362E-16
2 18	.82899281204938E-18	12 14	-.12991524441965E-16
2 20	-.16101555933395E-17	12 16	.15048974207966E-16
2 22	.14709918927718E-17	12 18	-.13093816244968E-16
2 24	-.14275625608520E-17	12 20	.14173449313260E-16
2 26	.80794594705213E-18	12 22	-.12370381360868E-16
2 28	.27696515098380E-18	12 24	.13722901324308E-16
4 4	.12272428479326E-17	12 26	-.13095558008867E-16
4 6	-.16293048932063E-17	12 28	.98763727647548E-17
4 8	.23862161543863E-17	14 14	.15790424642680E-16
4 10	-.20594222289284E-17	14 16	-.16811021070720E-16
4 12	.22350957089756E-17	14 18	.14689051839059E-16
4 14	-.13661327627724E-17	14 20	-.12270514883256E-16
4 16	.23157825799380E-17	14 22	.10833472257364E-16
4 18	-.24963911640746E-17	14 24	-.12222162085146E-16
4 20	.46819637432056E-17	14 26	.15182178471157E-16
4 22	-.42778006417160E-17	14 28	-.13382477505778E-16
4 24	.41073787756931E-17	16 16	.19822001805150E-16
4 26	-.23452550266630E-17	16 18	-.16843799924431E-16
4 28	-.66543282896704E-18	16 20	.16975282572324E-16
6 6	.23622663372187E-17	16 22	-.13812015790649E-16
6 8	-.35123533205048E-17	16 24	.15741741509831E-16
6 10	.33845001209633E-17	16 26	-.16229028762581E-16
6 12	-.36614960476057E-17	16 28	.14763762496582E-16
6 14	.26810329289111E-17	18 18	.17022171205191E-16
6 16	-.37982912074692E-17	18 20	-.17601080121954E-16
6 18	.42960385117915E-17	18 22	.16267221370710E-16
6 20	-.70190894835867E-17	18 24	-.15007124172032E-16
6 22	.66297319695961E-17	18 26	.14882671779542E-16
6 24	-.61064099387155E-17	18 28	-.10987068174600E-16
6 26	.36662592168055E-17	20 20	.25936077118387E-16
6 28	.17523420880234E-18	20 22	-.22780966672889E-16
8 8	.55321349322923E-17	20 24	.22121704419582E-16
8 10	-.56190839300943E-17	20 26	-.14808343656958E-16
8 12	.66124793356412E-17	20 28	.64571107136990E-17
8 14	-.53309868517976E-17	22 22	.23449769693599E-16
8 16	.72017054640601E-17	22 24	-.20347548319296E-16
8 18	-.73458936194835E-17	22 26	.15290872533794E-16
8 20	.11193280408343E-16	22 28	-.47921576485707E-17
8 22	-.10316100024246E-16	24 24	.23556131496919E-16
8 24	.98652863221099E-17	24 26	-.17426574103048E-16
8 26	-.65588482566393E-17	24 28	.99472024892936E-17
8 28	.13904354298525E-17	26 26	.22332943556028E-16
10 10	.68650465547862E-17	26 28	-.12834742986458E-16
10 12	-.86742258955936E-17	28 28	.24855275414208E-16
10 14	.86384038796786E-17		

Table 2. **GEM-T1 covariance matrix elements for the even zonal harmonic coefficients: $\sigma_{l_1 l_2}$ is the (l_1, l_2) element of P**

given orbit, is solely determined by the values of the correlation coefficients ρ_{a_e}, ρ_{ai}, ρ_{ei}. Second, since the quadric surface is the locus of the (1-sigma) injection error bounds, the only meaningful quadric in the present context is an ellipsoid, because only then are the errors finite. In this case, any triplet $(\sigma_a, \sigma_e, \sigma_e)$ from the solution space belongs to the interior of the ellipsoid.

There are two major consequences to these observations. The first is that the requirement that (20) be an ellipsoid places a restriction on the possible values of the correlation coefficients. The second is that the complete specification of the error space requires the specification of the semi-axes and the orientation of the ellipsoid, or, what amounts to the same, the eigenvalues and the eigenvectors associated with (20). Although theoretically clear, this way of specifying error bounds turns out to be impractical because these error bounds are correlated. It would be more desirable to specify the error bounds in terms of a parallelepiped instead. In that case, the error space can be characterized completely through the inequalities

$$\begin{aligned} |a^{III} - a^{I}| &\le \sigma_a \\ |e^{III} - e^{I}| &\le \sigma_e \\ |i^{III} + i^{I} - \pi| &\le \sigma_i \end{aligned} \tag{21}$$

in terms of *mutually independent* error bounds σ_a, σ_e, σ_i. We will now see how the method of equal influences can be used to achieve this.

2.2.2.1. Zero Correlation Analysis Application of the method of equal influences to equation (20) requires that all six terms on the r.h.s. have the same value. However, this is generally impossible because the constraints thus put on the coefficients of the quadric can only be satisfied under special circumstances. This leads to the ancillary assumption that the correlation coefficients be all zero, that is $\rho_{a_e} = \rho_{ai} = \rho_{ei} = 0$. From the positive definiteness of the covariance matrix **P** it then follows that equation (20) indeed defines an ellipsoid. The solution of the inverse problem is therefore given by

$$\begin{aligned} \sigma_a &= \frac{2\sigma^2_{\dot{\Omega}^*}}{(3\dot{\Omega}_{aJ}\,\mathbf{P}\,\dot{\Omega}^T_{aJ})^{1/2}} \\ \sigma_e &= \frac{2\sigma^2_{\dot{\Omega}^*}}{(3\dot{\Omega}_{eJ}\,\mathbf{P}\,\dot{\Omega}^T_{eJ})^{1/2}} \\ \sigma_i &= \frac{2\sigma^2_{\dot{\Omega}^*}}{(3\dot{\Omega}_{iJ}\,\mathbf{P}\,\dot{\Omega}^T_{iJ})^{1/2}} \end{aligned} \tag{22}$$

It is interesting to note that, as may be easily verified, (22) is also the solution to the problem of finding the semi-sides of the parallelopiped of maximum volume inscribed in the ellipsoid defined by (20), centered at the origin of the σ_a, σ_e, σ_i-coordinates, and with faces parallel to the coordinate planes. Such a geometric interpretation of the result (22) provides an acceptable justification for adopting the Method of Equal Influences for the solution of the inverse problem in the Theory of Errors in terms of standard deviations. Using the full covariance (see Table 2), the solution is the following

$$\begin{aligned} |\Delta a| &\le 26.98 \quad \text{km} \\ |\Delta e| &\le 0.188 \\ |\Delta i| &\le 0.121 \quad \text{deg} \end{aligned} \tag{24}$$

It can be seen that using the method of equal influences and including the effects of correlations existing among the even zonal harmonics of the GEM-T1 geopotential solution has significantly increased the allowable injection errors, compared with the results of the previous section.

In the following the full covariance matrix for the even zonal GEM-T1 coefficients will be used (see Table 2).

2.2.2.2. Full Correlation Analysis The geometric interpretation of the equal influences solution as an error box of maximum volume can be used to extend the method to the case of non-zero correlation coefficients; that is, $\rho_{a_e}, \rho_{ai}, \rho_{ei} \neq 0$. The solution space in this case can be defined to be the parallelepiped with the same characteristics as before, only that it cannot be determined analytically, and numerical optimization techniques must be used.

In order to find this solution, the values of the correlation coefficients are needed. If this information is missing, as in the present case, the correlation coefficients can be considered as parameters, and a solution can be determined for an exhaustive set of combinations of their values. Since the value of any correlation coefficient belongs to the interval $[-1,1]$, a solution was computed for each combination of values of $\rho_{a_e}, \rho_{ai}, \rho_{ei}$ from this interval at increments of 0.2, excepting combinations for which the quadric had negative eigenvalues.

Rather than giving the full list, the results obtained will be compressed into the following statistics:

$$\begin{aligned} |\Delta a| &\le 29.70 \pm 10.20 \quad \text{km} \\ |\Delta e| &\le 0.202 \pm 0.068 \\ |\Delta i| &\le 0.117 \pm 0.028 \quad \text{deg} \end{aligned} \tag{25}$$

where the mean and the dispersion about the mean are shown.

It can be seen that the mean values of the error bounds, when the correlation coefficients are non zero, do not differ appreciably from the case of zero correlations. Also, varying the correlation values does not produce large dispersions about the means.

It must be realized that the error bounds given by the method of equal influences can be quite conservative and that if two of the elements have zero or negligible errors, then the error in the third element can be effectively increased by a factor of $\sqrt{3}$. For instance, if the bounds on Δa and Δe are set respectively at 10 km and 0.004, which seem to be routinely attainable accuracies, then the upper bound in the inclination error rises to 0.21 degrees, with a dispersion of 0.01 degrees.

3. Summary and Conclusions

The goal of the Lageos I/Lageos III experiment is the measurement of the precession of the average node of the two-satellite configuration with such an accuracy as to permit the recovery of the general relativistic Lense-Thirring precession. This work addresses the problem of establishing the bounds for the orbit injection errors of Lageos III based solely on the covariance of the even zonal harmonics of the gravitational field of the Earth. The criterion used is a 3% uncertainty in the Lense-Thirring precession.

The solution is found by accounting for the statistical properties of the gravitational coefficients of the GEM-T1 field in a progressively more refined way.

It is thus found that the restrictive limits of expression (16) imposed by an analysis based on the propagation of the maximum error are relaxed by a little more than an order of magnitude (see (24)) when they are computed in terms of standard deviations using the full covariance for the even zonal coefficients of GEM-T1 and the injection errors are assumed to be uncorrelated.

Parameterizing the solution with the correlation coefficients of the three orbit injection errors yields average error bounds close to the ones corresponding to the zero-correlation case. In particular, the inclination error bound is centered at 0.12 degrees with a dispersion of 0.03 degrees due to all the possible combinations of correlations with the semi-major axis and eccentricity errors. However, if the bounds on the semi-major axis and the eccentricity can be set to 10 km and 0.004, respectively, then the bound on the inclination increases to 0.21 degrees with a negligible dispersion.

Bibliography

1. Caputo, M. (1967), *The Gravity Field of the Earth from Classical and Modern Methods*, Academic Press, Orlando, Fl.

2. Ciufolini, I. (1986), "Measurement of the Lense-Thirring Drag on High-Altitude, Laser-Ranged Artificial Satellites," *Phys. Rev. Lett.*, **56**, 278-281.

3. Kaula, W. (1966), *Theory of Satellite Geodesy*, Blaisdell, Waltham, Mass.

4. Lense, J. and H. Thirring, (1918), "Uber den Einfluss der Eigenrotation der Zentralkorper auf die Bewegung der Planeten und Monde nach der Eisteinschen Gravitationstheorie," *Phys. Z.*, **19**, 156-163; English translation in B. Mashhoon *et al.*, *Gen. Relativ. Gravit.* , **16**, 727-741 (1984).

5. Marsh, J. G., F. J. Lerch, B. H. Putney, D. C. Christodoulidis, D. E. Smith, T. L. Felsentreger, B. V. Sanchez, S. M. Klosko, E. C. Pavlis, T. V. Martin, J. W. Robbins, R. G. Williamson, O. L. Colombo, D. D. Rowlands, W. F. Eddy, N. L. Chandler, K. E. Rachlin, G. B. Patel, S. Bhati, and D. S. Chinn (1988), "A New Gravitational Model for the Earth from Satellite Tracking Data: GEM-T1," *JGR*, **93** (B6), 6169.

6. Shchigolev, B. M. (1965), *Mathematical Analysis of Observations* , American Elsevier, New York, N.Y.

APPENDIX B

(under separate cover)

Agenzia Spatiale Italiana Investigations

Principal Investigator: Ignazio Ciufolini – CNR Frascati

Other Members:

Bruno Bertotti	–	Un. Pavia
Giuseppe Bianco	–	ASI Matera
Mario Carpino	–	Oss. Astr. di Brera
Marino Dobrowolny	–	CNR Frascati
Paolo Farinella	–	Un. Pisa
Luciano Iess	–	CNR Frascati
Anna Nobili	–	Un. Pisa
Francesco Vespe	–	ASI Matera
Susanna Zerbini	–	Un. Bologna

B-1. Effect of Particle Drag on the Lageos Node and Measurement of the Gravitomagnetic Field (Ignazio Ciufolini, Marino Dobrowolny, and Luciano Iess)

B-2 Effects of Thermal Thrust on the Node and Inclination of Lageos (Paolo Farinella, Anna M. Nobili, Francois Barlier, and Francois Mignard)

B-3. The Rotation of Lageos (Bruco Bertotti and Luciano Iess)

B-4. Nodal Perturbations Due to Earth-Reflected and Earth-Diffused Radiation Pressure on Lageos-Type Satellites (Paolo Farinella and D. Lucchesi)

B-5. Earth Satellites and Gravitomagnetic Field (Giuseppe Bianco, Ignazio Ciufolini, and Francesco Vespe)

B-6. Supplementary Satellites and Tidal Perturbations (Bruno Bertotti and Mario Carpino)

B-7. Proposal for a Thermal Characterization Test Campaign for Lageos-Type Satellites (Paolo Farinella and Silvana Rabbia)